

**STRUCTURAL AND PETROGRAPHIC FABRICS IN THE CHISAMBA AND  
KABWE AREAS, CENTRAL ZAMBIA: IMPLICATIONS FOR THE LATE  
PROTEROZOIC MWEMBESHI DISLOCATION ZONE**

**BY**

**CRISPIN KATONGO**  
**B. Min. Sc. (University of Zambia)**

**A dissertation submitted to the University of Zambia in fulfillment of the  
requirement for the degree of Master of Mineral Sciences (Geology)**

**School of Mines**  
**University of Zambia**

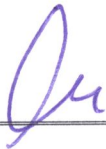
**July 1999**

20/8/99


## DECLARATION

I declare that this dissertation was written and submitted in accordance with the rules and regulations governing the award of the Master of Mineral Sciences of the University of Zambia. I further declare that the dissertation has neither in part nor in whole been presented as substance for award of any degree, either to this or any other University. Where other peoples work has been drawn upon, acknowledgement has been made.

Signature of author:

  
\_\_\_\_\_  
C. Katongo

Signature of supervisor:

  
\_\_\_\_\_  
Dr F. Tembo

Date:

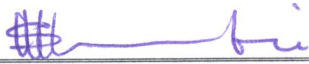
17.8.99

## APPROVAL PAGE

This dissertation of Crispin Katongo is approved as fulfilling the requirements of the  
Degree of Master of Mineral Science in Geology by the University of Zambia

Signature of Examiners

Chairman:

 18/08/99

First Examiner:



Second Examiner:

\_\_\_\_\_

External Examiner:

\_\_\_\_\_

**Dedicated to my wife Mirriam and my son Kapaya**



## CONTENTS

<b>ABSTRACT .....</b>	<b>IX</b>
<b>ACKNOWLEDGMENTS .....</b>	<b>XI</b>
<b>1.0 INTRODUCTION.....</b>	<b>1</b>
1.1 LOCATION AND ACCESS OF STUDY AREAS .....	2
1.2 OBJECTIVES OF THE RESEARCH .....	4
1.3 RESEARCH METHODOLOGY .....	4
1.3.1 <i>Field work</i> .....	4
1.3.2 <i>Sampling</i> .....	5
1.3.3 <i>Laboratory analysis</i> .....	6
1.4 PREVIOUS WORK .....	6
1.5 REGIONAL SETTING .....	11
1.6 GOLD MINERALISATION IN THE MWEMBESHI DISLOCATION ZONE.....	13
1.7 TECTONICS AND TIMING OF PAN-AFRICAN MOBILE BELTS .....	14
1.7.1 <i>Lufilian arc</i> .....	14
1.7.2 <i>Zambezi belt</i> .....	17
1.7.3 <i>Damaram belt</i> .....	18
1.8 GEODYNAMIC FRAMEWORK .....	19
<b>2.0 GEOLOGY .....</b>	<b>22</b>
2.1 CHISAMBA AREA.....	22
2.1.1 <i>Quartzo-feldspathic gneisses</i> .....	26
2.1.2 <i>Muscovite and muscovite-biotite quartzo-feldspathic gneisses</i> .....	26
2.1.3 <i>Calcareous gneisses</i> .....	28
2.1.4 <i>Garnet amphibolites in gneisses</i> .....	29
2.1.5 <i>Calc-silicate rock, scapolitic marble and amphibolite</i> .....	29
2.1.6 <i>Quartzites</i> .....	30
2.1.7 <i>S-L tectonite</i> .....	32
2.1.8 <i>Mylonitic rocks</i> .....	32
2.1.9 <i>Gabbro</i> .....	34
2.2 KABWE AREA.....	35
2.2.1 <i>Mwomboshi gneiss</i> .....	36
2.2.1.1 <i>Amphibolite</i> .....	40
2.2.2 <i>Chikonkomene Formation</i> .....	40
2.2.2.1 <i>Sericitic quartzite</i> .....	41
2.2.2.2 <i>Iron-banded quartzite</i> .....	42
2.2.2.3 <i>Polymictic metaconglomerate</i> .....	43
2.2.2.4 <i>Amygdaloidal epidosite</i> .....	44
2.2.2.5 <i>Chisamba Formation</i> .....	45
2.2.3 <i>Kangomba formation</i> .....	46
2.2.4 <i>Kasavasa gabbro</i> .....	47

2.3	DEPOSITION ENVIRONMENT.....	48
2.4	STRATIGRAPHY AND CORRELATION .....	49
2.4.1	<i>Chisamba area</i> .....	49
2.4.2	<i>Kabwe area</i> .....	51
3.0	PETROGRAPHY.....	54
3.1	INTRODUCTION .....	54
3.2	CHISAMBA AREA.....	54
3.2.1	<i>Garnet-biotite-muscovite quartzo-feldspathic gneiss</i> .....	54
3.2.2	<i>Banded gneiss</i> .....	55
3.2.3	<i>Kyanite-muscovite quartzite</i> .....	56
3.2.4	<i>Scapolite-diopside rocks</i> .....	59
3.2.5	<i>Garnet amphibolites</i> .....	63
3.2.6	<i>Mylonites</i> .....	66
3.2.6.1	Quartzo-feldspathic mylonites .....	66
3.2.6.2	Quartz-mylonite .....	70
3.2.6.3	Garnet-feldspar-quartz mylonite .....	71
3.2.6.4	Tourmaline-quartz mylonite .....	74
3.3	KABWE AREA.....	76
3.3.1	<i>Mwomboshi gneiss</i> .....	76
3.3.1.1	Less sheared biotite-muscovite-quartzo-feldspathic gneiss .....	76
3.3.1.2	Sheared biotite-muscovite- quartzo feldspathic gneiss .....	76
3.3.1.3	Biotite-muscovite schist .....	80
3.3.1.4	Protomylonitic fine-grained augen gneisses .....	82
3.3.1.5	Laminated feldspathic quartzite .....	85
3.3.1.6	Muscovite quartzite .....	86
3.3.1.7	Chlorite-epidote hornblende schist .....	89
3.3.2	<i>Chikonkomene Formation</i> .....	90
3.3.2.1	Sericitic quartzite .....	90
3.3.2.2	Iron-banded quartzite .....	93
3.3.2.3	Tourmaline quartzite pebble .....	94
3.3.2.4	Brecciated carbonaceous meta-siltstone .....	96
3.4	DISCUSSION AND SUMMARY.....	99
3.4.1	<i>Chisamba area</i> .....	99
3.4.2	<i>Kabwe area</i> .....	100
4.0	STRUCTURE.....	104
4.1	INTRODUCTION .....	104
4.2	CHISAMBA AREA.....	104
4.2.1	<i>Foliations</i> .....	104
4.2.2	<i>Lineations</i> .....	105
4.2.2.1	Stretching lineations .....	108
4.2.2.2	Mineral lineations .....	110
4.2.2.3	Crenulation lineation .....	110
4.2.2.4	Intersection lineation .....	110
4.2.2.5	Grooves and ridges .....	111

4.2.2.6	Boudins .....	111
4.2.3	<i>Folds</i> .....	111
4.2.4	<i>Shear zones and kinematic indicators</i> .....	116
4.2.4.1	<i>Mesososcopic structures</i> .....	117
4.2.4.2	Microscopic structures .....	118
4.2.4.2.1	Mica-fish .....	118
4.2.4.2.2	S-C and C' fabrics .....	119
4.2.4.2.3	Oblique grain shape fabric .....	119
4.2.4.2.4	$\sigma$ -type porphyroclast .....	121
4.2.5	<i>Faults</i> .....	121
4.3	KABWE AREA .....	122
4.3.1	<i>Foliations</i> .....	123
4.3.2	<i>Lineations</i> .....	126
4.3.2.1	Stretching lineations .....	126
4.3.2.2	Striations .....	127
4.3.2.3	<i>Boudins</i> .....	128
4.3.2.4	Crenulation lineation .....	128
4.3.2.5	Intersection lineation .....	128
4.3.3	<i>Folds</i> .....	130
4.3.4	<i>Faults</i> .....	135
4.3.5	<i>Shear zones and kinematic indicators</i> .....	135
4.3.5.1	Mwomboshi gneiss Formation .....	136
4.3.5.2	Chikonkomene Formation .....	140
4.3.6	<i>Strain analysis</i> .....	142
4.3.6.1	The Mwomboshi gneiss .....	142
4.3.6.2	The Chikonkomene Formation .....	143
4.4	DISCUSSION AND SUMMARY .....	146
4.4.1	<i>Chisamba area</i> .....	146
4.4.2	<i>Kabwe area</i> .....	147
5.0	<b>METAMORPHISM</b> .....	149
5.1	INTRODUCTION .....	149
5.2	CHISAMBA AREA .....	149
5.2.1	<i>Quartzo-feldspathic gneisses</i> .....	149
5.2.2	<i>Garnet-biotite-muscovite quartzo-feldspathic gneiss</i> .....	151
5.2.3	<i>Kyanite-muscovite quartzite</i> .....	152
5.2.4	<i>Scapolite-diopside rock</i> .....	152
5.2.5	<i>Garnet amphibolites</i> .....	153
5.2.6	<i>Mylonitic rocks</i> .....	154
5.2.7	<i>Mineral chemistry</i> .....	156
5.2.7.1	Garnet .....	156
5.2.7.2	Plagioclase .....	156
5.2.7.3	Hornblende .....	157
5.2.8	<i>Geothermobarometry</i> .....	157
5.2.8.1	Geothermometry .....	157

5.2.8.2	Geobarometry.....	161
5.3	KABWE AREA.....	163
5.3.1	<i>Mwomboshi gneiss</i> .....	163
5.3.2	<i>Quartzites</i> .....	163
5.3.3	<i>Chlorite-epidote hornblende schists</i> .....	164
5.3.4	<i>Chikonkomene Formation</i> .....	164
<b>6.0</b>	<b>FLUID INCLUSION COMPOSITIONS .....</b>	<b>165</b>
6.1	INTRODUCTION .....	165
6.2	SAMPLING FOR FLUID INCLUSION STUDIES.....	166
6.3	PETROGRAPHIC DESCRIPTION OF VEIN-QUARTZ SAMPLES .....	166
6.3.1	<i>Chisamba area</i> .....	166
6.3.2	<i>Kabwe area</i> .....	167
6.4	GEOMETRY OF FLUID INCLUSION TRAILS .....	169
6.5	MICROTHERMOMETRY ABBREVIATIONS.....	169
6.6	ANALYTICAL EQUIPMENT .....	170
6.7	FLUID INCLUSIONS .....	171
6.7.1	<i>Chisamba area</i> .....	171
6.7.1.1	H <sub>2</sub> O - CO <sub>2</sub> ±halite inclusions.....	171
6.7.1.2	H <sub>2</sub> O-halite inclusions.....	171
6.7.2	<i>Kabwe area</i> .....	173
6.7.2.1	H <sub>2</sub> O-halite inclusions.....	175
6.7.2.1	Low saline H <sub>2</sub> O inclusions.....	175
6.8	FLUID EVOLUTION.....	177
6.9	P-T CONDITIONS OF TRAPPING.....	177
6.10	DISCUSSION AND SUMMARY .....	179
<b>7.0</b>	<b>DEFORMATION HISTORY .....</b>	<b>181</b>
7.1	CHISAMBA AREA.....	181
7.2	KABWE AREA.....	184
7.2.1	<i>Mwomboshi gneiss</i> .....	185
7.2.2	<i>Chikonkomene Formation</i> .....	185
7.2.3	<i>Kangomba Formation</i> .....	186
<b>8.0</b>	<b>DISCUSSION AND CONCLUSIONS .....</b>	<b>189</b>
	<b>REFERENCES .....</b>	<b>194</b>
	<b>APPENDIX .....</b>	<b>203</b>

## LIST OF FIGURES

Figure 1.1: Location and geology of study areas. A: Chisamba area. B: Kabwe area. 1: Granite gneiss and sheared derivatives. 2: Schists and quartzites. 3: Quartzites. 4: Kundelungu. 5: Meta-carbonates. 6: Dolomites. 7: Alluvium. 8: Gabbros .....	3
Figure 1.2: Structural setting of study areas, A and B, showing distribution of dislocation zones in central Zambia. ....	9
Figure 1.3: Structural map of part of the Lufilian Arc and Zambezi Belt. ....	12
Figure 1.4: Groups of gold occurrences associated with the Mwembeshi, Zambezi and Kapiri-Mposhi-Mkushi zones. ....	15
Figure 1.5: A) Transcontinental Schliesen-Mwembeshi-Chimarilo (SMC) zone. B) Linked Pan-African Damaran-Lufilian-Zambezi belts. ....	21
Figure 2.1: Geological map of the Chisamba area, study area A. ....	23
Figure 2.2: Geological map of the Kabwe area, study area B. ....	37
Figure 4.1: Structural map and cross section along Y-Y' of the Chisamba area. ....	106
Figure 4.2: Equal area, lower hemisphere projection. Plot of dip direction and dip (a) Domain 1 (b) Domain 2 (c) Domain 3, and (d) lineations. ....	107
Figure 4.3: Structural map and cross-section along X-X' of the Kabwe area. ....	124
Figure 4.4: Equal area, lower hemisphere projection. Plot of dip-direction and dip. (a) Mwomboshi Formation (b) Chikonkomene Formation and (c) Lineations. ....	125
Figure 4.5: Flinn diagram plot of strain of xenoliths in the Mwomboshi gneiss and cobbles in the Chikonkomene Formation. ....	145
Figure 5.1: A) ACF diagram for mineral assemblages in calc-silicate rock and garnet amphibolite. B) AKF diagram for garnet-quartz mylonite and kyanite-muscovite quartzite. C) AKF diagram for quartzo-feldspathic gneisses. ....	150
Figure 6.1: Geometry of fluid inclusion trails: Chisamba area. ....	168
Figure 6.2: Intragranular trail of H <sub>2</sub> O-CO <sub>2</sub> , H <sub>2</sub> O-halite and low saline fluid inclusions. ....	172
Figure 6.3: Microthermometry histograms. ....	174
Figure 6.4: A) Plot of Th against salinity (Wt% NaCl EQ) of H <sub>2</sub> O-halite inclusions from the MDZ and NDZ. B) Plot of Ts against Th of H <sub>2</sub> O-halite inclusions from the NDZ. ....	176
Figure 6.5: Cross-cutting intragranular trails and clusters of H <sub>2</sub> O-halite and low saline inclusions from the NDZ. ....	178
Figure 6.6: Plot of isochores for H <sub>2</sub> O-CO <sub>2</sub> inclusions showing P-T trapping conditions from the MDZ. ....	180
Figure 8.1: Tectonic model showing dextral MDZ separating the Lufilian and Zambezi Belts. ....	193
Figure 8.2: Structural setting of the MDZ and associated second and third order structures. Insert showing orientation and sense of shear of second and third order structures consistent with a Riedel shear pattern. ....	193

## LIST OF TABLES

Table 2.1: Stratigraphic succession of the Chisamba area.....	25
Table 2.2: Straigraphic succession of the Kabwe area.....	38
Table 2.3: Stratigraphic correlation of lithologies in areas north and south of the MDZ. .	53
Table 4.1: Measurements of principal strain axes and strain parameters of (a) xenoliths and (b) pebbles and cobbles, X, Y, and Z cm.....	144
Table 5.1: Microprobe analyses of garnet.....	158
Table 5.2: Microprobe analyses of plagioclase.....	159
Table 5.3: Microprobe analyses of hornblende.....	160
Table 5.4: Garnet-amphibole geothermometer.....	162
Table 5.5: Garnet-amphibole-plagioclase quartz geobarometer.....	162
Table 7.1(a): Summary of the deformation history in the Chisamba area.....	183
Table 7.1(b): Summary of the deformation history in the Kabwe area.....	187

## LIST OF PLATES

Plate 3.1: Photomicrograph of garnet-muscovite-boitite gneiss showing poikiloblastic garnet with fine-grained inclusions. Sample KK56, x25, CPL. CH316308.....	57
Plate 3.2: Photomicrograph of banded biotite gneiss showing quartz ribbons and lozenge- shaped microcline porphyroclasts. Sample KK40, x25, CPL. CH319307.....	57
Plate 3.3: Photomicrograph of kyanite-muscovite quartzite, showing aligned kyanite blades partly retrograded to muscovite along the margins. Sample KK71, x100, CPL. CH174316.....	60
Plate 3.4: Photomicrograph of muscovite-biotite quartzite, showing inclusions of crystallographically aligned needles of rutile and biotite in quartz grains. Sample KK37, x200, CPL. CH316308.....	60
Plate 3.5: Photomicrograph of diopside scapolite calc-silicate rock, showing dynamically recrystallised scapolite along discrete shear zones. Sample KK11, x200, CPL. CH260349 .....	62
Plate 3.6: Photomicrograph of garnet-amphibolite showing a decompression assemblage indicated by a core of garnet surrounded by plagioclase II, and hornblende II. Sample KK08, x25, CPL. CH219346.....	62
Plate 3.7: Photomicrograph of quartzo-feldspathic protomylonite showing plagioclase porphyroclasts set in a fine-grained felsic matrix indicating marginal granulation. Sample KK18, x100, CPL. CH220358.....	69
Plate 3.8: Photomicrograph of quartzo-feldspathic protomylonite showing oblique shape fabric in the quartz ribbon indicating dextral sense of shear. Sample KK100, x25, CPL. CH106351.....	69
Plate 3.9: Photomicrograph of quartzo-feldspathic protomylonite showing chlorite (pale green) with needle-shaped rutile along its margins. Sample KK29, x200, PPL. CH216356.....	73

Plate 3.10: Photomicrograph of garnet-quartz mylonite showing dynamically recrystallised quartz ribbons and mica-fish. The mica-fish indicates ENE over WSW dextral sense of shear movement. Sample KK07, x25, CPL. CH220348.....	73
Plate 3.11: Photomicrograph of garnet-quartz-feldspar mylonite, showing dynamically recrystallised quartz. Mica-fish indicates SW over NE oblique thrust transport. Sample KK14, x25, CPL. CH217337. ....	75
Plate 3.12: Photomicrograph of tourmaline quartz-mylonite, showing dynamically recrystallised flattened quartz grains. Sample KK41, x25, CPL. CH301345. ....	75
Plate 3.13: Photomicrograph of sheared quartzo-feldspathic biotite gneiss at Nankuko quarry, showing S-C fabrics. Chlorite has grown along C-planes. Sample CK76, x100, CPL. KB442622. ....	78
Plate 3.14: Photomicrograph of protomylonitic augen gneiss showing quartz ribbons flowing around plagioclase. Sample CK58, x25, CPL. KB541695. ....	78
Plate 3.15: Photomicrograph of sheared biotite muscovite gneiss showing perthitic feldspar with inclusions of quartz biotite and exsolved twinned plagioclase. Sample CK17, x25, CPL. KB536726.....	84
Plate 3.16: Photomicrograph of sheared biotite-muscovite gneiss showing discrete narrow shear zones separated by an unsheared portion. Sample CK17, x25, CPL. KB536726. ....	84
Plate 3.17: Photomicrograph of protomylonitic augen gneiss showing myrmekitic intergrowths between plagioclase and microcline on grain faces parallel to the foliation. Sample CK66, x100, CPL. KB552677. ....	88
Plate 3.18: Photomicrograph of muscovite quartzite showing serrated grain boundaries and fine oriented muscovite inclusions in quartz. Sample CK90, x25, CPL. KB383496.....	88
Plate 3.19: Photomicrograph of hornblende schist showing S-C fabrics indicating sinistral sense of shear. Sample CK65, x25, PPL. KB552679.....	91
Plate 3.20: Photomicrograph of muscovite quartzite showing crenulated S <sub>1</sub> and crenulation cleavage S <sub>2</sub> , and recrystallised clasts of quartz aggregates. Sample CK40, x25, CPL. KB562777.....	91
Plate 3.21: Photomicrograph of phyllitic quartzite showing three overprinting S <sub>1</sub> , S <sub>2</sub> , and S <sub>3</sub> , and concentration of opaque minerals along S <sub>2</sub> . Sample CK30, x25, CPL. KB532777.....	95
Plate 3.22: Photomicrograph of kyanite pod showing randomly oriented kyanite blades, purple fluorite and quartzitic groundmass. Sample CK77, x25, CPL. KB454773.....	95
Plate 3.23: Photomicrograph of banded carbonaceous meta-siltstone showing F <sub>2</sub> gently folded bands. Sample CK01, x25, CPL. KB548738. ....	98
Plate 3.24: Photomicrograph of banded phyllite showing three overprinting cleavages defined by S <sub>1</sub> in the microlithons, S <sub>2</sub> crenulation domains and S <sub>3</sub> crenulation of S <sub>2</sub> . Sample CK86, x25, PPL. KB502858.....	98
Plate 4.1: Horizontal stretching lineation in quartzo-feldspathic protomylonite. Pencil parallel to lineation. CH106351. ....	109
Plate 4.2: Stretching lineation defined by quartz and quartzo-feldspathic aggregates indicating SW over NE oblique thrust transport. CH308308.....	109

Plate 4.3: Tourmaline filled grooves plunging SW on a probable fault plane quartz. CH301345. ....	112
Plate 4.4: S-L quartzitic tectonite. Lineation plunges to the SW. CH153316.....	112
Plate 4.5: Isoclinal intrafolial minor fold in muscovite quartzo-feldspathic gneiss. CH3232384.....	113
Plate 4.6: Loose block of biotite-quartzo - feldspathic gneiss showing tight folding. CH141275. ....	113
Plate 4.7: Folded diopside scapolite calc-silicate with dark iron-oxide bands outlining folds. CH219343. ....	115
Plate 4.8: isoclinal to tight intrafolial folds in banded scapolite marble. CH219342.....	115
Plate 4.10: Deflection of foliation into narrow shear zones (SZ) indicating dextral sense of shear in quartzo-feldspathic protomylonite.....	120
Plate 4.9: Sub-horizontal stretching lineation in calcareous quartzo-feldspathic gneiss. CH229358. ....	120
Plate 4.11: Sub-horizontal stretching lineation defined by quartz aggregates in quartzo- feldspathic gneiss. Lineation plunges to the west. KB537737.....	122
Plate 4.12: Stretched dark xenoliths and cross-cutting feldspathic veins in sheared quartzo- feldspathic gneiss. KB536726.....	129
Plate 4.13: Pseudo-conglomerate formed by boudinage of quartz veins in muscovite quartzite. KB563771 .....	129
Plate 4.14: Folding in sheared quartzo-feldspathic gneiss outlined by feldspathic veins. KB536726.....	132
Plate 4.15: Isoclinally folded quartz veins in muscovite quartzite. KB543764. ....	132
Plate 4.16: Highly stretched and folded cobbles in polymictic meta-conglomerate. KB543778.....	134
Plate 4.17: S-type folds outlined by quartz veins in conglomeratic muscovite quartzite. Vertical height is 6 m. Desi dam bridge. KB5333774.....	134
Plate 4.18: Rolled quartz vein in muscovite quartzite indicating south-over-north thrust transport. KB55779.....	137
Plate 4.19: Intricately folded quartz veins in a carbonaceous meta-siltstone at a major fault contact. KB547738. ....	137
Plate 4.20: Narrow shear zone (SZ) transecting relatively coarse-grained quartzo- feldspathic biotite gneiss at Nakunko quarry. Deflection of foliation into shear zone, indicates sinistral sense of shear. KB442622. ....	138
Plate 4.21: Phyllitic quartzite marking shear zone. Displacement of quartz veins on opposite sides of zone indicates dextral sense of shear. KB532777. ....	138
Plate 4.22: Rotated cobble in sericitic quartzite indicating sinistral sense of shear. KB543764.....	141
Plate 4.23: Brittle ductile shear zone indicating dextral sense of shear along a major fault contact. KB547738. ....	141



## **Abstract**

In the Chisamba area, some lithologies hitherto mapped as quartzites and dolomitic marbles are quartz mylonites and interbanded calc-silicate, marble and amphibolites, respectively.

Both meso- and microstructural fabrics in the Chisamba area indicate that deformation associated with shearing was predominantly crystal-plastic under low temperature conditions consistent with greenschist facies metamorphism, while deformation in the Kabwe area was predominantly cataclastic.

Mesoscopic and microscopic shear sense indicators are used for the first time to deduce sense of shear in the Mwembeshi Dislocation Zone (MDZ). Micro-textures such as asymmetric porphyroclasts, oblique grain shape-fabrics, S-C fabrics and mica-fish consistently indicate dextral strike-slip shear in the Chisamba area, whilst a sinistral shear sense is predominant in the Kabwe area. The plunging stretching lineation in the Chisamba area indicates similar oblique northeast thrust transport as that of the Lufilian Arc to the north.

Amphibolite facies assemblages were downgraded to greenschist facies assemblages during shearing in the Chisamba and Kabwe areas. Quartz and, in some instances feldspar, in both areas displays annealing textures, which are attributed to a major thermal episode associated with syntectonic magmatism, related to the MDZ. Breakdown of garnet to

plagioclase and hornblende in amphibolites in the Chisamba area, indicating decompression, is considered to be related to exhumation during Lufilian thrusting. The garnet-amphibole geothermometer indicates temperatures between 400°C and 600°C for the decompression reaction involving garnet.

The lithologies of the Chisamba Formation in the Kabwe area and Chunga Formation in the Chisamba area are continuous across the MDZ and are therefore considered to be one and the same Formation. The Lusaka dolomite is not juxtaposed against basement rocks along the MDZ but instead oversteps them. Amphibolite to eclogite facies metamorphic grades attained in both the Lufilian and Zambezi mobile Belts on either side of the MDZ suggest that, there is no metamorphic break across the zone.

Fluid inclusions in quartz veins from the Chisamba area consists of H<sub>2</sub>O-CO<sub>2</sub> +Halite, H<sub>2</sub>O-Halite, and low saline inclusions, whilst those from the Kabwe area comprise H<sub>2</sub>O-Halite, and low saline complex inclusions. P-T trapping conditions in the Chisamba area range from 200°C-350°C temperature; at pressure between 2 and 3 Kbars, consistent with greenschist facies grades. Fluid inclusions in the Kabwe area were trapped at relatively higher temperatures, ranging from 350°C-400°C.

## Acknowledgments

The research, which forms the basis for this thesis, was financially supported by a 2 year Staff Development Fellowship of the University of Zambia held by the author.

Dr F. Tembo, my supervisor, is thanked for the tireless guidance and support he rendered through out the research work and the write up of this thesis. I am also indebted to him for electron microprobe analyses and arranging for my stay at the University of Zimbabwe for fluid inclusion studies. Mr. W. Nundwe of the University of Zambia is thanked for his invaluable logistical assistance and companionship during fieldwork. Management of Dar-Farms and teachers Lukoshi Primary School are thanked for their hospitality and permission to set up camps on their premises in the Chisamba and Kabwe areas, respectively. The United Nations University Institute for Natural Resources in Africa-Mineral Resources Unit (UNU/INRA-MRU) is thanked for the use of computer facilities from inception of the research project to the write up of this thesis. Thanks are also due to Mr. A. K. Lloyd, Head of Mineralogy, Z.C.C.M, for accepting to have my thin sections prepared at his department and for use of microscope accessories. I would like to extend my sincere gratitude to Mr. J. Musonda, of Z.C.C.M, for preparing most of my thin sections. Mr. R. Jombolo, of the University of Zambia is also thanked for preparing some of my thin sections. I would like to express my sincere gratitude to Dr. H. Munyanyiwa, Chairman, Geology Department, University of Zimbabwe, for use of the fluid inclusion facility. Prof. T. Blenkisorp and Dr. P. Dirks are thanked for affording me an audience to discuss pertinent aspects of my research. Special thanks go to Dr. Hiellke Jelsma for

supervising and introducing me to fluid inclusion analyses. Finally, I am deeply and sincerely grateful to my wife Mirriam Siachuculi and my son Kapaya Katongo for their patience and endurance during my long absence from home in the course of my research.

## Chapter 1

### 1.0 INTRODUCTION

The late Proterozoic Mwembeshi Dislocation Zone (MDZ), is a prominent ENE trending lineament across central Zambia, which is of economic importance due to its spatial association with gold mineralisation throughout its 1000 km extent, but its tectonic and structural significance are uncertain. Despite its important geotectonic and economic setting, the MDZ has not been studied in detail to establish its structural and kinematic evolution. It was first mapped in the 1960's on a reconnaissance basis by the Geological Survey of Zambia. From a geotectonic point of view, the MDZ has been interpreted to be the trace of a suture representing the boundary between the Congo and Kalahari cratons.

Very few detailed studies have been done on the MDZ and this is evident from the lack of publications that address specific aspects. The most recent and more focused studies of the MDZ are by Hanson et al., (1993) and Kasolo (1992), on the age of shear movement along the MDZ and on fluid channeling in relation to gold mineralisation, respectively. This research project arose from the need to understand the structure and kinematics of the MDZ in more detail than is the present situation and is the first of its kind.

Over the past years, the geotectonic development and sense of shear of the MDZ have been a matter of conjecture and several genetic models have been proposed. This study presents new data on the structural and kinematic development of the MDZ in the

Chisamba area. The study of the Kabwe area is used as check to compare deformation and metamorphic processes with those of the Chisamba area.

### **1.1 Location and access of study areas**

The Chisamba and Kabwe areas were selected for the study; one located within and the other outside the MDZ, Chisamba (study area A) and Kabwe (study area B) areas, respectively (Fig. 1.1).

The Chisamba area is the principal study area and covers the entire width of the MDZ, as it is known today. The Chisamba area is located 30 Km north of Lusaka in the Chisamba West Farming Block. It is bounded by latitudes  $14^{\circ} 25' S$  and  $15^{\circ} 25' S$  and longitudes  $28^{\circ} 00' E$  and  $28^{\circ} 12' E$ . The Great North Road (GNR) forms the eastern boundary of the area. There are several gravel roads that join the GNR, but the best road branches off due west at Twin Palms Motel. The MDZ is well defined in the Chisamba area and it is in the location, which marks the boundary between the Lufilian Arc and the Zambezi belt.

The Kabwe area is located north of the MDZ. It has been included in the study in order to compare the structural and metamorphic differences with the principal study area. The Kabwe area is bounded by latitudes  $14^{\circ} 39' S$  and  $14^{\circ} 48' S$  and longitudes  $28^{\circ} 24' E$  and  $28^{\circ} 29' E$ . Access to the area is by gravel road which branches off the GNR at the Kasavasa junction 14 Km south of Kabwe.

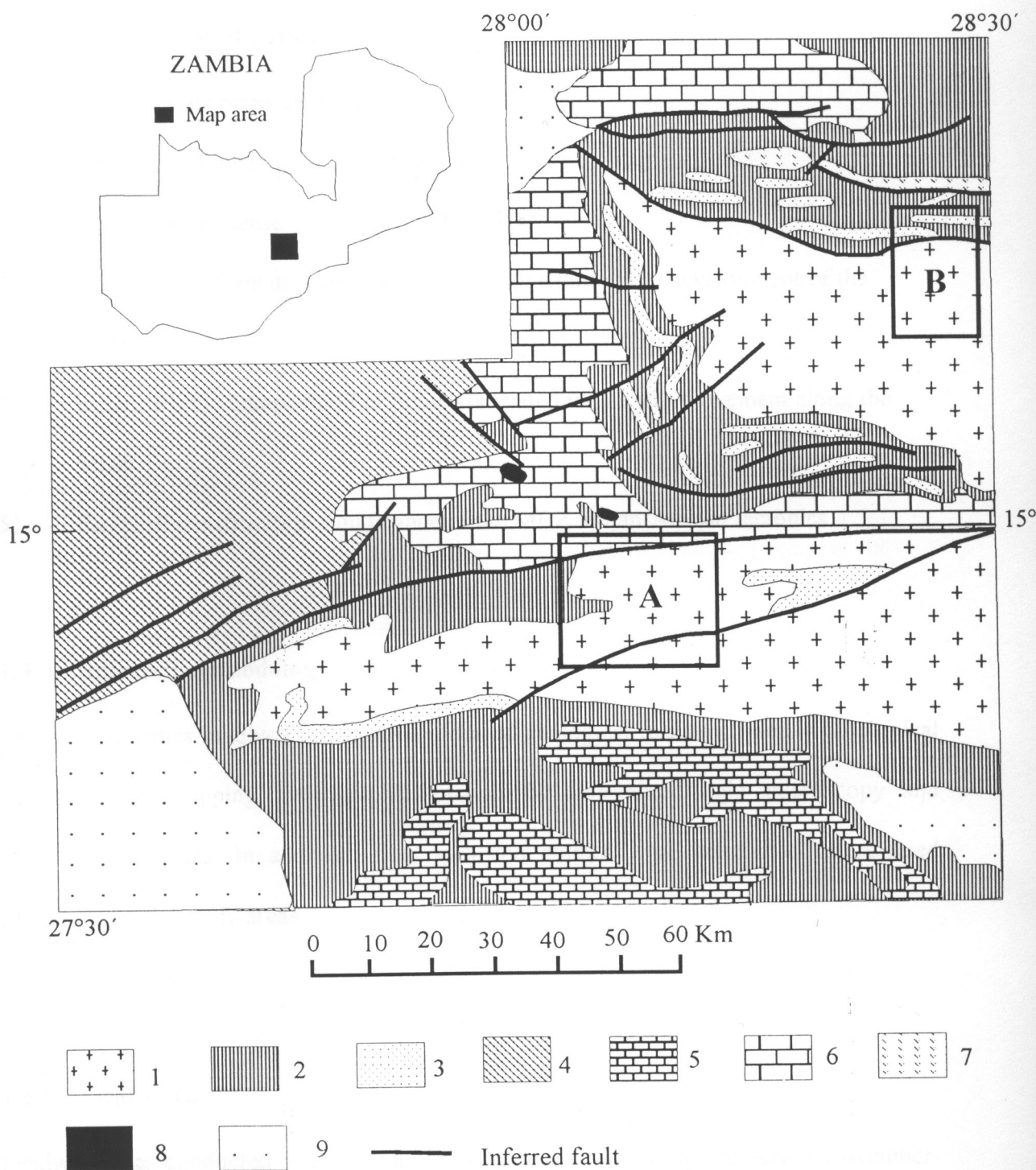


Fig. 1.1: Location and geology of study areas. A: Chisamba area. B: Kabwe area. 1: Granite gneiss and sheared derivatives. 2: Schists and quartzites. 3: Quartzites. 4: Kundelungu. 5: Meta-carbonates. 6: Dolomite. 7: Metavolcanic rocks. 8: Gabbro. 9: Alluvium (after Thieme and Johnson, 1981)

## **1.2 Objectives of the research**

The objectives of the research were to:

- 1) Characterize the structure of the MDZ
- 2) Determine the sense of shear along the MDZ
- 3) Determine deformation mechanisms operative during the development of the MDZ
- 4) Determine the composition of fluids associated with shear movement along the MDZ
- 5) Establish the structural significance of the MDZ in Pan-African tectonics.

## **1.3 Research methodology**

Research activities involved principal methods of geological research, namely lithological and structural mapping, petrographic analysis by transmitted light microscopy and microprobe analysis. In addition, fluid inclusion studies were conducted on selected samples from the study areas.

### **1.3.1 Field work**

Fieldwork was conducted over a total number of 80 days, during the period November-December, 1996 in the Kabwe area, and September-October, 1997 in the Chisamba area.

Satellite imagery and aerial photographs were studied before and during fieldwork. The satellite images available are MSS black and white prints at a scale of 1:100,000. The



ENE-WSW trending lineament of the MDZ stands out prominently on the satellite images. Aerial-photographs at scales of 1:30,000 and 1:20,000 of selected sections of the study area were also studied. Ridges and fault trends are very distinct and are easily traced over long distances.

Fieldwork involved detailed structural mapping of sections of the study areas at scales of 1:25,000 and 1:50,000 in the Kabwe and Chisamba areas respectively. The Chisamba area was mapped at relatively small scale due to the paucity of outcrops. The area is located in the Chisamba Farming block dominated by game and cattle ranching, as such vegetation is not burnt. The scarcity of outcrops of certain lithologies is compounded by large patches of wetland with thick vegetation and soil cover. Exposure in the Kabwe area is relatively better particularly in the Chikonkomene range of Hills. The larger scale of mapping was necessitated by the rapid variation in lithologies in the metasedimentary sequence.

### **1.3.2 Sampling**

Representative oriented samples from each lithology were collected for petrographic analysis, microprobe analysis, and fluid inclusion studies. Sixty samples were collected from the Chisamba area and fifty from the Kabwe area, out of which fifty thin sections were prepared at the ZCCM, Technical Services Mineralogy Department laboratories, Kalulushi.

Six oriented vein-quartz samples were collected for fluid inclusion studies. However, following petrographic analysis, only two samples, one from each area, were found suitable for analysis.

Sample numbers referred to in descriptions refer to thin sections in which a particular feature was observed. KK and CK sample number prefixes denote samples collected from the Chisamba and Kabwe areas, respectively. Similarly CH and KB grid reference prefixes refer to localities in the Chisamba and Kabwe areas.

### **1.3.3 Laboratory analysis**

Petrographic analyses were conducted at the University of Zambia, Geology Department, whilst fluid inclusions were analysed at the University of Zimbabwe, Geology Department, during the period January-February, 1998. Dr F. Tembo of the University of Zambia carried out Microprobe analyses on one sample at Goettingen University, Germany, 1998.

## **1.4 Previous work**

There are several ENE trending dislocation zones that transect central Zambia (Fig. 1.2). Among these, the MDZ is the most prominent due to its structural significance and association with base and precious metal mineralisation (De Swardt et al., 1964; Mbumba, 1990; Kasolo, 1992)

The MDZ was first described in the Mwembeshi River area, after which it was named (Simpson, 1962). The MDZ was later mapped in other areas along its strike length by the Geological Survey Department (GSD) and recognised as a regional lineament of considerable transcurrent WSW over ENE sinistral displacement (De Swardt et al., 1964).

In the Mwembeshi River area, Simpson (1962) described the MDZ as a zone of prominent faults with ENE-NE trends. The ENE faults extend in the Lusaka area and mainly affected basement rocks and were mapped as dextral strike slip faults (Simpson et al., 1963). De Swardt et al. (1964) however, attribute the dextral sense of shear to lagging of some crustal slices during a dominantly sinistral movement. The sinistral movement is based on the deflection of NW foliation trends in the ENE trend of the MDZ.

Further east in the Chainama Hills area, the MDZ produced extensive shearing and granulation coupled with a near-vertical crenulation cleavage and greenschist facies metamorphic grades (Garrard, 1968).

In the Luano valley the Karoo faults parallel to the MDZ trend. This signifies that rifting in the Luano valley made use of the weak zones established by the MDZ. In the basement complex of the Luano valley region, Reichwalder (1978) found no evidence for sinistral movement but reported NE directed thrusting.

In the Sasare area, movement along the Chinkombe zone, which is considered to be part of the MDZ (De Swardt et al., 1964) transposed and sheared out bedding into a new

foliation (Barr and Drysdall, 1972). Although Barr and Drysdall (1972) did not find evidence for displacement along the zone, Johns et al. (1989) demonstrated that the Chinkombe-Ilinda zone formed as a result of a transpressive ENE over WSW dextral strike slip motion. Shearing in the Chikombe zone occurred under amphibolite facies conditions coupled with an increase in grain size of the lithologies, in contrast to retrograde greenschist facies metamorphism which is accompanied by grain size reduction reported in other parts of the MDZ.

Southwest of Mumbwa, Abell (1970) deduced sinistral displacement on the basis of deflection of NW primary Lufilian trends into the ENE zone. He also noted that the Hook Granite Massif (HGM) was little affected by the main MDZ, but sheared and granulated along secondary splay faults. De Swardt et al. (1964) considered the HGM to have acted as a buttress during the development of the MDZ. A U-Pb Zircon age of  $551 \pm 19$  Ma (Hanson et al., 1993) obtained from syntectonic rhyolite from an MDZ fault in the HGM indicates that the massif intruded during or soon after the development of the MDZ. This explains why the HGM appears to be little affected by the MDZ.

South of the Mumbwa district in the Lui Hills area (Degree Sheet 1527 NW Quarter) displacement of the northern ENE trending ovoid body of the Matala Dome relative to the southern body, along an MDZ fault is WSW over ENE sinistral. On this basis Phillips (1958) considered the MDZ to possess the same sense of shear.

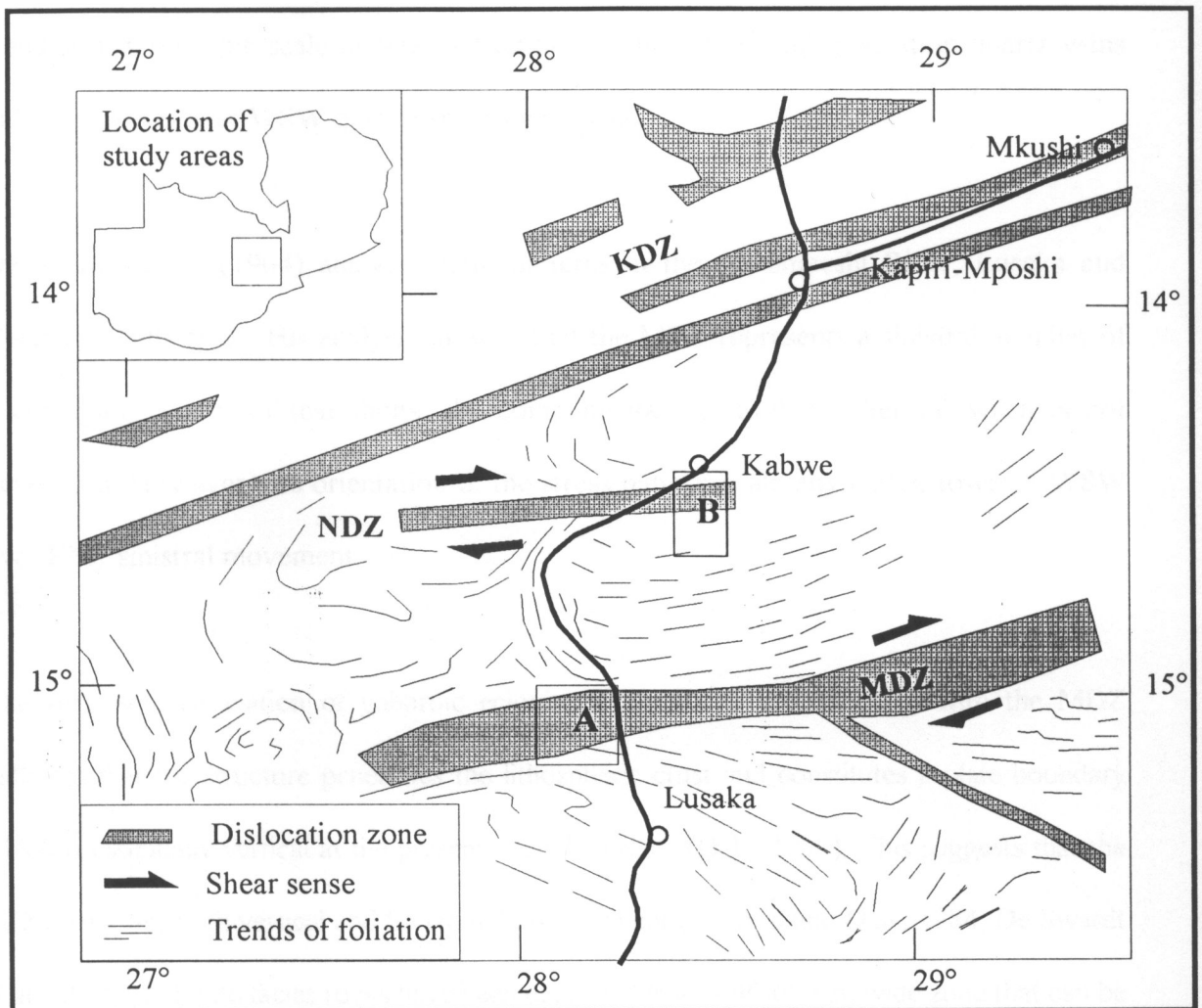


Fig.1.2 : Structural setting of study areas, A and B, showing distribution of dislocation zones in central Zambia. MDZ: Mwembeshi Dislocation Zone; NDZ: Nyama Dislocation Zone; KDZ: Kapi-Mposhi Dislocation Zone (after de Swardt et al., 1964)

However, in the vicinity around Mumbwa, Minex Department (Sliwa, 1981) mapped NW trending macroscopic scale mineralised tension gashes of second generation quartz veins indicating ENE over WSW dextral shear movement.

De Swardt et al. (1964) analysed fault patterns in the Mwembeshi River, Lusaka and Chainama Hills areas. His analysis showed that the MDZ represents a sinistral member of a conjugate system of tear faults, the complimentary dextral member of which is not developed. However, the orientation of the stress pattern is already biased towards WSW over ENE sinistral movement.

The supposed association of gabbroic eclogite (Prasad and Vrana, 1972) with the MDZ indicates that the structure penetrates the lithospheric crust and constitutes a plate boundary which is essentially vertical at the present erosion surface (Daly, 1986). This suggests that the MDZ comprise both vertical and horizontal displacement (Coward and Daly, 1984; De Swardt et al., 1965). Eclogite facies rocks have been described from a 40-60 Km wide zone that can be traced along the Lufilian Arc (Cosi et al., 1992) across the MDZ and along the Zambezi belt west and south of Lusaka (Vrana et al., 1975) up to the northern edge of the Zambezi belt (Fig.1.3) suggesting that the MDZ may no be laterally associated with these rocks. The formation of eclogites thus appears to have preceded the development of the MDZ. In the Damara belt, the southeastern extension of the MDZ in Namibia is known as the Schliesen zone. In the Schliesen zone, basic and ultrabasic rocks with ophiolite affinities indicate the presence of an old plate boundary (Coward and Daly, 1984). Although similar rock assemblages have not been reported in the MDZ, Coward and Daly (1984) suggested that it

could well represent the same plate boundary and explained the high pressure metamorphic assemblages, in the Zambezi belt, to have resulted from oblique collision along a Pan-African transform-type plate boundary. Metamorphism south of the MDZ, in the Zambezi belt, is stratigraphically controlled (Munyanyiwa, 1985). Petrographic studies of small eclogite bodies around Lusaka and Chombwa area 37 Km south of Mumbwa showed that they were formed as a result of metamorphism of gabbros (Prasad and Vrana, 1972). However, the association of some of the eclogites with ultramafic rocks suggests that some of the eclogites were sourced from deep crustal levels by exhumation during the extension phase of the Zambezi orogeny.

It is evident from the above review that the structure of the MDZ has not been studied in great detail. Since the publication of De Swardt et al. (1964), sinistral shear movement has been entrenched in literature and the same has been used in geodynamic models for Pan-African tectonics. It is also clear that no attempt has been made to deduce the sense of shear movement on the MDZ from reliable kinematic and shear sense indicators.

## **1.5 Regional setting**

The MDZ is structurally located at the boundary between two Pan-African mobile belts; the Lufilian Arc to the north and the Zambezi Belt to the south. The two mobile belts display different geotectonic histories, opposite tectonic transport and different ages of tectonism (Unrug, 1983; Coward and Daly, 1984 (Fig.1.3); Ring, 1993). The MDZ forms part of a transcontinental crustal scale lineament stretching from the Atlantic to the Indian Ocean. In the west and east it is considered to be continuous with the Schliesen zone of

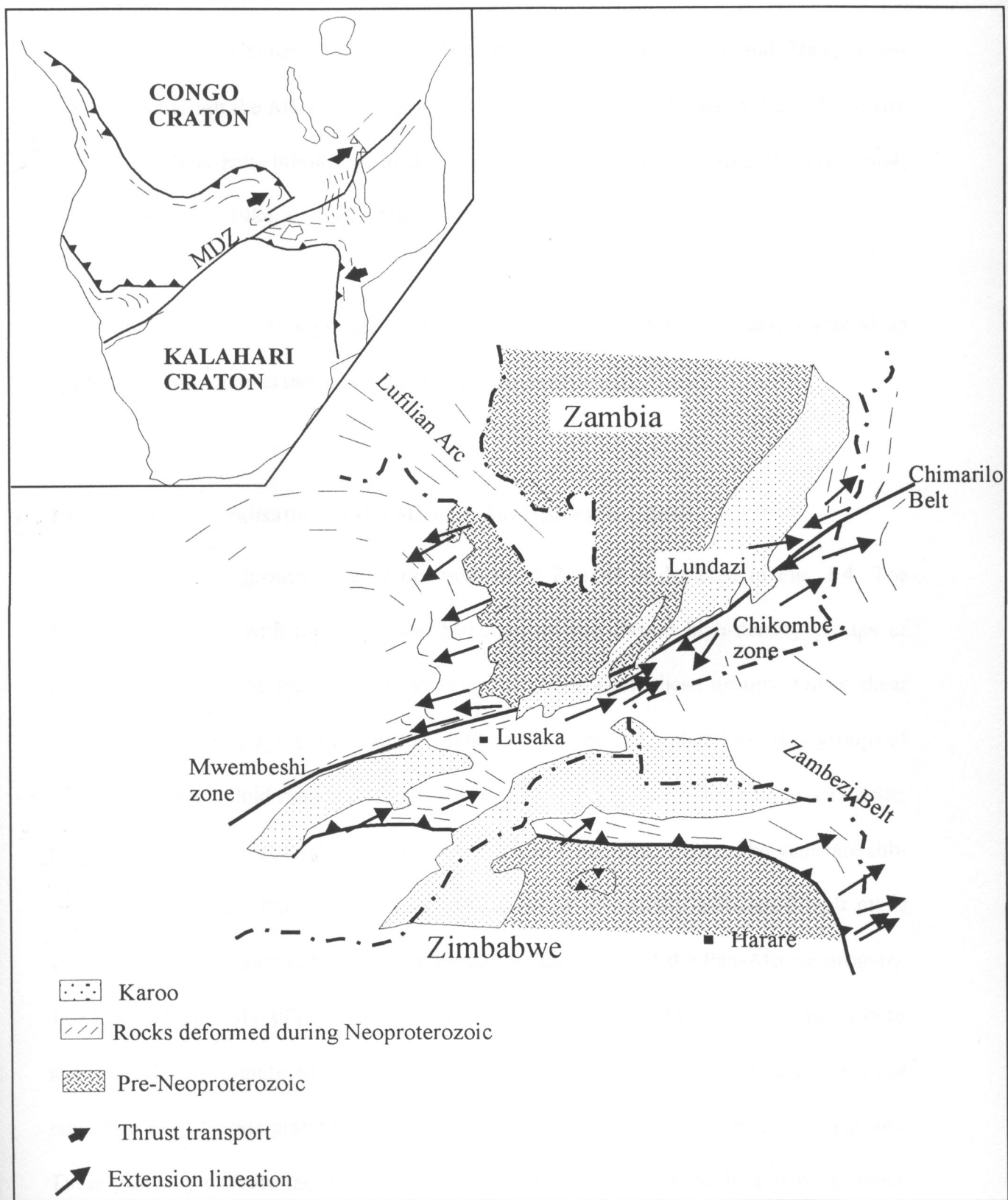


Fig.1.3: Structural map of part of the Lufilian Arc and Zambezi belt (after Coward and Daly, 1986)



Namibia and the Chimarilo zone of Malawi, respectively (Coward and Daly, 1984. Fig.1.5). Although the MDZ forms an apparent structural break between the Lufilian Arc and the Zambezi belt, lithologies in the two belts have been correlated (Moore, 1964; Coward and Daly, 1984, Liyungu, 1986. Table 2.3)

De Swardt et al. (1964) suggested that movement along the MDZ probably followed an ancient zone of weakness that was determined by Irumide trends.

## **1.6 Gold mineralisation in the Mwembeshi Dislocation Zone**

The distribution of groups of gold occurrences in Zambia is depicted in Fig. 1.4. The MDZ is associated with the Mumbwa, Mwomboshi and Sasare high-density groups of gold occurrences. The main gold producers have been from these groups. Other shear zones of Proterozoic age, parallel to the MDZ, are also spatially related to other groups of gold occurrences. Gold mineralisation is found in quartz veins with bismuth, arsenopyrite, pyrite, anomalous base metals and carbonates of iron (Mbumba, 1990). The veins are sub-parallel to the major fault zones. Gold mineralisation is spatially associated with mafic volcanic rocks and granitoids emplaced during the late stages of the Pan-African orogeny. The Hook Granite Massif (HGM) is spatially related to the Mumbwa and Lubungu groups and Chapalapata granite to the Sasare group. A few of the gold occurrences are not related to any obvious granitoids but to domes of minor felsic to intermediate intrusions. These probably indicate the presence of major granitoid bodies at shallow depths, which raised the temperature to remobilise fluids from which gold was deposited. The

association of gold mineralisation with mafic meta-volcanics is less obvious than granitoids. The major areas of mafic meta-volcanic rocks are the Kafue, Rufunsa and Sasare of the Mesoproterozoic Mpanshya group. The Kafue meta-volcanic rocks occur near the Mpande dome, which is surrounded by numerous gold occurrences. The Rufunsa and Sasare meta-volcanics occur near the Rufunsa and Sasare gold occurrences, respectively. However, gold occurrences of the Matala group are not associated with any meta-volcanics. The Sasare group is located at an extensional fault jog, at which the MDZ swings from an ENE trend to a NE trend. The presence of conglomerates, mafic meta-volcanic rocks and felsic intrusions suggests a pull-apart basin or dilation zones (Mbumba, 1990). The pull-apart basins or dilation zones are second and third order structures associated with the MDZ (Kasolo, 1992).

## **1.7 Tectonics and timing of Pan-African mobile belts**

Three Pan-African (600-500 Ma) orogenic belts transect south-central Africa; the Lufilian, Zambezi and the Damaran belts (Fig. 1.5). The Lufilian and Zambezi belts are separated by the ENE trending MDZ and considered to be linked to the Damaran belt (De Swardt et al., 1965; Unrug, 1983; Coward and Daly, 1984).

### **1.7.1 Lufilian arc**

The Lufilian Arc is a large arcuate, northwest convex-shaped geological structure covering eastern Angola, southern Zaire and north-western Zambia, which is well known

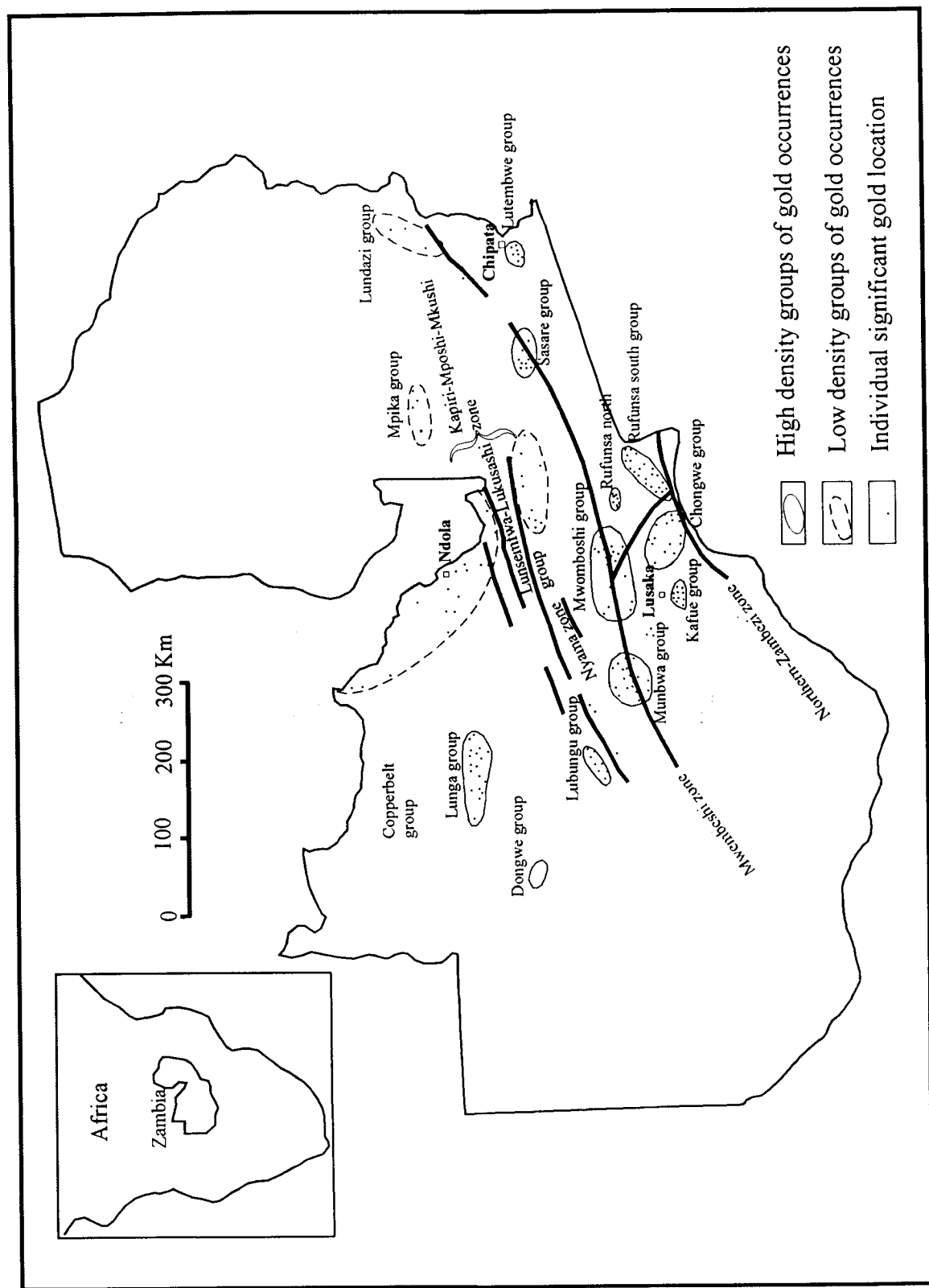


Fig.1.4 :Groups of gold occurrences associated with the Mwembeshi, Zambezi and Kapiri-Mposhi-Mkushi zones

for its vast Copper-Cobalt deposits hosted in the metasediments of the Katanga Supergroup (Unrug, 1983). The southern boundary of the Lufilian Arc is considered to be the MDZ (Coward and Daly, 1984; Hanson et al., 1993). Daly (1986) distinguished two kinematic phases in the Lufilian Arc. An early ( $K_1$ ) ENE directed phase involving thrusting of the basement and cover sequences coupled with folding and development of bedding parallel shears. The northerly directed second phase ( $K_2$ ) affected the Domes region and is considered to be responsible for the emplacement of the Kolwezi klippe and several smaller thrust sheets north of the of the Lufilian Arc.

In the Domes region, Cosi et al., (1992) distinguished an early NW and a later northerly directed thrusting phase and suggested that the former occurred before the onset of the main Lufilian deformation. On this basis, Tembo (1994) equated the thrusting event in the Domes region and Copperbelt to the 820 Ma Zambezi deformation of Hanson et al., (1988).

The timing of peak deformation in the Lufilian is poorly constrained (Tembo, 1994). Ages ranging from 692 to 456 Ma, obtained from dating of mainly U-bearing hydrothermal veins are reported by Cahen et al., (1984). In the Domes region Cosi et al., (1992) estimated the main Lufilian deformation to have occurred about 750 Ma based on Rb-Sr mineral and whole rock dating and obtained K-Ar mineral ages of 525 Ma. The latter dates indicate late Lufilian deformation. U-Pb zircon ages ranging from 570-560 Ma (Hanson et al., 1993) from the Hook Granite Massif (HGM), which marks the southern extremity of the Lufilian Arc suggests that orogenesis in this part of the of the belt

occurred later than the north (Tembo, 1994). This also implies that the  $551 \pm 19$  Ma of Hanson et al. (1993) for shearing in the MDZ is syntectonic with the late phase of Lufilian orogenesis.

### **1.7.2 Zambezi belt**

In the Zambezi belt, structures dip SW-SSW with NW-SE strike. The Zambezi belt has recorded amphibolite grade of metamorphism coupled with occurrences of eclogitic gabbro bodies (Vrana et al., 1975; Barr and Drysdall, 1972; Munyanyiwa, 1985). The Eclogitic gabbros in the Zambia belt indicate high pressures an episode of Zambezi belt orogenesis. Ramsay and Ridway (1977) reported widespread occurrences of kyanite in the Lufilian Arc indicating moderate to high-pressures of deformation. Talc-kyanite bearing rocks and eclogitic meta-gabbros in the Domes region also indicate high-pressures attained in the Lufilian Arc. Coward and Daly (1986) suggested that deformation in the Lufilian Arc and Zambezi belt occurred under similar metamorphic conditions and involved deep crustal metamorphic rocks with high pressure mineral assemblages (Barr, 1974) and patches of eclogites (Vrana et al, 1975). However, it must first be proved that deformation in the amphibolite facies Zambezi belt occurred at greenschist facies as in the Lufilian Arc and then isothermally derived rocks produced the amphibolite facies rocks observed now. Daly (1988) recognised two kinematic phases in the east-west part of the Zambezi belt; an early ( $K_1$ ) WSW directed thrusting, from extension and thrusting geometries and a later ( $K_2$ ) southerly directed thrusting phase. In the same area, however, Wilson et al. (1993) found no evidence for the second kinematic phase. In contrast to thin

skinned deformation in the Lufilian Arc, deformation in the Zambezi belt involved interslicing of basement and Katangan metasediments (Unrug, 1983).

On the basis of parallelism of deformation fabrics within the, Lufilian Arc, MDZ and Zambezi belt, Daly (1988) concluded that, the three structures are coeval and kinematically related and considered the MDZ to have acted as a major transform for the opposed belts. Coward and Daly (1984) suggested that this transform represents the boundary between the Congo and the Kalahari plates. This is further supported by recent dates ranging from 500-550 Ma (Dirks et al., 1998) from northeast Zimbabwe suggesting that Zambezi belt experienced its peak metamorphic event during the same Late Proterozoic to early Paleozoic, similar to the Mozambique belt and Lufilian Arc (Dirks et al., 1998).

### **1.7.3 Damaran belt**

According to Coward and Daly (1984), the Damara belt of Namibia is part of the north-south trending Pan-African orogenic system of the west coast of Africa which comprises a north-south arm and an east-north-east arm which projects inland into central Africa. Coward (1983) identified three kinematic phases in the Damara belt. The earliest ( $K_1$ ) is southwest directed and the second ( $K_2$ ) involved major southwest overthrusting on flat lying planes. Southeast overthrusting indicates  $K_3$ . The Schiessen zone is a major lineament in the east-north-east arm of the Damaran belt associated with southwest thrusting. The Schiessen zone displays WSW over ENE sinistral displacement dating between 675-550

Ma (Coward, 1983). The occurrence of basic and ultramafic rocks of ophiolite affinities indicates that the zone is a plate boundary between the Kalahari and Congo plates (Coward and Daly, 1984). On the basis of lateral continuity, the Schliesen zone is the western continuation of the MDZ along the same plate boundary despite the absence of similar rock assemblages (Coward and Daly, 1984; De Kock, 1996). Ring (1993) considers the absence of rocks with ophiolite affinities in the MDZ to be due to a large component of pure strike-slip shear motion.

The MDZ is also considered to be continuous northeastwards with the Chimarilo zone of Malawi (Coward and Daly, 1984; Ring, 1993). The Chimarilo zone displays ENE over WSW dextral transcurrent motion considered to have occurred between 740 and 600 Ma during early Pan-Africa orogenesis (Ring, 1993).

On the basis of reconstruction of large-scale tectonics, Hoffman (1991) determined ENE over WSW dextral transcurrent motion along the MDZ.

## **1.8 Geodynamic framework**

Several geodynamic models have been postulated for the Pan-African orogenic belts. The MDZ and its western and eastern extensions play a central role in the geodynamics of central Africa.

Coward and Daly (1984) postulated that, the MDZ is a transform type plate boundary along which the Congo and Kalahari plates collided. The occurrence of eclogite bodies is attributed to high pressures (11 Kbar, Barr, 1976) generated during oblique collision. Although Coward and Daly (1984) subscribe to WSW over ENE sinistral motion along the MDZ, their tectonic model of the relationship between the Schliesen-Mwembeshi-Chimarilo (SMC) zone and the two plates indicates ENE over WSW dextral displacement.

Porada (1989) attributes the sinistral motion along the SMC to opening of the west-Congolian-Brasilano rift. The rifting set into motion the Congo and Kalahari plates eastwards, but the Kalahari plate is believed to have been moving relatively faster compared to the Congo plate. The WSW over ENE sinistral displacement is considered to have been the net effect of the relative velocities of the two plates.

Unrug (1983) considers the WSW over ENE sinistral strike slip displacement along the MDZ to be a result of crustal shortening during clockwise rotation of the Congo craton.

Based on kinematic indicators in the network of Pan-African orogenic belts and their associated shear zones, Coward and Daly (1984) and Daly (1986), concluded that the relation between shear zones and adjacent orogenic crustal scale thrust belts which share the same movement direction, resembles the flat lateral ramp geometry commonly described in foreland thrust belts. The Lufilian Arc, Zambezi belt and the MDZ was taken as an example of such a relationship.



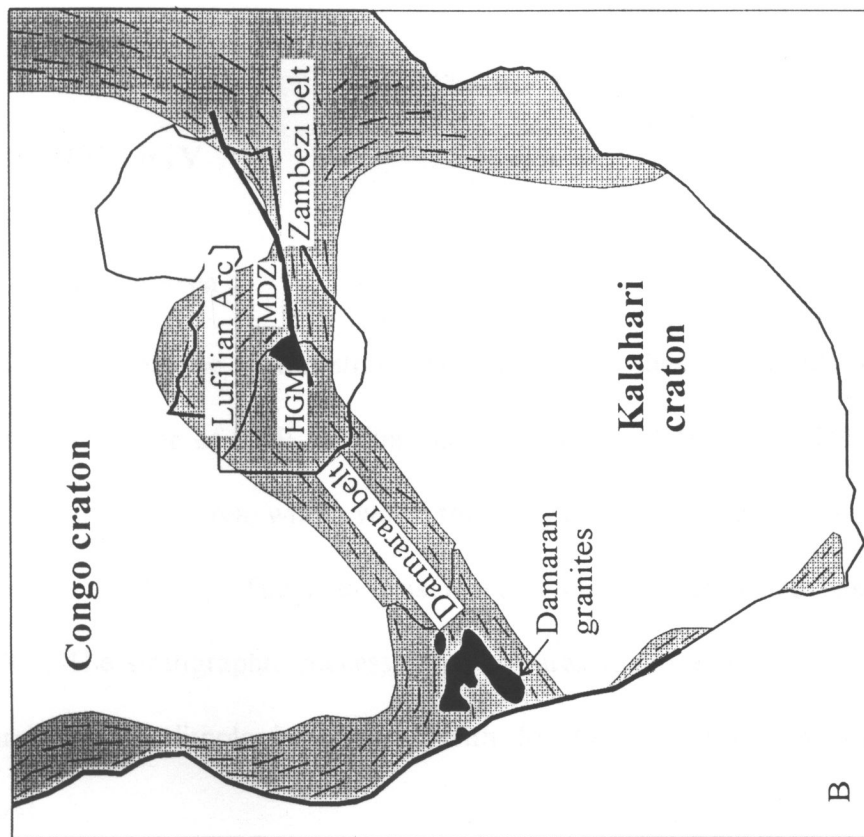
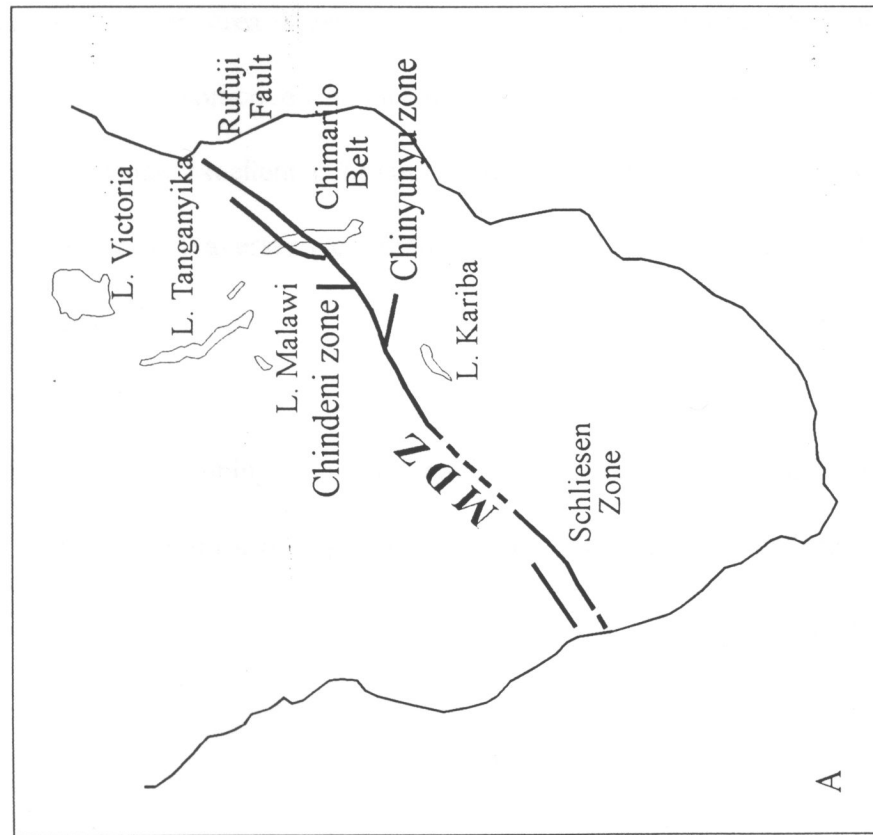


Fig. 1.5: A) Transcontinental Schliesen-Mwembeshi-Chimarilo (SMC) zone. B) Linked Pan-African Damaran-Lufilian-Zambezi Belts (after Coward and Daly, 1986; Hanson et al., 1993)

## **Chapter 2**

### **2.0 GEOLOGY**

#### **2.1 Chisamba area**

Study area A forms the northeastern corner of degree sheet 1528, NW Quarter which is transected by a zone of ENE trending faults of the MDZ (Fig.2.1). The only publication on the geology of the area, within which the study area is located, is a geological report by Simpson et al. (1963). The area was mapped on reconnaissance basis at a scale of 1:100,000. The stratigraphic succession of the area is presented in Table 2.1. However, the parallelism of lithologic contacts with foliation suggests that the succession is structural.

Rock exposure in this area is generally poor. Rocks crop out in stream sections whereas thick vegetation and soil cover the interfluvies. Quartzitic rocks form prominent ridges and hills. These provide excellent continuous outcrops, which can be followed along strike over long distances. Traverses were therefore taken along streams and in hilly areas across the general strike.

Detailed structural mapping was conducted only in areas with good exposures. Oriented samples were collected for both petrographic and micro-tectonic analysis.

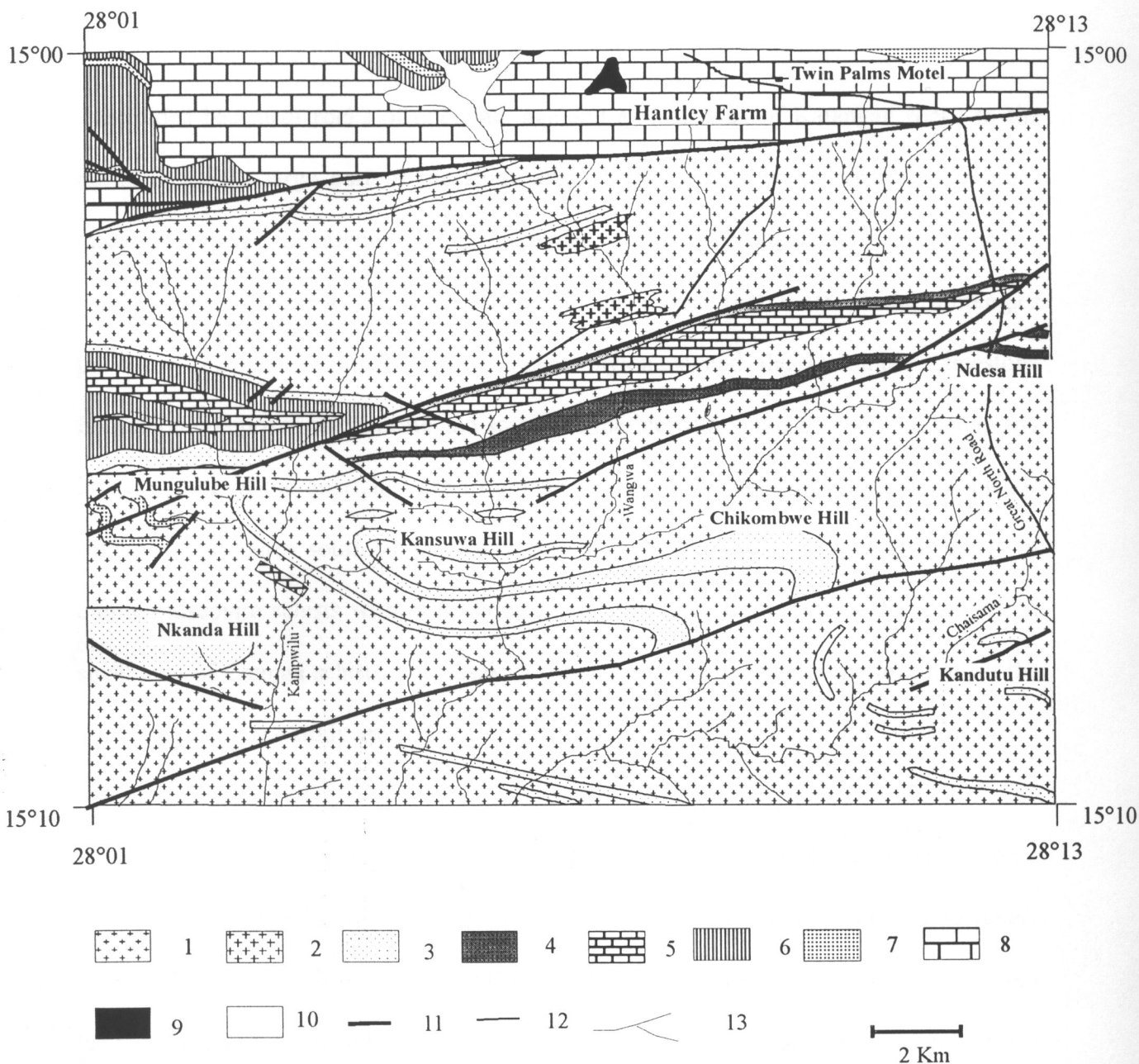


Fig. 2.1: Geological map of the Chisamba area: Study area A. 1: Granite-gneiss and sheared derivatives. 2: Calcareous gneiss. 3: Muscovite quartzite. 4: Quartz mylonite. 5: Interbanded calc-silicate, scapolitic marble, and minor amphibolite. 6: Garnet muscovite schist. 7: Iron-banded quartzite. 8: Dolomite. 9: Olivine gabbro. 10: Alluvium. 11: Inferred fault. 12: Road. 13: Stream

Interfolded basement rocks of uncertain age and a small area of Katangan rocks to the north underlie a large part of the study area. The basement rocks consists of biotite-muscovite gneiss, calcareous gneiss, quartzites, and impure limestone (Simpson et al., 1963). Mapping during the current research has shown that most of the lithologies previously mapped as quartzites are quartz mylonites and the Dolomitic Limestone Formation comprises calc-silicate and scapolitic marble with minor amphibolite bands and blocks. Some of the quartzites are Iron-banded, current bedded quartzites, lithologically similar to quartzites south of the study area in the Chunga Formation. Thin bands of biotite-muscovite schists with or without garnet were also found within the gneisses. A small area of Chunga schists and Lusaka Dolomite of the Katangan Supergroup form the northern part of the study area.

A zone of ENE-NE strike-slip faults exhibiting dextral sense of displacement affects both basement and Katangan rocks (Simpson et al., 1963). However, it is difficult to detect these faults in the field. At locality CH220348 quartz mylonite coincides with an inferred fault suggesting that the lineaments interpreted as faults on aerial photographs and landsat images may be discrete shear zones. Most of the ‘faults’ in the area are shown to have dextral sense of displacement (Simpson et al., 1963), in contrast to the assumed sinistral sense of displacement (De Swardt et al., 1964).

The interfolding of lithologies in the study area makes it difficult to construct a stratigraphic succession. On the basis of lateral continuation of lithologies in adjacent areas, Thieme (1984) compiled a 1:250,000 geological map of Lusaka, sheet No. SD-35-

Table 2.1: Stratigraphic succession of the Chisamba area (after Simpson et al., 1963)

Age	Supergroup	Formation	Lithologies
Neo-Proterozoic		Post Katangan Gabbro Lusaka granite	-Small plugs intruding Cheta formation and Lusaka dolomite -Coarse grained granite
	Upper Katanga	Lusaka Dolomite	-dolomite and limestone with various intermediate types
	Mid-Katanga	Cheta	-Quartz-muscovite schist, phyllite and micaceous flags -Gray-white and gray banded limestone and dolomite -Quartz-muscovite and micaceous chlorite schists and micaceous flags -Gray white and gray banded limestone and dolomite
	Lower Katanga	Chunga	-Quartz-muscovite-biotite-garnet schist and flaggy micaceous quartzite -Thin impure limestone and calc-silicate schist -Black banded current bedded quartzite - limestone, calc-silicate rocks
		-unconformity-	
Meso-proterozoic	Muva		- pure quartzites, micaceous quartzites, and tectonites
		-unconformity-	
Palaeo-proterozoic		Basement Gneiss	-biotite gneiss and pegmatitic gneiss and their sheared derivatives

15 and assigned gneisses to the basement of uncertain age; quartzites to the Muva Supergroup (Mesoproterozoic) and the carbonate rocks, calc-silicates and schists to the lower Katangan Supergroup (Neoproterozoic).

### **2.1.1 Quartzo-feldspathic gneisses**

Gneisses occupy a large portion of the study area. They are generally highly weathered and are best exposed in the Kampwilu and Wangwa rivers (Fig. 2.1). Four types of gneisses can be distinguished on the basis of mineral composition. These are biotite-muscovite-quartz-feldspar gneiss, muscovite quartz-feldspar gneiss, granite gneiss and calcareous gneiss. The gneisses have undergone various intensities of shearing producing narrow bands of schists and mylonites. The calcareous gneiss crops out in isolated lenses with limited strike length in the Wangwa stream north of the main road (Fig. 2.1).

### **2.1.2 Muscovite and muscovite-biotite quartzo-feldspathic gneisses**

Muscovite-quartz-feldspar gneiss and muscovite-biotite-quartz-feldspar gneiss are intercalated in some areas, but each one is more predominant in one part of the area than the other. The biotite-muscovite gneiss occurs mainly in the tributary of the Wangwa stream and Chaisama stream east of the GNR (Fig. 2.1). This rock is highly weathered and friable. It is composed of feldspar, quartz, muscovite and subordinate biotite. The micas define the main foliation. Along the Kampwilu stream, it is intercalated with weathered muscovite quartz-feldspar gneiss.

The muscovite-quartz-feldspar gneiss is the main rock type in the area. It is widely distributed especially south of the main road in the study area. The muscovite-rich gneiss is highly weathered. The rock is fine-medium grained, composed of feldspar, quartz and abundant muscovite along the foliation plane. Feldspar is pink in colour in relatively fresh samples. At CH139299, in the Kampwilu stream, the gneiss is locally banded. Thin (2-3 cm) tourmaline bands define the banding. The occurrence of tourmaline bands parallel to the gneissic foliation suggests circulation of boron-rich fluids during shearing of the gneiss. However, it is also possible that the banded gneiss was derived from shearing of tourmaline-rich pegmatitic granite.

At some outcrops, the gneiss possesses two foliations, one cutting across the other. The foliations in the gneisses consistently strike ENE-WSW and their dip ranges from 40° S to 90° with occasional northerly dips, indicating that the rock has undergone at least two deformation phases.

A thin band of garnet biotite-muscovite schist occurs in the Kampwilu stream at CH140280. Simpson et al. (1963) described similar lithologies in the Chunga Formation and therefore the band probably represents schists of the same Formation.

The gneisses are evidently folded at least twice, as suggested earlier. At CH141275, loose block of banded gneiss is folded into a tight overturned fold verging north (Plate 4.6). The foliation is axial planar to the fold.

South of the Chikombwe hill, in the Wangwa stream and immediately to the east of the Nkanda hill, there are extensive outcrops of coarse, pinkish, augen gneiss composed of pink feldspar, quartz, muscovite and minor biotite. The gneiss has a weak, ENE trending, foliation, implying that the gneisses are pre to syntectonic with respect to regional deformation. Contacts between the coarse augen gneiss and the surrounding sheared gneiss were not observed. The gneiss has survived shearing which is prominent in other parts of the area. It probably represents a low strain region. The occurrence of relatively finer-grained muscovite gneiss is more likely a sheared derivative of this coarse augen gneiss.

Complete mineralogical compositions could not be determined in the field because of the severity of weathering. The mineralogical composition of garnet biotite-muscovite schist, as far as can be determined in hand specimen, suggests a sedimentary parentage. Some schistose bands in the main gneiss are certainly due to shearing, but others however, are sedimentary.

### **2.1.3 Calcareous gneisses**

Calcareous gneiss crops out in the Wangwa stream north of the main road. It is intercalated with the leucocratic muscovite gneiss. The intensity of deformation in the area would suggest that this intercalation is tectonic. The gneiss is light gray in colour, fine- to medium-grained, weakly foliated and fizzes weakly with dilute HCL.



In some places thin amphibolitic bands occur parallel to the main foliation,  $S_1$ , in the calcareous gneiss, indicating that deformation was accompanied by amphibolite facies metamorphism

#### **2.1.4 Garnet amphibolites in gneisses**

Amphibolites occur as concordant lenses (e.g. CH235381) in sheared gneisses in the stream that drains into the Wangwa stream from Hartley farm (Fig. 2.1). Contacts with immediate host were not observed. The amphibolites are characteristically dark green and fine-grained consisting of a well-developed linear parallelism of hornblende prisms with interstitial elongate felsic aggregates and garnet porphyroblasts.

#### **2.1.5 Calc-silicate rock, scapolitic marble and amphibolite**

Calc-silicate rocks and marble are intimately associated and best exposed in the Wangwa stream (CH219342). They extend along strike over a considerable distance. An isolated outcrop of marble inter-banded with amphibolite occurs in the Kampwilu stream west of the Nkanda hill. Calc-silicates have a brownish buff weathered surface, but greenish on a fresh surface. The rock fizzes weakly with dilute HCL. The foliation in the calc-silicate is expressed as a steep axial planar cleavage. Banded calc-silicates exhibit normal overturned parallel folds verging south. The banding consists of alternating calc-silicate, and relatively thin dark iron-oxide bands. The rock could originally have been composed of interbedded

iron-oxide and calcareous layers, which were later metamorphosed to the iron-banded calc-silicate rock.

An extensive outcrop of scapolitic marble occurs along the Wangwa stream. The marble fizzes vigorously with HCL. Unlike the calc-silicate rocks, marble is disharmonically folded. The banded marble exhibits minor intrafolial, isoclinal folds. White bands mark the folds in gray marble.

Within the same formation, a lens of collapse breccia of about 10 m in extent consists of boulders of white marble and talcose rocks in gray marble.

In some places, thinly bedded amphibolite is interbedded with white marble. In other places, rounded boulders of amphibolite float within flow banded marble. The amphibolite boulders are not boudinaged here, however, Simpson et al. (1963) reported boudinage of amphibolite in the area. At CH219342, marble is amphibolitised at the contact with layered amphibolite, either indicating an intrusive contact or a reducing front during metamorphism.

#### **2.1.6 Quartzites**

Quartzitic lithologies which are considered as quartzites are relatively fine to medium grained consisting of equigranular crystalline quartz and possess a spaced cleavage defined by muscovite trails, which in some cases cuts across bedding. The cleavage is sub-parallel

to the bedding and dips in the same direction at a low angle to bedding indicating tight folding. Quartzites generally form E-W trending prominent ridges interfolded with other lithologies.

Quartzites at Kandutu hill consist of bands of tourmaline ranging from a few mm to 1 cm in thickness. Some of the bands are folded and appear to mimic folded bedding planes. At the same locality highly sheared quartzite consists of lens shaped enclaves of unsheared quartzite demonstrating strain partitioning.

Banded iron-oxide quartzite occurs at Mungulube hill. The iron-oxide bands occur as thin laminae defining trough cross bedding. The quartzite is fine to medium grained, with muscovite defining  $S_1$  along bedding parallel foliation. The cross bedding indicates SE-NW current transport direction. A steeper  $S_2$  spaced cleavage, striking  $060^\circ$  and dipping  $40^\circ$  S, cuts across bedding. The bedding/cleavage ( $S_0/S_2$ ) intersection lineation plunges  $14^\circ$  towards  $222^\circ$ .

Mungulube Hill is the only locality where iron-banded quartzite was seen. The iron-banded quartzite in this area is similar to that observed in the Kabwe area to the north, although some of the iron-bands in the Kabwe area range up to 10 cm thick. Simpson et al. (1963) described hematite cross-bedded quartzites in the Chunga Formation south of the study area. The quartzites at Mungulube hill correlate well with Chunga and Chikonkomene Formation cross-bedded quartzites.

### **2.1.7 S-L tectonite**

An S-L quartzitic tectonite forms a 4m band of limited lateral extent within muscovite quartzite (CH153316). The rock is characterized by a stacking of elongate and flattened quartzitic boudins (Plate 4.4), which are bounded by very small amount of micaceous matrix. The long axes of the boudins define a plunging lineation, which indicate ENE thrust transport. The tectonite was formed from a protolith consisting of alternating argillaceous and quartzitic layers. The more competent quartzitic layers were boudinaged during an extension episode, probably during the Irumide orogeny, followed by stretching along the long axis of the boudins, during Lufilian orogeny. Similar S-L quartzitic tectonite, previously mapped as quartzite, was observed in the Mwembeshi River Area (1527 NE; MW815295), on the western side of the Chisamba area. The tectonite in the Mwembeshi River Area contains more micaceous matrix than that observed in the Chisamba area and hence has preserved a better record of the deformation history. The boudins in the Mwembeshi tectonite exhibit isoclinal folding and imbricate structures in the XZ plane. The imbricate structures indicate NE directed Lufilian thrust transport. The boudins are highly flattened and tongue-shaped, with curved hinge lines, resembling sheath folds. The rock thus displays a complex deformation history involving both extension and compression.

### **2.1.8 Mylonitic rocks**

Lithologies in the Chisamba area are generally sheared, but some are more strongly sheared to produce mylonitised equivalents.

Zones of quartzo-feldspathic mylonites were only observed in the northern part of the area in calcareous gneisses. Textural features in the sheared micaceous quartzo- feldspathic gneisses are obscured by severe weathering to a friable white micaceous rock. Quartzo-feldspathic mylonites are fine- to medium-grained and have a strong steep to vertical mylonitic foliation, defined by micas mainly muscovite, subordinate biotite, and stretched quartz ribbons and felsic aggregates. The lineation is sub-horizontal. On the basis of the abundance of porphyroclasts relative to matrix, the mylonites developed in quartzo-feldspathic lithologies may be referred to as protomylonites.

Quartz-mylonites are fine to medium grained and possess a mylonitic foliation defined by muscovite and stretched quartz.

A band of quartz mylonite trending E-W was encountered at CH217337. An oblique mineral stretching lineation pitching with a low angle on southerly dipping shear foliation indicates that the mylonite developed in a thrust zone. In thin section mica-fish (Plate 3.11) indicates NE directed thrust transport (discussed in more detail in section 4.2.4.2.1).

Another band with the same trend is located to the north of the above-described mylonite and dips steeply to the southeast. It is composed of stretched quartz and garnet porphyroblasts with abundant muscovite defining a mylonitic foliation. The stretching lineation is sub-horizontal, 5° towards 250°, indicating a large component of strike slip shear movement.

Very fine-grained milky white quartz mylonite with interfolded bands of relatively coarse-grained tourmaline occurs at Ndesa hill along the GNR. Quartz grains are stretched and are strongly dynamically recrystallised. The mineral stretching lineation is sub-horizontal. Unlike other quartz mylonites, muscovite is not present.

A kyanite quartz mylonite encountered at CH174316 is strongly lineated with the lineation defined by an intersection of thin beds (3 cm) and cleavage defined by micas. The cleavage is sub-parallel to the bedding ( $050^{\circ}/60^{\circ}$  S) but with a shallower dip in the same direction ( $080^{\circ}/40^{\circ}$  S) and defined by muscovite, and dynamically recrystallised quartz. Kyanite is oriented in the cleavage plane.

A thin band (2 m wide) of silicified mylonitic epidosite was mapped within gneiss at CH232386. The rock is pale-green in colour, very fine-grained, hard and compact. The mylonitic foliation is defined by very fine streaky laminar of alternating pale-green epidote and quartz layers oriented parallel to the general trend in the area.

#### **2.1.9 Gabbro**

A small hillock of fine-medium grained gabbro at CH215420, outside the fault zone that defines the MDZ, has a relatively coarse-grained core, surrounded by a fine-grained margin. The fine-grained margin is concentric and unfoliated, indicating variation in cooling rates rather than shearing. There are no outcrops near the contacts of the intrusion.

## 2.2 Kabwe area

The only available publication on the geology of the area is a Geological Survey Report by Moore (1964). Rock types of the Kabwe area are presented in Table 2.2. The Mwomboshi gneiss, Chikonkomene and Kangomba Formations underlie the study area. Moore (1964) has attributed the dominant structure in the Chisamba area to large-scale WSW over ENE sinistral drag between the Kapiri-Mposhi and Mwembeshi Dislocation Zones (Fig. 1.2). Moore (1964) reported shear zones in the Mwomboshi gneiss, but did not mention the predominant sense of shear and how they relate to the sinistral drag.

The Mwomboshi gneiss is referred to as granite-gneiss on the basis of mineralogical composition. It is not established whether it is a paragneiss or an orthogneiss.

Moore (1964) placed the Chikonkomene Formation in the Basement, which comprised the Mwomboshi gneiss unconformably overlain by the Chikonkomene Formation. At the time a large part of the country was not mapped. He correlated the Chikonkomene Formation with the Muva Supergroup-Musofu Formation, of Mkushi and Kapiri-Mposhi areas. An attempt is made to establish depositional-type environment of the Chikonkomene Formation despite the intensity of deformation.

Generally, rocks are best exposed in rivers and streams (Fig. 2.2). The best exposures are found in the Munyama River, which cuts across strike of the various rock types. Exposure along the Lukoshi River is poor, and outcrops are highly weathered. Except for quartz veins, there are generally no outcrops on the interfluvies, which are extensively cultivated. The northern part of the area consists of the E-W trending Chikonkomene

range of hills. In the Chikonkomene hills, exposure is fairly good, with insitu outcrops occurring at the foot of the hills or low ridges. North of the hills, exposure is extremely poor. The southern portion is relatively flat and exposures are generally restricted to streams with no outcrops on the interfluves.

### **2.2.1 Mwomboshi gneiss**

The Mwomboshi gneiss Formation is best exposed in the Muyama River and underlies more than two thirds of the study area (Fig. 2.2). It is composed of foliated medium-grained, leucocratic and mesocratic gneisses and their sheared derivatives.

Localised intense shearing in the Mwomboshi gneiss has produced schistose and quartzitic rocks in shear zones described in detail in chapter 3. The predominant EW-ENE structural trend in the gneiss is ascribed to the Irumide orogeny, which culminated at ca. 1355 Ma (Cahen et al., 1984). In some places, pegmatitic bands intrude the gneisses. In many places, gneisses are composed of alternating fine-grained, dark, biotite-rich bands and light felsic bands. The felsic bands are folded about an axial planar foliation.



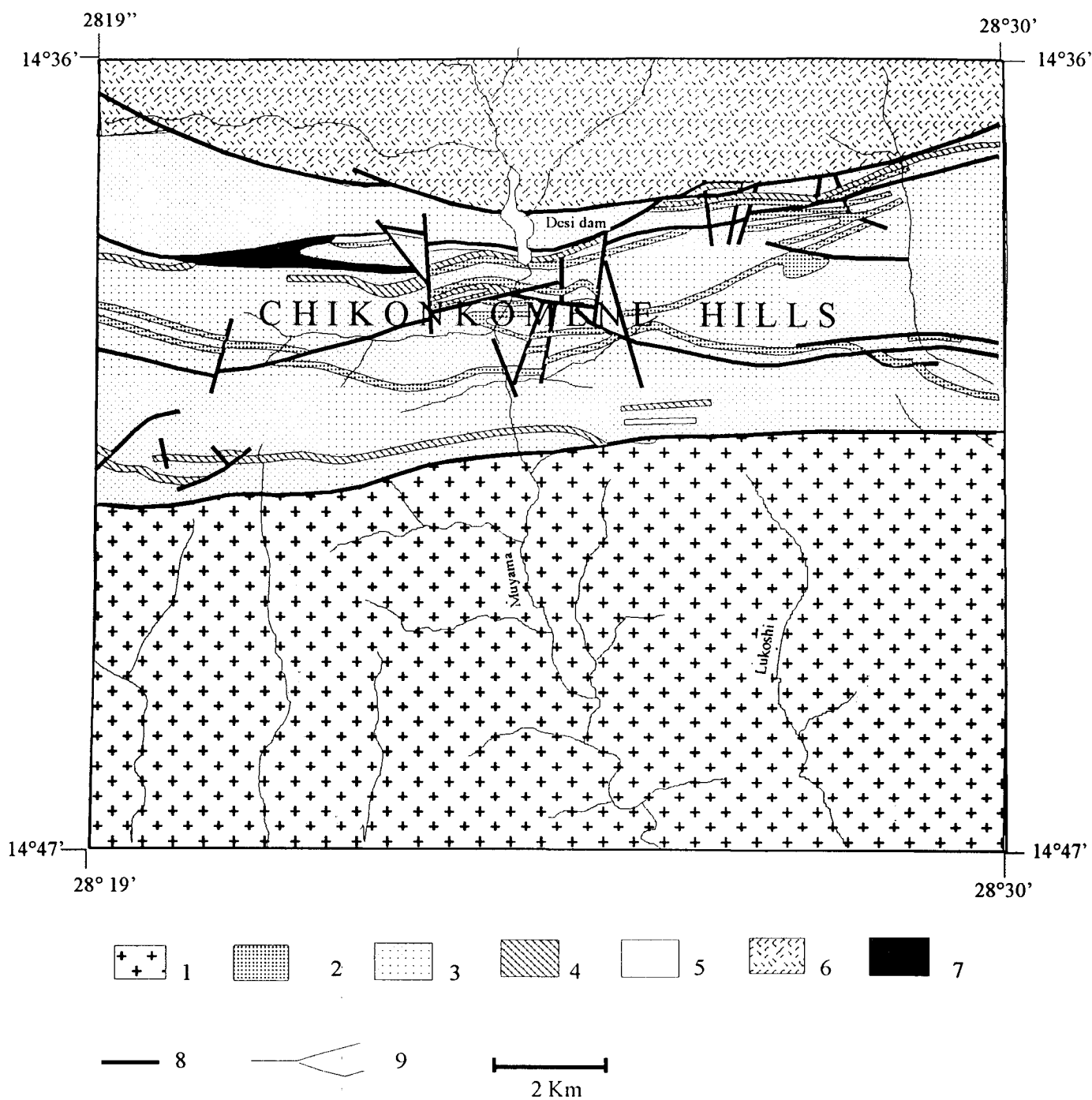


Fig. 2.2: Geological map of the Kabwe area: study area B. 1: Granite gneiss and sheared derivatives. 2: Polymitic meta-conglomerate. 3: Sericitic quartzite. 4: Iron-banded quartzite. 5: Gritty quartzite. 6: Interlayered phyllite, slate and marble. 7: quartz vein. 8: Inferred fault. 9: Stream

Table 2.2: Stratigraphic succession of the Kabwe area (after Moore, 1964)

Age	Supergroup	Formation	Lithologies
Neo-Proterozoic	Katanga	Post Nyama Intrusive rocks	Gabbro, pegmatites and iron bearing quartz veins
		Nyama	Limestone and dolomite with thin graphitic sandstone and intercalated shales
			-----? Unconformity ?-----
		Kangomba	Interbedded phyllites, shales, quartz-muscovite schists and dolomite with thin, impersistent quartzites and arkose
			-----unconformity-----
Meso-Proterozoic	Muva	Chisamba	Garnet-quartz muscovite schists and fine-grained quartz sericite schists with interbedded thin quartzites and iron-stones; sheared gneiss and granite
			-----unconformity-----
Palaeo-proterozoic		Chikonkomene	Schistose sericitic quartzites and quartz sericite schists, with iron-banded horizons, Polymictic meta-conglomerates and gritty quartzites.
			Metavolcanic rock: Amydaloidal epidosite -----faulted unconformity-----
		Mwomboshi gneiss	Quartz-feldspar-biotite gneiss with sheared Derivatives.

The leucocratic gneiss has a granitic composition consisting of muscovite, quartz, and K-feldspar. The dark grey gneiss has a granodioritic composition consisting mainly of plagioclase with subordinate quartz, biotite and muscovite. The micas define a crude foliation. Coarse-grained weakly foliated grey biotite gneiss used to be quarried at Nankuko quarry (KB442622). The dark grey gneiss represents the weakly deformed granodiorite, which in other places, is sheared to the dark grey protomylonite.

Very fine-grained dark elongated xenoliths were observed within the Mwomboshi gneiss at KB536726. The elongation of the xenoliths is aligned parallel to the east- west trend of the foliation. The xenoliths have the same composition as the host gneiss but with more biotite.

The preservation of the xenoliths implies that their original composition was of a higher temperature mineral assemblage at the time of emplacement of the host, such that the temperature introduced was not high enough to remelt and assimilate the xenoliths. Assimilation of wall rocks depends on mineral constituents of the wall rock and crystallising minerals from the magma (William et al., 1982). The fine-grained nature of the xenoliths probably means that there was no room for recrystallisation to take place.

On the basis of the occurrence of xenoliths, the Mwomboshi gneiss is considered to be an orthogneiss. It is also evident that the Mwomboshi gneiss was not derived from a homogeneous igneous body as demonstrated by the variation in mineralogy. The

mineralogically distinct gneiss probably represents two phases of intrusions. However, it is difficult to tell the age relations between the two.

#### **2.2.1.1 Amphibolite**

Fine-grained amphibolite lenses occur within the Mwomboshi gneiss. At KK552679, the amphibolite is composed predominantly of fine-grained hornblende with subordinate elongate felsic aggregates. The rock is slightly weathered and the outcrop is flat making it difficult to take measurements. A flat surface on a handspecimen after cutting with a rock-saw exhibits S-C fabrics indicating ENE over SWS with a sinistral shear movement. The rock is retrograded to chlorite-schist along shear planes.

#### **2.2.2 Chikonkomene Formation**

The Chikonkomene Formation makes up the Chikonkomene range of hills and immediate surroundings. It is composed of sericitic quartzites, iron-banded quartzites and polymictic meta-conglomerate (Fig. 2.2). The iron-banded quartzites and the meta-conglomerate form ridges running roughly E-W. The sericitic quartzites also form ridges but occur predominantly in low-lying areas between the ridges. Lithological boundaries between members range from sharp to transitional. The meta-conglomerate is composed of pebbles and cobbles set in a quartzitic matrix. With decreasing amounts of pebbles and cobbles, the meta-conglomerate grades into sericitic or iron-banded quartzite.

### 2.2.2.1 Sericitic quartzite

Sericitic quartzite constitutes the bulk of the Chikonkomene Formation and is intercalated with the meta-conglomerate and iron banded quartzite. It is whitish grey in colour, fine-to medium-grained and has a strong ENE crenulation cleavage ( $070^{\circ}/30^{\circ}$  N) defined by sericite, which in some places is copper coloured. The intensity of deformation in the area implies that, to a large extent grain size is a function of recrystallisation rather than sedimentary processes. Fine specks of hematite are disseminated in the rock. The shallow dipping ENE trending crenulation cleavage ( $070^{\circ}/30^{\circ}$  N),  $S_2$  foliation cuts an early steeper ( $075^{\circ}/45^{\circ}$  N)  $S_1=S_0$  foliation. The sparsely cleaved sericitic quartzite grades into a meta-conglomerate with an increase in pebbles and cobbles.

In many places, sericitic quartzite appears to have been mylonitised. The quartz is fine-grained and equigranular and white mica occurs in place of the copper coloured sericite. The mylonitic quartzite in some places consists of discontinuous quartzite white bands.

At KB543764, quartz veins are boudinaged parallel to the trend of the main foliation, trending  $060^{\circ}$ , implying an extension episode in the NE-SW direction. In other places, the quartz veins are refolded. The rock thus suffered extension followed by a compressive episode, which is expressed as folds (**Fig. Field sketch**)

At KK557768, quartz veins are folded within the banded mylonitic quartzite. Fold closures were noted in the fold noses indicating refolding. The folded quartz veins exhibit pinch and swell features and are boudinaged in places. However, the thickened portions of

the veins may well be due to refolding in the fold noses (**Fig. Field sketch**). An  $S_2$  crenulation cleavage ( $065^\circ/28^\circ$  N) is developed as axial planar foliation to the folded veins. A thick iron band (3 cm wide) representing  $S_0$  is gently folded on  $S_2$  axes.

Shear zones, probably on thrust planes are marked by banded mylonitic quartzites at KK531759 and KK554767. The quartzites are sub-horizontal with dips ranging from  $5^\circ$  to  $10^\circ$  N towards  $160^\circ$ , a sharp contrast from the steeper attitudes in the adjacent meta-conglomerates.

At KK532747, one set foliation dips steeply at  $75^\circ$  N whilst the other, 5-10 m apart, dips shallowly at  $10^\circ$  N, indicating a south facing overturned fold. At the same locality, the quartzite is composed of silt-sand size quartz and some feldspar with scattered iron oxides and fine mica along the foliation planes.

#### **2.2.2.2 Iron-banded quartzite**

The main rock type is a sericitic quartzite, which has iron bands up to 5 cm thick. It has a characteristic rippled surface due to differential weathering, with the iron bands being more resistant. The iron-banded quartzite invariably forms ridges due to its resistant nature, and is easily traced on aerial photographs. Iron-banded quartzites grade into sericitic quartzite with a decrease in iron-bands and also grade into meta-conglomerate with an increase in pebbles and cobbles. In the iron-banded quartzite  $S_1$ , which is expressed as a spaced cleavage, is parallel to  $S_0$ . Thin laminae of iron bands define cross-

lamination showing a younging direction to the north. The iron-bands thus represent original bedding  $S_0$  which in places have been gently folded. The paleocurrent direction may not be reliable as the metasediments are multiply deformed and only observed in a loose boulder of iron-banded quartzite. This is also suggested by tight folding of iron bands. Outside the study area, along strike, brecciated kyanite pods were found within faulted iron-banded quartzite. The kyanite pods and the host are invaded by a net work of thin purple fluorite veins.

The iron-banded quartzite contains some feldspar, in the quartzitic bands with sericite defining cleavage. The presence of feldspar in the iron-banded quartzite indicates the proximity of the source material to the area of deposition.

#### **2.2.2.3 Polymictic metaconglomerate**

The meta-conglomerates of the Chikonkomene Formation are matrix supported and consist of well rounded, flattened pebbles and cobbles, which in many places are crenulated about an axial planar crenulation cleavage ( $060^\circ/20^\circ$  N). The matrix consists of quartz with subordinate, aligned sericite cementing the pebbles and cobbles. The pebbles and cobbles consist of a mixture of fine-grained dark chert, tourmaline and white quartzite. Oxidised purplish to reddish cobbles make up a small component. Other pebbles and cobbles are dark fine-grained quartz-tourmaline rock, grey metasilstone, vein quartz, jasper and white fine-grained quartzite. In some places pseudoconglomerate is

characterized by boudinaged quartz veins which resemble flattened rock fragments of sedimentary origin.

Marked variations in grain sizes from the matrix to pebbles and cobbles is indicative of poor sorting and rapid deposition of debris flow type. However, pebbles and cobbles are well rounded either through long distance transportation or multiple reworking of sediments prior to final deposition. The sericite content of the quartzitic matrix probably reflects the argillaceous component of the deposit. The conglomerates consist of sub-rounded to rounded clasts of grey siltstone enclosed in a darker grey sand-size matrix indicating that the conglomerates of the Chikonkomene Formation are products of the reworking of an earlier conglomerate.

#### **2.2.2.4 Amygdaloidal epidosite**

Metavolcanics occur within the Chikonkomene Formation and the Mwomboshi gneiss and have been completely metamorphosed to amygdaloidal epidosites. A large part of the Chikonkomene Formation in the Chipembi area (Degree Sheet 1428, SE Quarter) located adjacent and west of the Kabwe area (Newman and Smith, in press), is made up of epidote-bearing amygdaloidal meta-volcanics. The amygdaloidal epidosites in the Kabwe area are pale yellow-green, massive and dense. The amygdales are irregularly shaped, composed of quartz or epidote pseudomorphs. In thin section, the amygdaloidal epidosite consists of about 80 % of epidote and the rest constitutes pale green actinolite and minor quartz. The epidote in many places is seen to form at the expense of actinolite. In



amygdales, epidote forms coarse radiating pseudomorphic prisms. In the Chipembi area the meta-volcanic rocks are weakly to strongly foliated and greenish, with epidote-filled amygdaloides (Newman and Smith, in press). The epidote-bearing amygdaloid meta-volcanic rocks in the Chipembi area consist of quartz, epidote, iron ore, actinolite and minor chlorite with epidote and quartz in the amygdaloides. The meta-volcanic rocks described in the Kabwe and Chipembi areas are principally the same. Geochemical analysis of the Mulungushi meta-volcanic rocks in the Chipembi area showed that they are altered basic lavas (Munyanyiwa, 1983)

#### **2.2.2.5 Chisamba Formation**

The Chisamba Formation is composed of quartzites, schists, sheared gneisses and granites (Moore, 1964). This unit was not investigated in detail due to poor exposure, but its southward continuity in the Chisamba area, where it is described as the Chunga Formation (Simpson et al., 1963) has a significant bearing on the MDZ.

Moore (1964) interpreted the Chisamba Formation to be a tectonic unit derived from shearing of the Mwomboshi gneiss. In his stratigraphic succession, Moore (1964) placed the Chisamba Formation at the top of the Nyama Formation, as he believed that the unit formed under a sedimentary cover during Lufilian deformation. In the Mwomboshi gneiss, tectonic quartzites and schists are evidently sheared derivatives of the gneiss. At locality KB552677, gneiss grades into a relatively fine-grained strongly foliated (laminated) quartzitic rock. Sheared fine-grained biotite schistose rocks were observed at several

localities in the Mwomboshi gneiss. However, the shearing event in the Mwomboshi gneiss that produced these shear zones is considered to be related to the Irumide orogeny or an older deformation event on the basis of metamorphic history. Although Moore (1964) mapped remnants of sheared gneiss within the Chisamba Formation at Chibombo (KB160790) and along Kamano (KB555510) and Kalangwa Rivers (KB600470), indicative of the tectonic origin of the Chisamba Formation, associated quartzite members are of sedimentary origin as suggested by the presence of detrital tourmaline grains observed in thin section. This seems to suggest that Chisamba Formation has both tectonic and sedimentary components.

The outcrop of the Chisamba Formation extends into the Lusaka area (1528 NE) of which study area A constitutes a small part, where it is mapped as Chunga Formation. The Chunga Formation is correlated with lower Katanga metasediments of the Copperbelt (Mendelsohn, 1961). On the basis of continuity of outcrop of lithologies and similarity in metamorphic grade (almandine-amphibolite facies) of the Chisamba and Chunga Formations, which are here considered to be one and the same lithology across the MDZ, it is concluded that the MDZ does not juxtapose lithologies of different ages as previously believed.

### **2.2.3 Kangomba formation**

The Kangomba Formation is faulted against the Chikonkomene Formation. Exposure is extremely poor. The Kangomba Formation is composed of phyllites, banded slates, fine-

grained quartz-muscovite schist, sugary quartzites, arkoses and thin dolomites. The quartzites of the Kangomba Formation are derived from the Chikonkomene Formation (Moore, 1964).

A traverse along the Kasavasa stream, outside the map area, shows highly weathered and dense greenish schistose rocks (probably mafic source). Pale yellowish green amygdaloidal epidosite veins occur within the green mafic schistose rock. The irregularly shaped amygdales are formed by quartz. These veins are similar to those observed near Nyama siding (KK463807) and those noted within the Mwomboshi gneiss formation in a shear zone at KK541703. The veins may have formed in extensional shear fractures.

#### **2.2.4 Kasavasa gabbro**

A small gabbro body forms Kabweso hill at Kasavasa siding (KB487877). Textural characteristics are similar to the olivine-gabbro in study area A. It is also composed of a coarse-grained core and fine-grained margin but it differs in mineral composition which comprises hornblende, augite and plagioclase with secondary actinolite and chlorite. Fine-grained yellow green epidote veinlets transect the gabbro. The most striking feature of this gabbro is the occurrence of mafic pegmatite vugs composed of coarse-grained plagioclase and hornblende laths.

### **2.3 Deposition environment**

The structures observed in the Chikonkomene Formation indicate tight folding, shearing and faulting. As such, most of the primary sedimentary structures have been obliterated and /or overprinted, and the stratigraphic succession distorted. In this section, the depositional environment of the Chikonkomene Formation is discussed on the basis of textural and petrographic characteristics of the lithologies in the area.

Sandstones and conglomerates can be deposited in various environments but their composition and texture reflect their mode of deposition and source rock (Pettijohn, 1975). The meta-conglomerates in the Chikonkomene Formation are polymictic, therefore derived from mechanical weathering of different rock types. The composition, shape, sorting and roundness of pebbles and cobbles are discussed in section 2.2.2.3. None of the pebbles and cobbles has the same composition as that of the Mwomboshi gneisses. This indicates that the meta-conglomerates were not derived from the underlying Mwomboshi gneiss in the depositional basin, but from a number of protoliths reflected by the composition of the clasts. The polymictic meta-conglomerate is matrix supported. The matrix consists of recrystallised quartz with subordinate amounts of muscovite, which defines the foliation. The absence of feldspar in the matrix indicates a mature sedimentary protolith. Although all the clasts are flattened and stretched the well roundedness is, to a large extent, through sedimentary processes and therefore attributed to reworking. The polymictic meta-conglomerate is poorly sorted suggesting deposition by debris flow. Some of the pebbles and cobbles consist of smaller rounded clasts suggesting reworking of an earlier conglomerate.

The intervening sericitic and iron banded quartzites lack feldspar, indicating high maturity of the protolith. In some places sericitic quartzite is cross bedded defined by thin iron oxide laminae, probably indicating deposition in braided rivers.

The above sedimentary characteristics suggest that the Chikonkomene Formation represents alternating or successive deposition by debris flow in an alluvial fan setting and less turbulent episodes in braided rivers.

There is a complete lack of carbonate rocks in the Chikonkomene Formation. The lack of carbonate sequences and predominant clastic metasedimentary rocks in the Chikonkomene Formation in the Kabwe area implies that the Irumide basin never attained a stable character during deposition. The presence of meta-basalts (Munyanyiwa, 1983) in the Chikonkomene Formation is indicative extreme attenuation of Muva continental crust (Daly, 1988).

## **2.4 Stratigraphy and correlation**

### **2.4.1 Chisamba area**

On a regional scale, the basement gneiss of the Chisamba area has been correlated with the Mkushi gneiss. The granitoid precursor of the Mkushi gneiss gave an emplacement Rb-Sr age of  $1777 \pm 89$  Ma and deformed during the Irumide orogeny at c. 1350 Ma (Ng'ambi et al., 1986). The basement gneiss is therefore probably Palaeoproterozoic in age.

Basement rocks underlie a large portion of the Chisamba area with small areas to the north and east being of Katangan meta-sedimentary rocks. The absolute age for the basement gneiss is unknown. The composition of basement is given in Table 2.1. However, some of the constituent lithologies are here believed to belong to the Muva and/or Katangan Supergroups on the basis of structural and petrographic similarities with other lithologies in the region. The iron- banded, cross-bedded quartzites mapped in the area are similar to those described in the Chunga Formation in the Lusaka area. The iron-banded, cross-bedded quartzites in the area are thus younger than the other basement lithologic units. The tourmaline and kyanite bearing quartzites in the area probably belong to the Muva Supergroup as they rest directly on Basement gneiss. The same quartzites are similar to those of the Chikonkomene Formation mapped in the Kabwe area.

The tourmaline and recrystallised quartzites are interfolded and appear to sit directly on basement gneiss. Thieme (1984) assigned all the quartzites, which are intimately associated with basement gneisses in the Lusaka area to the Muva Supergroup. This presupposes that the gneiss is orthogneiss, on top of which the metasediments were deposited.

Calcareous gneiss, calc-silicates, and marbles are assigned to the Basement Complex. Carbonate rocks on the Copperbelt are Upper Katangan, Kundelungu Supergroups. In the Lusaka area rocks with carbonate affinities are widespread in the Chunga and Cheta Formations. Calcareous gneisses in the Zambezi belt south of Lusaka have also been assigned to Katanga. On the basis of the widespread occurrence of calcareous and

carbonate rocks in the Katangan Supergroup, similar rocks in the Chisamba area may also be of the same age. However, it is possible that the same rocks could be older, but there is no evidence to support an older age.

The outcrop of Chunga Formation schists in the Lusaka area (Simpson et al., 1963) is continuous with that of the Chisamba Formation in the Chisamba area (Moore, 1964) in the region of the MDZ (Fig. 1.1). The latter is believed to be a tectonic unit it contains remnants of gneisses from which it was derived by shearing (Moore, 1964). However, the schists in the Chunga Formation are interpreted as a metasedimentary unit. A strip of Lusaka dolomite forms the boundary between the Chisamba and Lusaka areas and bounded by an inferred fault on the southern side. Simpson et al. (1963) and De Swardt et al. (1964) consider this fault to have juxtaposed younger Lusaka dolomite against older basement to the south. However, field relations suggest that the carbonate strip oversteps the Chisamba Formation to the north and Chunga and basement rocks to the south, which are essentially continuous across the fault. It is evident therefore that the MDZ does not juxtapose younger lithologies against older ones.

#### **2.4.2 Kabwe area**

The Mwomboshi gneiss and the Chikonkomene Formation constitute the basement of the Kabwe area. The Chikonkomene Formation is here considered to belong to the Mesoproterozoic Muva Supergroup due to its lithological similarities with Formations

assigned to the Muva Supergroup in other areas eg Copperbelt, Mkushi and Kapiri-Mposhi. The Chikonkomene Formation has a striking resemblance with the Muva of the Copperbelt (Mendelsohn, 1961), Musofu and Mkushi Formations of the Musofu river, Mkushi (Stillman, 1965) and Kapiri-Mposhi area (Smith, 1966). On the Copperbelt, the Mesoproterozoic rudaceous group south of Mufurila, consists of intensely sheared conglomerate with intervening beds of quartz-mica schist (Mendelsohn, 19961). The Musofu Formation includes quartzites and interbedded conglomeratic horizons (Stillman, 1965; Smith, 1966). By extrapolation along strike from the Mwembeshi, Chainama, and Rufunsa areas, some of the quartzites in the basement of the Lusaka area belong to the Muva Supergroup (Stillman and Simpson, 1963). Table 2.3 presents a proposed stratigraphic correlation of areas north and south of the MDZ. Previously (De Swardt et al. (1964); Moore (1964); Coward and Daly (1984); Liyungu (1986)) equivalents of the amphibolite facies Chunga Formation to the south of the MDZ were correlated with greenschist facies Lower Roan north of the MDZ. This led to the conclusion that the MDZ separates rocks of higher metamorphic grades to the south from lower metamorphic grades to the north. The proposed correlation, coupled with other evidence discussed elsewhere in this thesis indicates that there is no metamorphic break across the MDZ.



Table 2.3: Stratigraphic correlation of lithologies in areas north and south of the MDZ

NORTH OF MDZ			SOUTH OF MDZ	
Luiru Hills Phillips (1958)	Chisamba Moore (1964)	Copperbelt Mendelsohn (1961)	Mwembeshi Simpson (1962)	Lusaka Simpson et al. (1963)
Rudaceous Group		Upper	Post-Kawena Conglomerate	
-----	-----	-----	-----	-----
Calcareous- Arenaceous Group			Kawena sand stone	Kawena Sand stone
-----	-----		-----	-----
Transition beds		Middle	Kawena Argillite	Kawena Argillite
-----	-----	-----	-----	-----
Carbonate argillite group	Nyama Formation	Lower Mwashya group	Lusaka Dolomite	Lusaka Dolomite
-----	-----	-----	-----	-----
Quartzite schist group	Kangomba Formation		Cheta Formation	Cheta Formation
-----	-----	-----	-----	-----
	Chisamba Formation	Lower Roan Group	Chunga Formation	Chunga Formation
	-----	-----	-----	-----
	Chikonkomene Formation	Muva	Mwembeshi Quartzites	Quartzites
-----	-----	-----	-----	-----
Paragneiss Group	Mwomboshi gneiss	Basement	Kembe gneiss and schist	Basement Gneiss

## **Chapter 3**

### **3.0 PETROGRAPHY**

#### **3.1 Introduction**

This chapter presents petrographic and microstructural data from the Chisamba (MDZ) and Kabwe areas.

Modal mineralogical analyses are based on visual estimates. Mylonitic rocks have a wide range of grain sizes and some rocks are banded or laminated. For this reason, modal percentages could not be quantified by point counting.

Thin sections were prepared from oriented samples and represent sections cut parallel to the lineation and perpendicular to the foliation in the XZ plane of the strain ellipsoid.

#### **3.2 Chisamba area**

##### **3.2.1 Garnet-biotite-muscovite quartzo-feldspathic gneiss**

This lithology was observed at one locality. As such the description is based on one sample, KK 56. The rock consists of a medium-grained equigranular intergrowth of quartz (40%) plagioclase (30%) K-feldspar (15%), garnet (5%) and Micas (10%), mainly muscovite, with subordinate biotite occurring in alternating layers which define the main foliation and a weak, probably, earlier foliation.

Plagioclase (An<sub>60-52</sub>) generally has straight twin lamellae, but occasionally, deformation twins are present. The K-feldspar is microcline.

The schistosity is defined by cross-cutting flakes of oriented muscovite and minor biotite. The dihedral angle between the foliations is small indicating tight folding and renders deciphering of age relations difficult. Biotite appears to form along the margins of muscovite. Micas in the felsic zones occur at grain boundaries of quartz and feldspar.

The garnet is poikiloblastic, containing inclusions of mainly fine-grained quartz, green biotite, feldspar and muscovite, indicating that there has been grain size growth (Plate 3.1). The garnet is also fractured, along which it is downgraded to biotite. The foliation wraps around the garnet.

### **3.2.2 Banded gneiss**

Banded gneiss is a sheared derivative of the biotite gneiss. It occurs in a narrow shear zone, 5 m wide. The rock is fine-grained and composed of alternating pink K-feldspar-rich and quartz-rich bands, which range in thickness from 1-3 mm. The pink bands consist mainly of K-feldspar with subordinate quartz. The quartz bands consist wholly of crystalline quartz and appear to be recrystallised foliation parallel quartz veins.

The feldspar is predominantly microcline with subordinate plagioclase. A few bands comprise plagioclase with minor amounts of microcline and quartz. The feldspar in the feldspar-rich

bands is anhedral and generally shows deformation twins and undulose extinction. A few grains are fractured, but fracturing does not seem to have played an important role in the deformation. Plagioclase is moderately sericitised, such that the twin lamellae are obscured. Grain boundaries between feldspar are straight and regular indicating annealing. Muscovite in some layers occurs in significant amounts. Thin polycrystalline quartz ribbons, one grain wide occur in feldspar-rich layers and are oriented parallel to the banding.

The quartz-rich bands are composed of coarse aggregates (1-2 mm) of quartz grains, flattened and stretched in the banding plane. The grains are transected at a high angle to the stretching direction ( $050^\circ$ ) by intergranular fluid inclusion trails. Grain boundaries between adjacent quartz grains are irregular and lobate. The grains show patch extinction due to subgrain development. Some subgrains are elongated parallel to the fluid inclusion trails. Quartz in ribbon aggregates hosts fine inclusions of mica possessing a strong fabric. As in many other specimens this predates static growth of quartz. The quartz grains were however, deformed after recrystallisation as indicated by undulose extinction. Thin isolated layers of lozenge (spindle) shaped feldspar aggregates or individual grains occur within the quartz bands (Plate 3.2).

### **3.2.3 Kyanite-muscovite quartzite**

The quartzites in the study area are generally sheared and in many cases mylonitised. They are composed of strained quartz, muscovite and minor biotite defining the foliation. Many of the quartzite bodies contain oriented kyanite blades. The quartzites are relatively coarse-grained

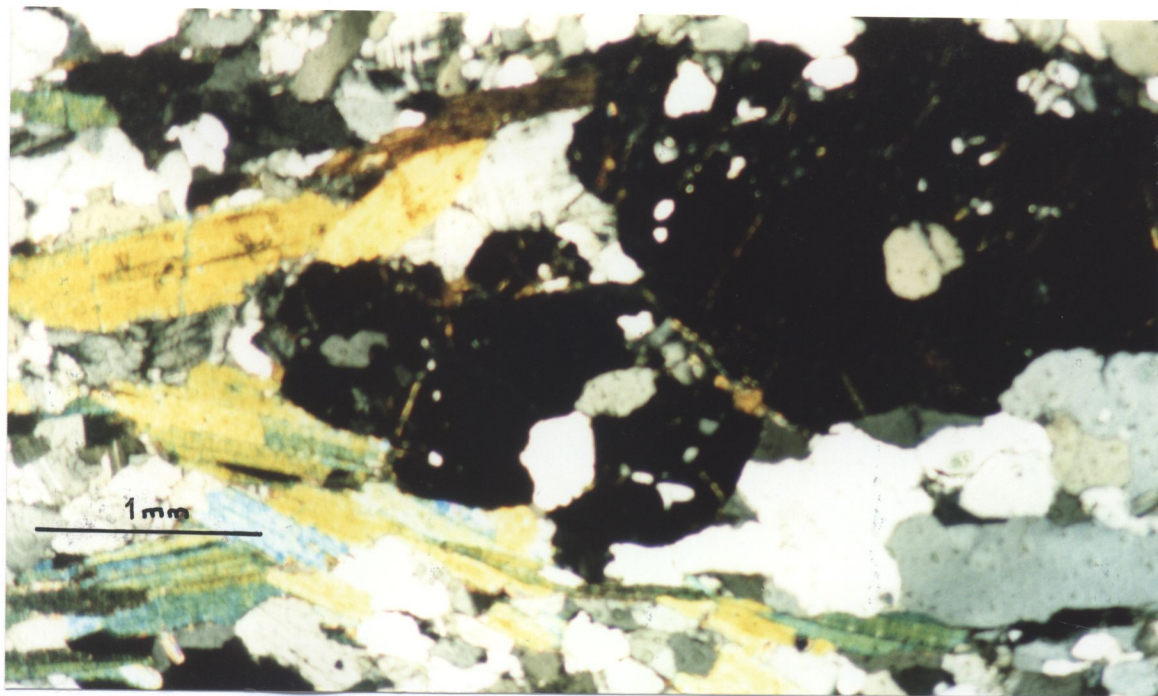


Plate 3.1: Photomicrograph of garnet-muscovite-biotite gneiss showing poikiloblastic garnet with fine-grained inclusions. Sample KK56, x25. CPL. CH316308.

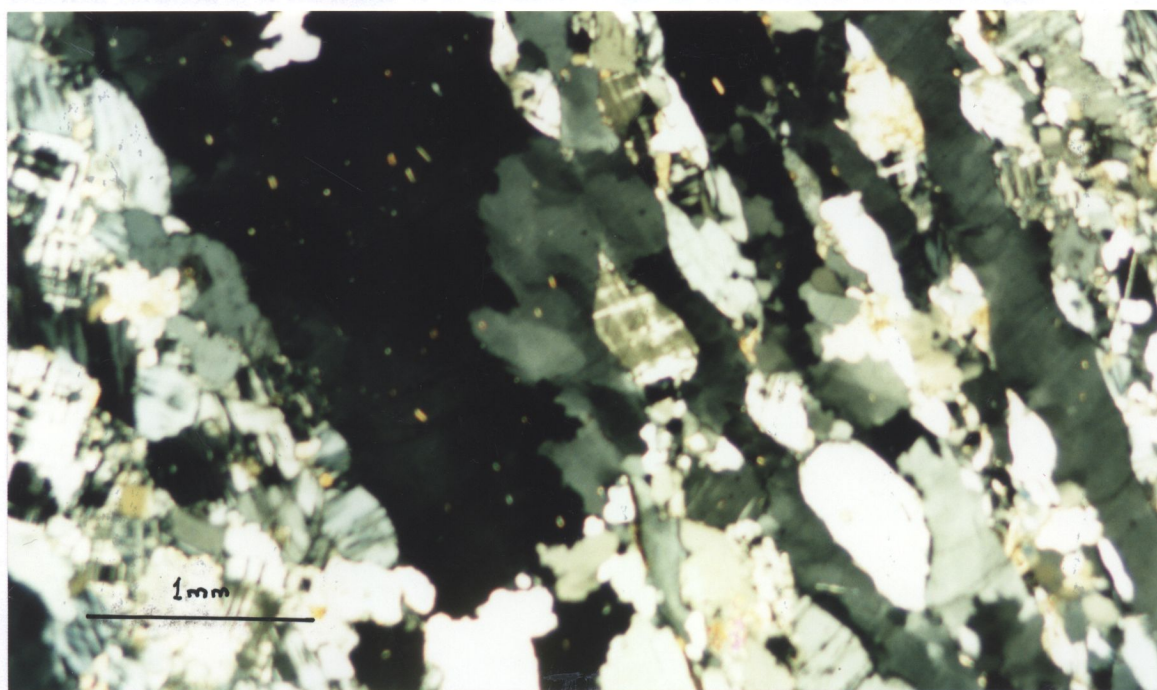


Plate 3.2: Photomicrograph of banded biotite gneiss showing quartz ribbons and lozenge-shaped microcline porphyroclasts. Sample KK40, x25, CPL. CH319307.

due to static recrystallisation as at Chikombwe hill. In thin section the quartzites consist of fine- to medium-grained, strained and in some cases flattened quartz, muscovite and sparsely distributed kyanite porphyroblasts. Accessories include tourmaline zircon and sphene.

Quartz grains hosts fine inclusions of muscovite, biotite and kyanite (sample KK71) which define a strong internal fabric parallel to the external foliation. The parallel orientation of the internal fabric in quartz with the external foliation in the rock indicates that quartz overgrew the internal fabric by static recrystallisation, which outlasted the fabric forming deformation event. The quartz grains exhibit undulose extinction, core and mantle structures and deformation bands. In sample KK32, the inclusions in quartz define two foliations, one is parallel to the external foliation and the other is at an acute angle to the external foliation suggesting tight folding of the rock. Some mica occurs at grain boundaries indicating impinging of grain growth. In the same sample the quartz grains are irregularly shaped with boundaries ranging from slightly serrated to smooth. In contrast relatively coarse elongate quartz grains in sample KK71 are set in finer-grained groundmass of subhedral to euhedral polygonal quartz grains, indicating core and mantle structures. Porphyroblasts of sparsely distributed kyanite occur as oriented prisms in the foliation, and define a sub-horizontal ENE mineral lineation (Plate 3.3). Kyanite is mantled by muscovite along the margins, indicating breakdown of the former. In some samples green tourmaline (2%) occurs both as inclusions in quartz and as isolated grains. Some tourmaline grains host small inclusions of quartz. This implies that the quartzite was finer-grained than the present and grew in size by annealing.

The main mica in the quartzite is muscovite, but small amounts of brown biotite are present. The micas define a foliation. Some mica appear to be drawn into mica-fish but are so extensively sheared out that the fish structure is destroyed.

Sample KK37 is a muscovite-biotite quartzite interlayered and probably interfolded with biotite gneiss. The main mica is biotite whilst muscovite is subordinate. Quartz is fine-to medium-grained with serrated and irregular grain boundaries. Subgrains are oriented at a high angle to the foliation. The foliation is defined by aligned biotite. The biotite layers alternate with quartz layers defining a compositional banding. Unlike other quartzites, this particular quartzite contains lozenge shaped feldspar. The most striking textural feature in the quartzite is the occurrence of needles of crystallographically orientated inclusions of rutile in quartz (Plate 3.4). This texture is known as sangenite structure. In addition to rutile, fine biotite also occurs as inclusions with the same orientation as rutile. The occurrence of rutile and biotite indicates static growth of the host quartz.

### **3.2.4 Scapolite-diopside rocks**

Calc-silicate rocks and amphibolite rocks occur as bands in scapolitic marble. Calc-silicates crop out at two localities along strike at localities CH219342 and CH260349, respectively (Fig. 2.1).



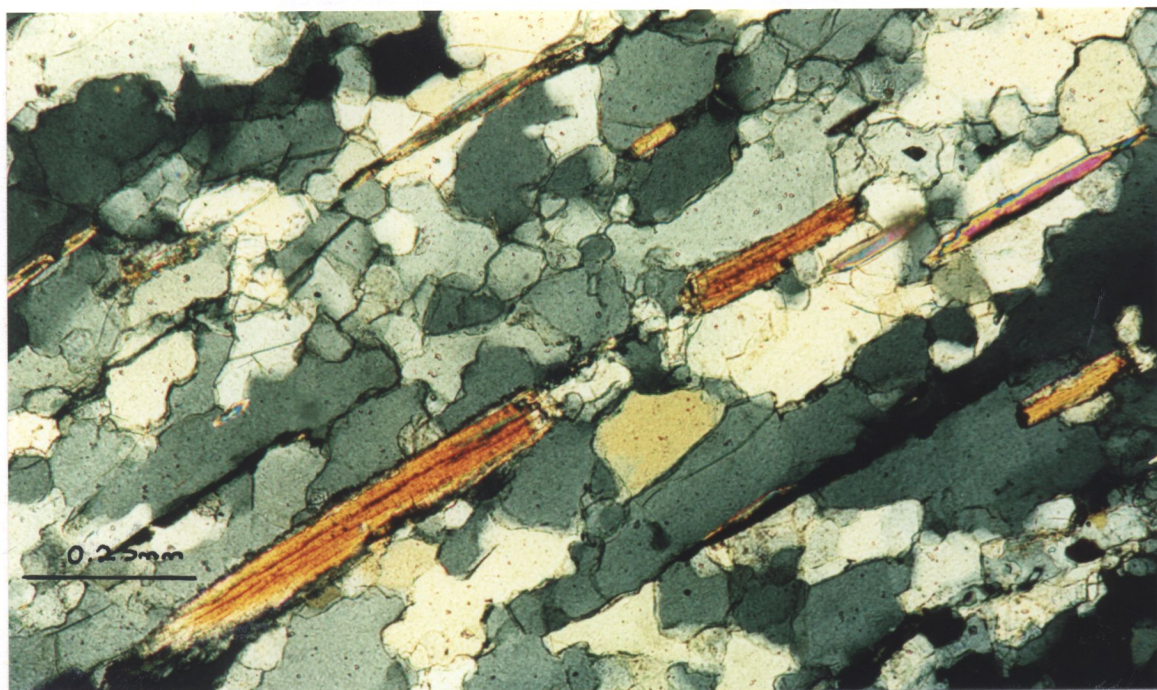


Plate 3.3: Photomicrograph of kyanite-muscovite quartzite, showing aligned kyanite blades partly retrograded to muscovite along the margins. Sample KK71, x100, CPL. CH174316.

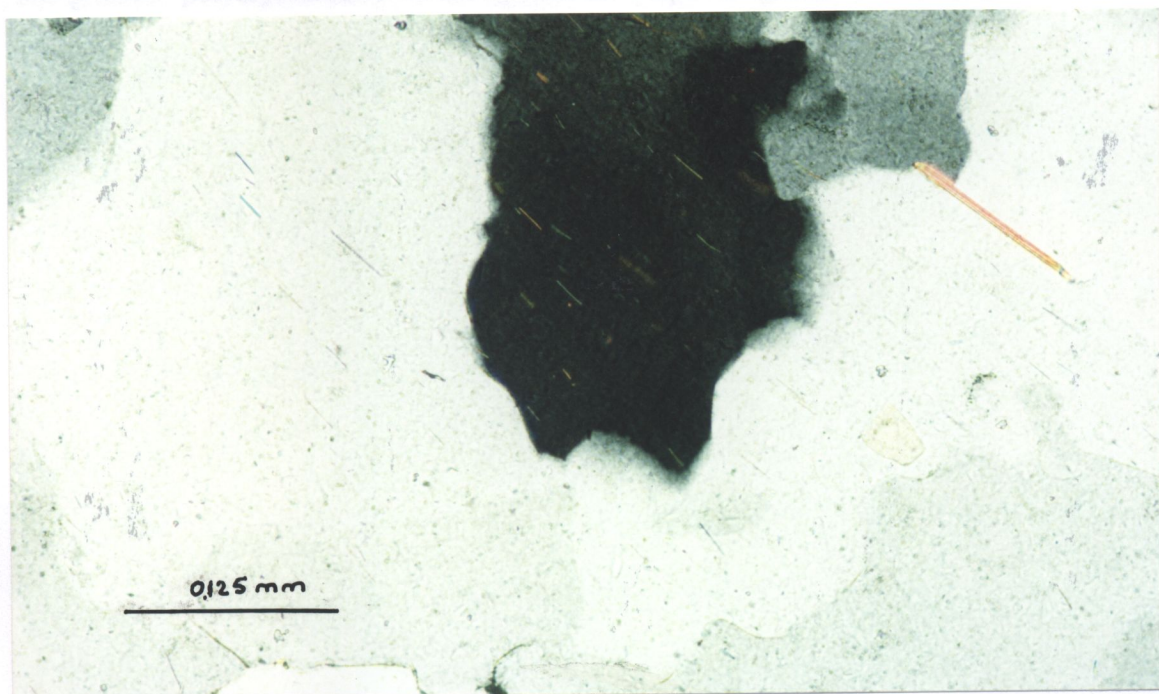


Plate 3.4: Photomicrograph of muscovite-biotite quartzite, showing inclusions of crystallographically aligned needles of rutile and biotite in quartz grains. Sample KK37, x200, CPL. CH316308.



The calc-silicate rocks are composed mainly of oriented subhedral to anhedral prisms of diopside (75%) and subordinate scapolite (20%), plagioclase (2%), epidote (2%), carbonate (1%) and minor phlogopite.

The rocks consist of alternating fine-grained and relatively coarse-grained layers of diopside and scapolite defining a textural banding. In sample KK92 coarse-grained layers or lenses are composed of unoriented mineral grains, whilst minerals in fine-grained layers are aligned parallel to the banding. Scapolite occurs in both layers whilst elongate epidote is restricted to the fine-grained layers. The rock is characterized by anastomosing zones of fine-grained mineral aggregates parallel to the foliation. Along the fine-grained zones, scapolite occurs as fine-grained polycrystalline aggregates. Some scapolite grains exhibit core and mantle structures, subgrains and undulose extinction (Plate 3.5). The fine-grained zones are considered to be discrete shear zones along which dynamic recrystallisation of scapolite occurred. In some zones fine-grained scapolite surrounds large strained diopside. Grain boundaries of diopside adjacent to the shear zones are granulated as shown by smaller highly undulose fragments, indicating a cataclastic deformation mechanism.

Diopside has typical pyroxene cleavage parallel to the C-axis but basal sections show two cleavage traces cross cutting at  $\approx 90^\circ$  to each other. Polysynthetic twinning and undulose extinction are not uncommon. In sample KK11 the diopside shows cruciform twins. In some cases the twin lamellae are developed in one portion of the crystal, indicating deformation. Kinking perpendicular to elongation is evident in some grains. Grain boundaries vary from straight to irregular.

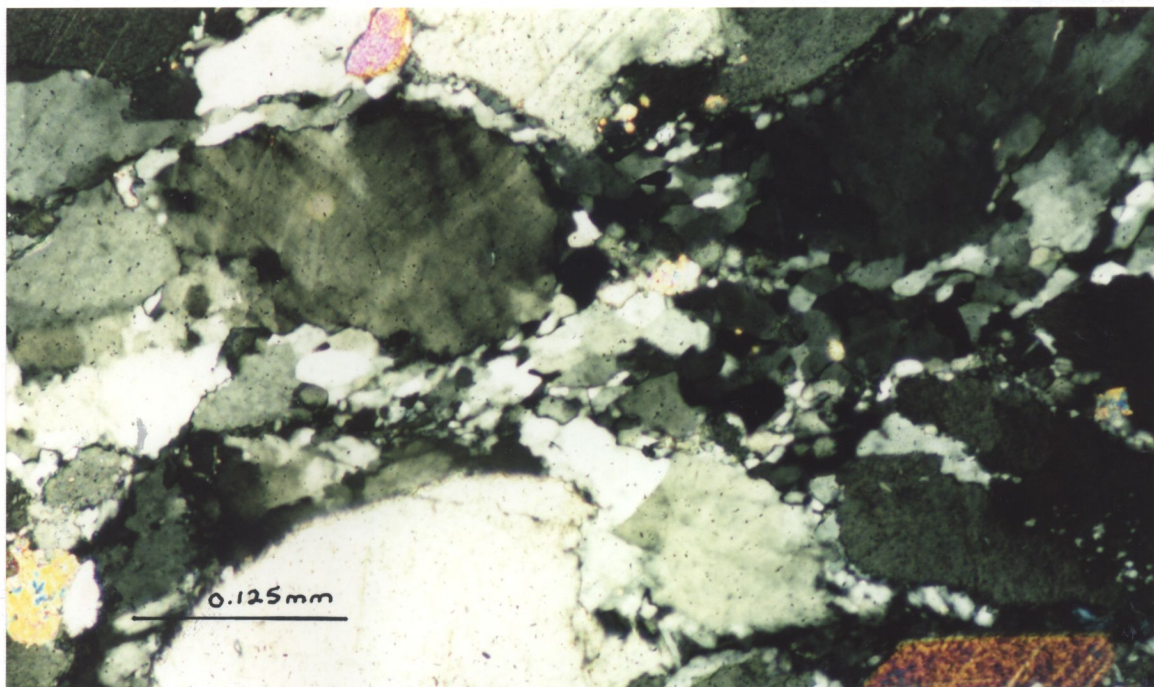


Plate 3.5: Photomicrograph of diopside-scapolite calc-silicate rock, showing dynamically recrystallised scapolite along discrete shear zones. Sample KK11, x200, CPL. CH260349.

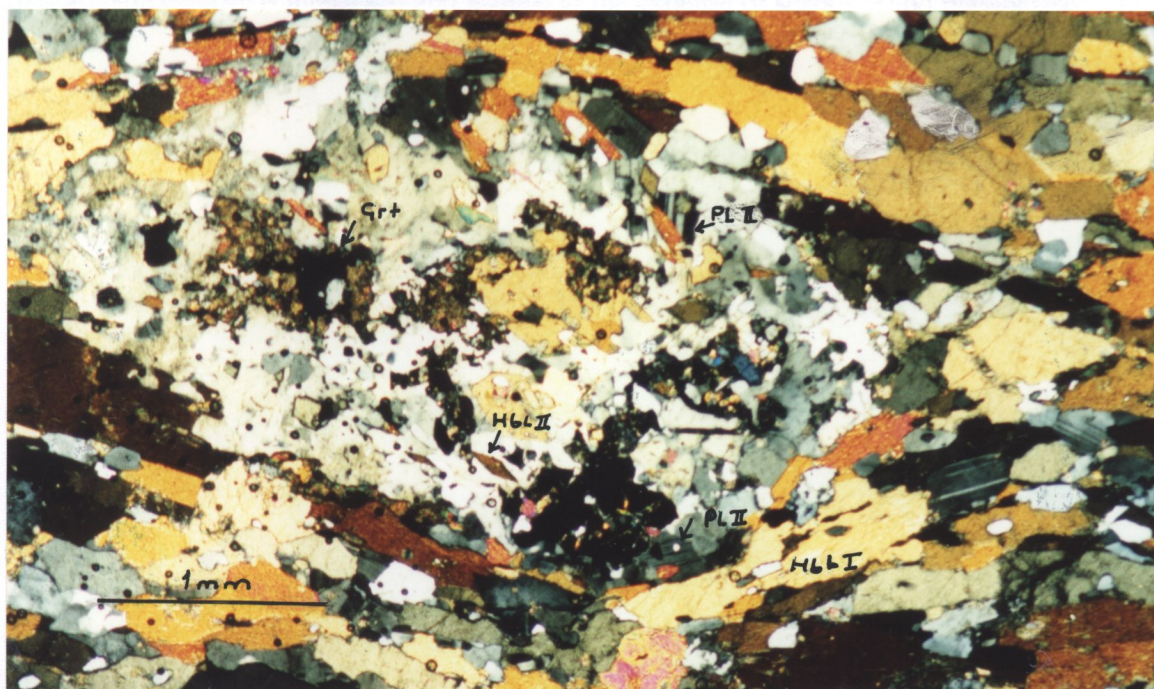


Plate 3.6: Photomicrograph of garnet amphibolite, showing a decompression texture indicated by remnants of garnet in the core surrounded by plagioclase II, hornblende II. Sample KK08, x25, CPL. CH219346.

Scapolite constitutes about 20% of the rock and occurs as porphyroblasts enclosing diopside in a pseudo subophitic texture. The grain boundaries are straight but the grains show undulose extinction. Cleavage is parallel to the long dimension of grains, but some sections show two cleavages at 90°. Epidote and phlogopite replace scapolite. Scapolite is distinguished from plagioclase ( $n=1.53$ ) by a slightly higher relief ( $n=1.54$ ). In sample KK11 scapolite is kinked perpendicular to foliation and in some grains, fractures at a high angle to foliation are filled by quartz. The composition of scapolite was not determined. Plagioclase is identified by its lower refractive index and slight turbid surface due to alteration. Twinning in plagioclase is vaguely discernible making An-content determination difficult. Some dark grey grains have cross-hatch twinning reflecting microcline.

Indigo blue epidote is interstitial and formed at the expense of scapolite and plagioclase.

### **3.2.5 Garnet amphibolites**

Garnet amphibolites consist mainly of parallel oriented prisms of green hornblende (75%) with interstitial plagioclase (15%) and quartz (5%) in elongate lenses. Garnet (5%) porphyroblasts are sparsely disseminated. Amphibolites that occur in association with carbonates contain scapolite, (sample KK08) whilst those in gneisses are devoid of the same mineral (KK110). The mineral composition of the amphibolites depends on the host rock. Basal sections of hornblende exhibit two characteristically intersecting cleavages and simple twinning. Other sections show one cleavage parallel to the long axis of the mineral. Hornblende defines the main foliation and lineation but a few hornblende prisms are oriented at a high angle to the

main foliation, defining a weak younger foliation. Some hornblende grains are retrograded to chlorite and zoisite along fractures and grain boundaries. In sample KK110, chlorite has preferentially developed along one of the cleavage traces. A discrete crenulation or kink cuts across the main foliation in the same sample. Hornblende and plagioclase along the crenulation band have broken down to an aggregate of chlorite, epidote and quartz.

Quartz occurs as single grains and aggregates stretched parallel to the foliation. The quartz grains show irregular grain boundaries and undulose extinction.

Plagioclase in sample KK110 exhibits deformation twins indicated by interfingering twins and bent twin lamellae. Some kinked porphyroblasts of untwinned albite are poikiloblastic with inclusions of hornblende, quartz, calcite, epidote and garnet. The internal fabric in the albite is parallel to the external fabric indicating that the albite is post tectonic. In sample KK08, the An-content of twinned plagioclase determined from growth twins ranges from  $A_{45-52}$  indicating andesine-labradorite composition. The plagioclase in the same sample is partly to completely replaced by scapolite.

Garnet is wrapped around by the hornblende foliation. The garnet has broken down to plagioclase, and to hornblende in gneiss-hosted-amphibolites and plagioclase, quartz, hornblende and biotite in carbonate-hosted-amphibolites. These assemblages are indicative of decompression (Plate 3.6). The hornblende and plagioclase represent second generation phases. The first generation phases occur in the foliation. The second-generation hornblende is idiomorphic.

In the carbonate-hosted-amphibolites a core of garnet with a corona of plagioclase, biotite, carbonate, epidote, hornblende, sphene and opaque minerals characterizes the decompression texture. The assemblage governed by decompression is wrapped around by the hornblende foliation indicating that garnets originally occurred as porphyroblasts pre-dating the foliation. The light brown biotite is associated with the decompression assemblage. However, biotite in the foliation occurs at the margins of hornblende after which it formed. In some places biotite occurs at the contact between hornblende and plagioclase. Biotite is itself being replaced by chlorite.

Scapolite porphyroblasts are associated with plagioclase both in the foliation and decompression assemblage. It is evidently forming at the expense of plagioclase. Some scapolite host inclusions of hornblende, epidote, carbonate and biotite.

Epidote is common as inclusions in scapolite and associated with garnet. The former case indicates that epidote predates the scapolite. In some instances, epidote forms large poikiloblasts enclosing carbonate, hornblende and biotite, but not scapolite. In some cases, epidote replaces plagioclase.

Sphene is quite abundant in the groundmass. In some cases it is closely associated with an opaque mineral, probably ilmenite.

Similarly the decompression assemblage in gneiss- hosted amphibolite consists of relic garnet in the core, surrounded by plagioclase, and blue-green actinolitic hornblende.

The garnet is further retrograded to chlorite along the fractures. Pale brown patches within and along margins of chlorite indicate that, the latter formed at the expense of biotite. This implies that the garnet had broken down to biotite during the decompression reaction and in turn retrograded to chlorite in a subsequent metamorphic event.

### **3.2.6 Mylonites**

Mylonites are generally developed in narrow discrete shear zones of varying sizes at several localities in the gneiss and quartzite. There are two lithologically distinct mylonites; quartzo-feldspathic mylonite and quartz mylonite with or without feldspar, garnet or kyanite. The mylonites formed in gneisses are characterized by marked grain size reduction, and a strong mylonitic foliation defined by alternating felsic and mica layers. Quartz ribbons and felsic aggregates define a stretching lineation. Similarly, quartz mylonites are characterized by a strong fabric defined by alternating flattened quartz and thin mica layers. Quartz grains define a strong stretching lineation.

#### **3.2.6.1 Quartzo-feldspathic mylonites**

Quartzo-feldspathic mylonites occur at very few widely spaced localities. For this reason, the description is based on few samples. In thin section the mylonites are invariably composed of fine- to medium-grained augen shaped feldspar porphyroclasts alternating with, quartz ribbons

and mica-rich layers, set in a fine-grained quartzo- feldspathic matrix. The matrix constitutes less than 10% of the mylonites. The foliation wraps around relatively large feldspar porphyroclasts. The mylonites are thus classified as protomylonites following the classification scheme of Sibson (1977).

Plagioclase occurs mainly as elongate or lens shaped felsic aggregates and to a lesser extent as single clasts. The plagioclase is either twinned or untwinned with intensities of alteration varying from one sample to the other. The breakdown of plagioclase is mainly due to sericitisation, though saussuritisation, indicated by a mixture of sericite, zoisite and carbonates is also evident.. The twin lamellae in the plagioclase are generally straight. The anorthite content of the plagioclase determined by the extinction angle method in sections perpendicular to X, showing the (001) cleavage trace ranges from  $An_{0-20}$ . This indicates a composition range from albite to oligoclase. The plagioclase is commonly fractured. In KK29, the fractures are oriented at a high angle to the foliation. Some plagioclase porphyroclasts are surrounded by small plagioclase grains, which are strongly undulose indicating marginal granulation (Plate 3.7).

Augen shaped felsic aggregates are composed of an equigranular intergrowth of mostly plagioclase and minor quartz with no apparent fabric orientation.

Individual grains and aggregates of quartz are drawn out into ribbons and elongate lenses, which define a strong sub-horizontal stretching lineation. In many cases, the ribbons wrap around plagioclase porphyroclasts. The ribbons are generally composed of an aggregate of



small elongate grains which are generally oriented parallel to the foliation, but occasionally and common in all the samples, the stretched quartz grains are oriented at an oblique angle to the long axis of the ribbon. The obliquity of the stretched grains to the shear plane indicates a ENE over WSW dextral shear movement (Plate 3.8). In sample KK100 the obliquity of the grains gradually grades into a granoblastic mosaic within the same ribbon aggregate. Some ribbons or lenses are composed of relatively coarse granoblastic quartz grains. The quartz grain boundaries in ribbons range from serrated to straight. Subgrains ranging in shape from elongate to small equant grains are common in quartz. In some cases feldspar is caught up in polycrystalline quartz ribbons and drawn into augens and lozenge shapes (samples KK101 and 29).

Generally the groundmass is relatively finer-grained than the porphyroclasts and composed of an intergrowth of 95% feldspar and 5% quartz. The plagioclase is severely altered to sericite (KK103 and 101) such that the texture is obscured. The grains are anhedral to subhedral. The majority of the plagioclase in the groundmass is twinned, though a few are untwinned or obscured by sericitisation. The groundmass plagioclase has the same composition as the porphyroclasts and exhibits deformation twins indicating low temperature crystal plastic deformation. Kinking is also evident in some plagioclase crystals. The quartz in the groundmass is strained. Isolated chlorite porphyroblasts occur in the groundmass (sample KK101).

Mica-rich zones are oriented parallel to the ribbons and wrap around the pophyroclasts. The mica-rich zones are composed of muscovite, brown biotite and subordinate chlorite. The biotite



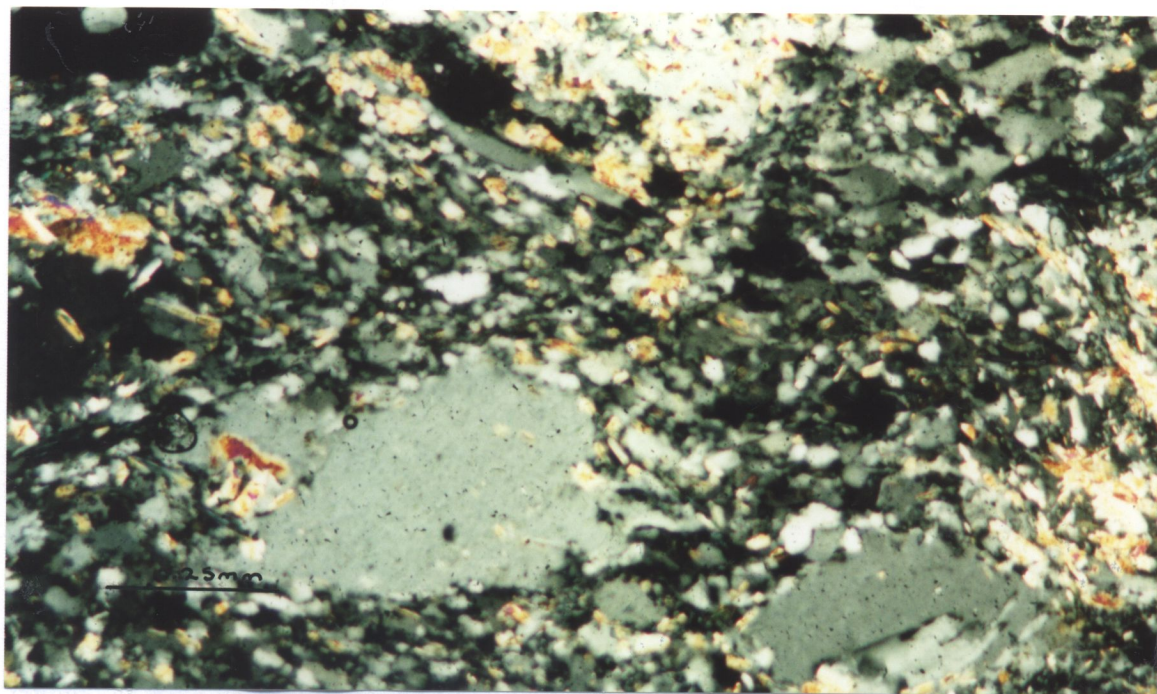


Plate 3.7: Photomicrograph of quartzo-feldspathic protomylonite, showing plagioclase porphyroclasts set in a fine-grained felsic matrix indicating marginal granulation. Sample KK18, x100, CPL. CH220358.

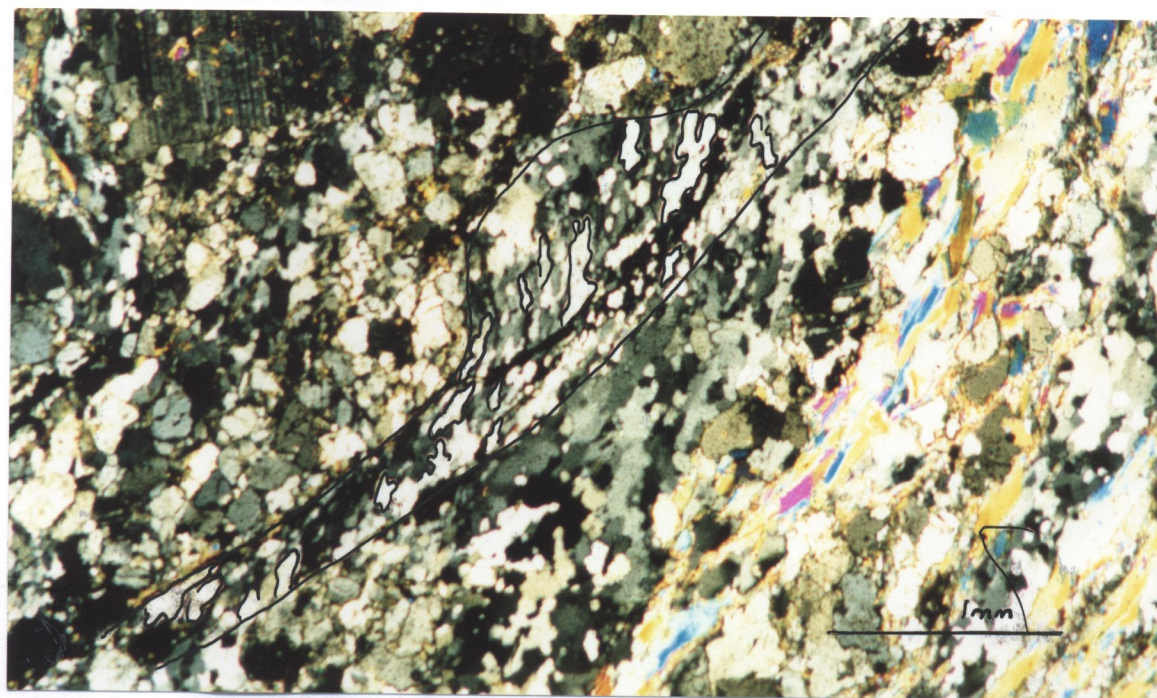


Plate 3.8: Photomicrograph of quartzo-feldspathic protomylonite showing oblique shape fabric in the quartz ribbon indicating dextral sense of shear. Sample KK100, x25, CPL. CH106351

is partly replaced by chlorite along the margins. Porphyroblasts of chlorite pseudomorph after biotite. In sample KK29, the replacement of biotite by chlorite was accompanied by a substantial formation of acicular rutile (Plate 3.9). The rutile generally occurs as needles radiating from the margins of chlorite. The formation of rutile may be explained by the breakdown of biotite at greenschist facies metamorphic conditions. Interstitial calcite is present in KK29. In KK100 mica-fish porphyroblasts occur in the mica rich zones.

K-feldspars in the mylonites occur in minor amounts (KK100). Accessory minerals are commonly epidote, zircon, apatite and rutile.

#### **3.2.6.2 Quartz-mylonite**

Quartz-mylonite is only represented by one sample (KK07). Outcrops along strike on the basis of aerial photograph interpretation could not be located. The outcrop coincides with the location (CH220348) of a aerial photograph linear feature, which was inferred to be fault.

The rock has a strong mylonitic foliation, defined by alternating layers of quartz aggregates and aligned muscovite, with sparsely disseminated stretched garnet porphyroclasts.

In thin section the rock consists of highly stretched quartz grains interspaced by layers of thin mica trails defining a foliation. A few (200-400  $\mu\text{m}$ ) garnet porphyroclasts are stretched in the foliation. Ovoid pseudomorphs of fine-grained aggregates of muscovite occur within mica-rich foliation. Tourmaline, zircon, and rutile occur in accessory amounts.

Quartz ribbons are composed of aggregates of stretched grains, which define a stretching lineation. The quartz grains exhibit strong undulose extinction due to deformation bands. Small equant new grains occur along the margins of the coarse quartz grains displaying core and mantle structures. These microstructures indicate dynamic recrystallisation.

Muscovite generally occurs as mica-fish indicating ENE over WSW dextral shear movement (Plate 3.10). The micas are commonly kinked perpendicular to the foliation.

The garnet is fractured and retrograded to chlorite.

### **3.6.2.3 Garnet-feldspar-quartz mylonite**

The rock is pinkish in colour, and possesses a mylonitic foliation defined by stretched quartz and aligned micas. The quartz ribbons define a strong oblique lineation. Pinkish garnet porphyroclasts are discernible in hand specimen.

In thin section the rock is composed of polycrystalline layers of recrystallised quartz grains (100-200  $\mu\text{m}$ ). The elongate quartz layers alternate with muscovite trails. Relatively coarse (up to 1 mm) augen to lozenge shaped porphyroclasts of feldspar are sporadically distributed throughout the section. Elongate-garnet porphyroclasts, fish-shaped sphene and tourmaline are minor constituents.

The quartz aggregates consist mostly of recrystallised grains exhibiting granoblastic texture, with subordinate grains showing irregular boundaries and weak undulose extinction. Some grains are composed of small (20-30  $\mu\text{m}$ ) euhedral equant subgrains. Most of the quartz show a uniform colour when a gypsum plate is inserted in Cross Polarised Light (CPL). This indicates that the grains have a strong Crystallographic Lattice Orientation (CLO).

Feldspar porphyroclasts comprise, plagioclase and microcline as shown by albite and cross-hatch twins, respectively. However, the twin lamellae are bent, tapered and are vaguely discernible. The feldspar porphyroclasts are lozenge shaped, with the long axis parallel or slightly oblique to the main foliation. The feldspars are altered to sericite around the margins and in some cases in strain shadows constituting tails or wings. The shape of the feldspar as noted in other sections indicates low temperature deformation mechanisms.

The asymmetric shape and stair stepping of the tails of the mica-fish structure indicate thrusting from SW to NE or top over bottom with a lateral strike-slip component (Plate 3.11).

A euhedral sphene porphyroblast possesses a fish-like structure with a slight obliquity to the main shear foliation, indicating dextral shear movement.

Garnet porphyroclasts are sparsely dispersed. They are fractured and retrograded to biotite or muscovite. Some small garnets are elongated parallel to the shear foliation. Most garnet porphyroclasts host small inclusions of quartz and feldspar. This indicates that the precursor rock was finer-grained than the present size, which is due to static recrystallisation.



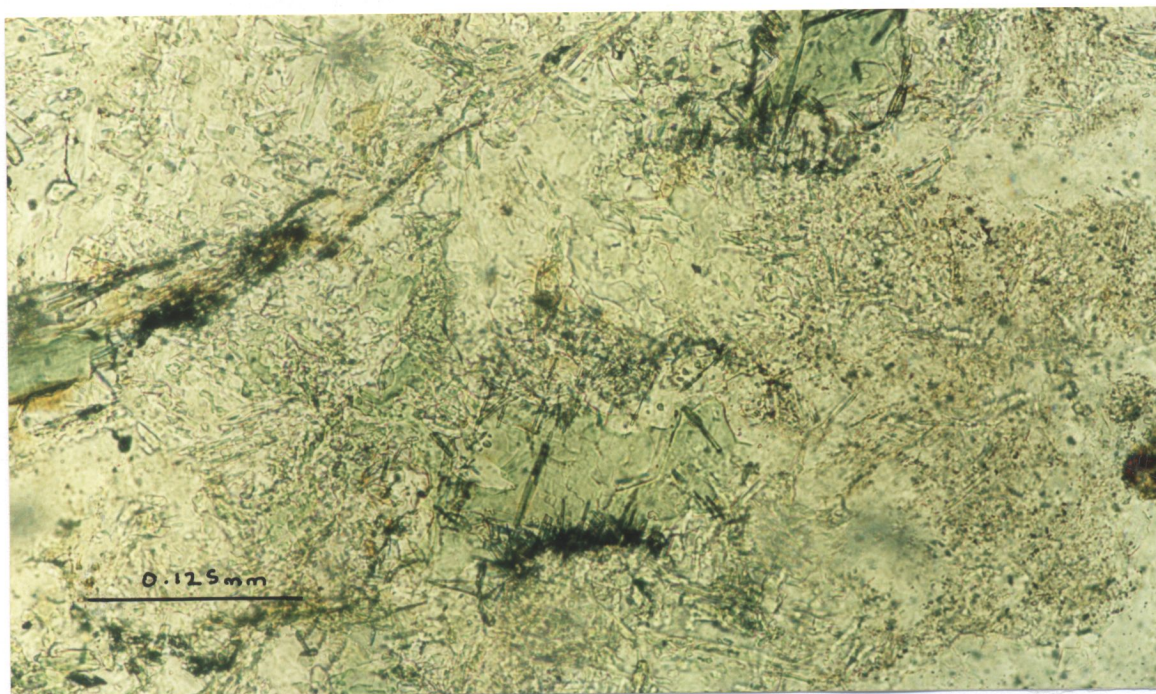


Plate 3.9: Photomicrograph of quartzo-feldspathic protomylonite, showing chlorite (pale green) with needle shaped rutile along its margins. Sample KK29, x200, PPL. CH216356.

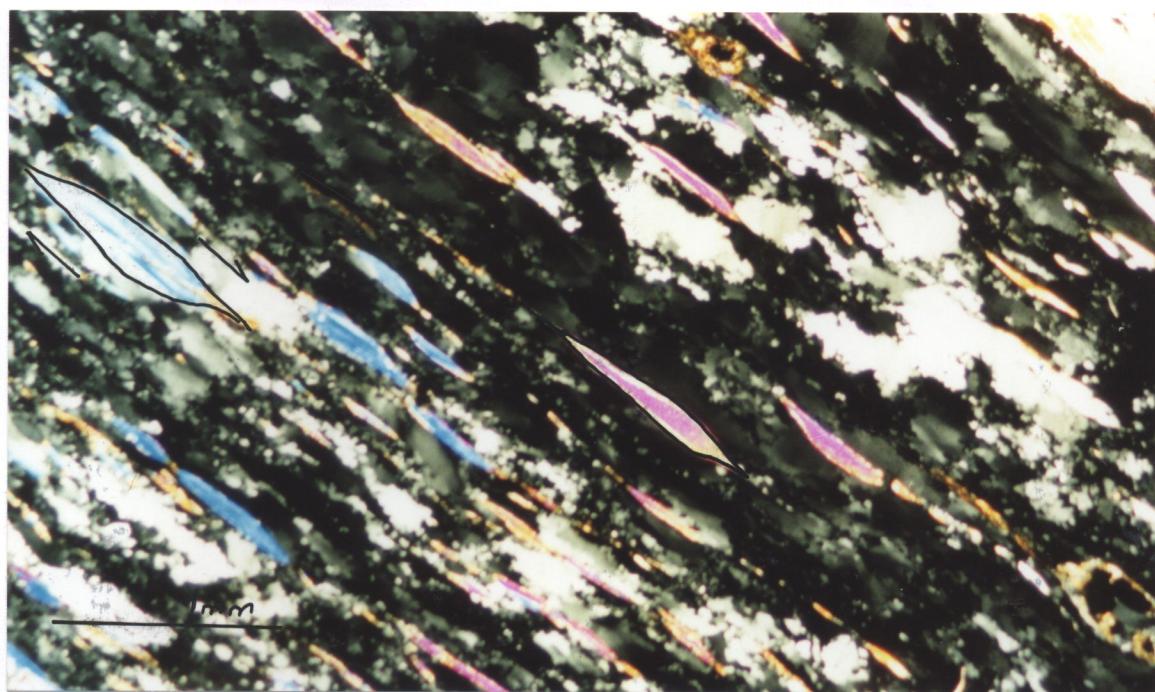


Plate 3.10: Photomicrograph of garnet-quartz mylonite, showing dynamically recrystallised quartz ribbons and mica-fish. The mica-fish indicates ENE over WSW dextral shear movement. Sample KK07, x25, CPL. CH220348.

#### **3.2.6.4           Tourmaline-quartz mylonite**

The rock consists predominantly of dynamically recrystallised ribbon quartz and elongate polycrystalline quartz (Plate 3.12). Tourmaline occurs in significant amounts.

The ribbons, consisting of individual quartz grains, are highly stretched and flattened. The grains are strongly strained as indicated by a strong wavy undulose extinction. In some grains the undulose extinction is due to deformation bands developed at a high angle to stretching axis.

Both ribbons and aggregates exhibit core and mantle structures shown by small (10-30µm) new grains around a core of strained quartz (Plate 3.12). Subgrains are not uncommon in most old grains. In some cases the ribbons or aggregates have completely dynamically recrystallised to a fine-grained aggregate (Plate 3.12. Lower left corner). The quartz grains show a strong CLO.

Tourmaline occurs as coarse fractured grains. Some fractures are v-shaped, perpendicular to the shear plane and filled in by quartz, indicating that the deformation was accompanied by pressure solution. Some studies have used v-shaped pull-apart fractures to deduce the sense of shear (Hippertt et al., 1993). This criterion could not be applied to these fractures because they are not consistent.



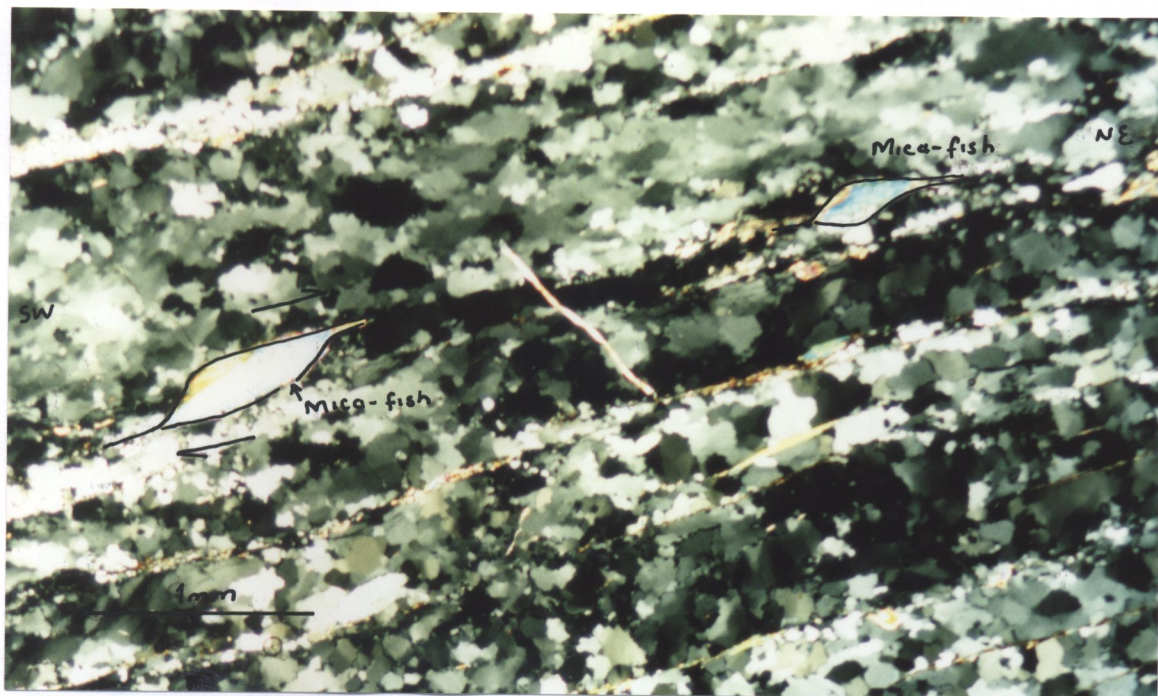


Plate 3.11: Photomicrograph of garnet-quartz-feldspar mylonite, showing dynamically recrystallised quartz. Mica-fish indicates SW over NE oblique thrust transport. Sample KK14, x25, CPL. CH217337.

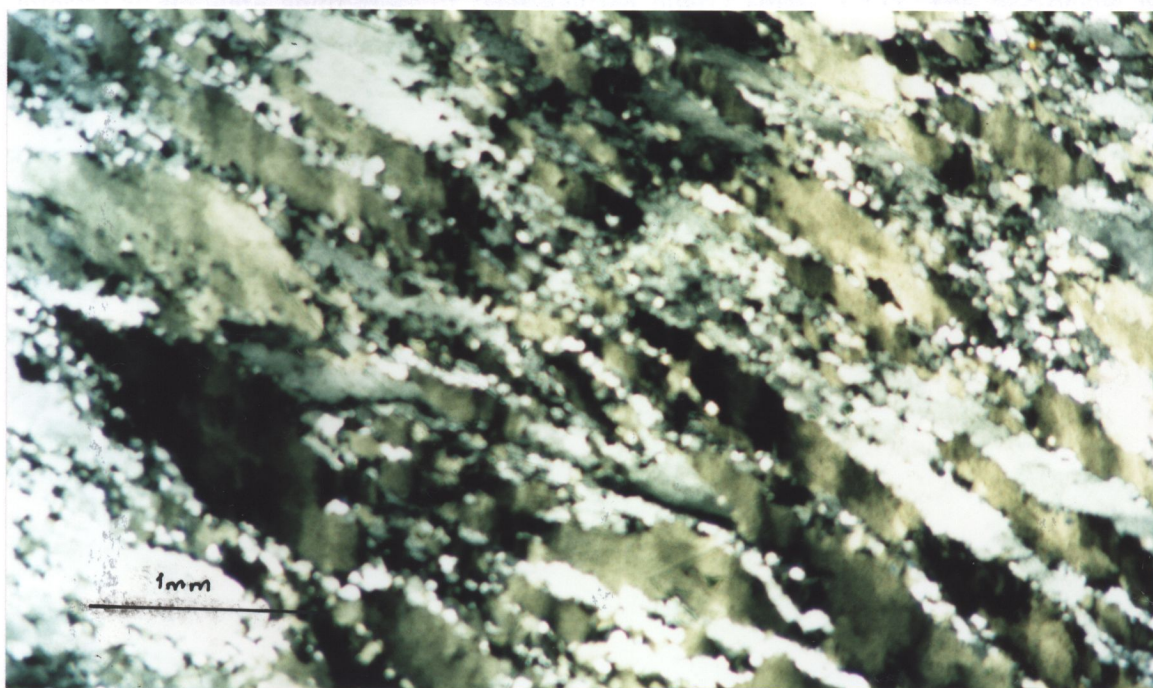


Plate 3.12: Photomicrograph of tourmaline quartz mylonite, showing dynamically recrystallised flattened quartz grains. Sample KK41, x25, CPL. CH301345.

Other tourmaline grains are not fractured and are zoned indicating that they have recrystallised to the present size.

### **3.3 Kabwe area**

#### **3.3.1 Mwomboshi gneiss**

##### **3.3.1.1 Less sheared biotite-muscovite-quartz-feldspathic gneiss**

At Nankuko quarry (KB442622), coarse-grained, weakly foliated quartz-feldspathic biotite gneiss is sheared along narrow discrete shear zones. The coarse-grained gneiss consists mainly of strained plagioclase, subordinate poikiloblastic microcline, and minor interstitial elongate aggregates of recrystallised quartz (Plate 3.13). The microcline has aligned twinned plagioclase, quartz and biotite indicating that it was introduced later by metasomatic processes.

##### **3.3.1.2 Sheared biotite-muscovite- quartz feldspathic gneiss**

The sheared derivative of the Nankuko quarry gneiss, is fine-grained and dark grey in colour. It is composed of alternating less sheared, felsic and more sheared biotite-rich zones.

The felsic zones consist mainly of plagioclase, microcline and interstitial quartz. Quartz in elongate aggregates and ribbons is unstrained and exhibits polygonal textures. Fine oriented inclusions of micas in quartz and granoblastic textures indicate annealing.



Plagioclase, which constitutes about 90 % of the feldspars is generally untwinned and moderately altered to sericite in the cores, but in some instances, the grains breakdown to sericite, carbonate, quartz and epidote. Small strongly undulose grains feldspars around porphyroclasts of plagioclase and microcline indicate grain size reduction by cataclastic deformation. Isolated carbonate grains are interstitial and also occur along fractures in feldspars.

Biotite-rich zones consist mainly of fine green biotite and subordinate muscovite defining S-C fabrics (Plate 3.13). The quartz and feldspar are finer grained than in the felsic zones, but a few porphyroclasts of feldspars are present. The finer grain size is attributed to comminution during shear movement. S-C fabrics are well developed in the finer-grained zones. Chlorite is developed along C-planes as a secondary mineral (Plate 3.13).

Another group of sheared rocks along the Munyama river are also dark, fine-grained and strongly foliated. They are composed of small augen shaped porphyroclasts of K-feldspar and plagioclase set in fine-grained micaceous matrix. Some microcline porphyroclasts have smaller strained grains around them, indicating marginal granulation. Other samples consist mainly of sericitised plagioclase with subordinate amounts of microcline. Most of the microcline encloses smaller grains of slightly sericitised, twinned plagioclase and quartz (Plate 3.15), suggesting that they formed by metasomatic processes.

The matrix consists of an intergrowth of quartz, feldspar, and oriented micas. The feldspars exhibit strong undulose extinction whilst the quartz is unstrained.

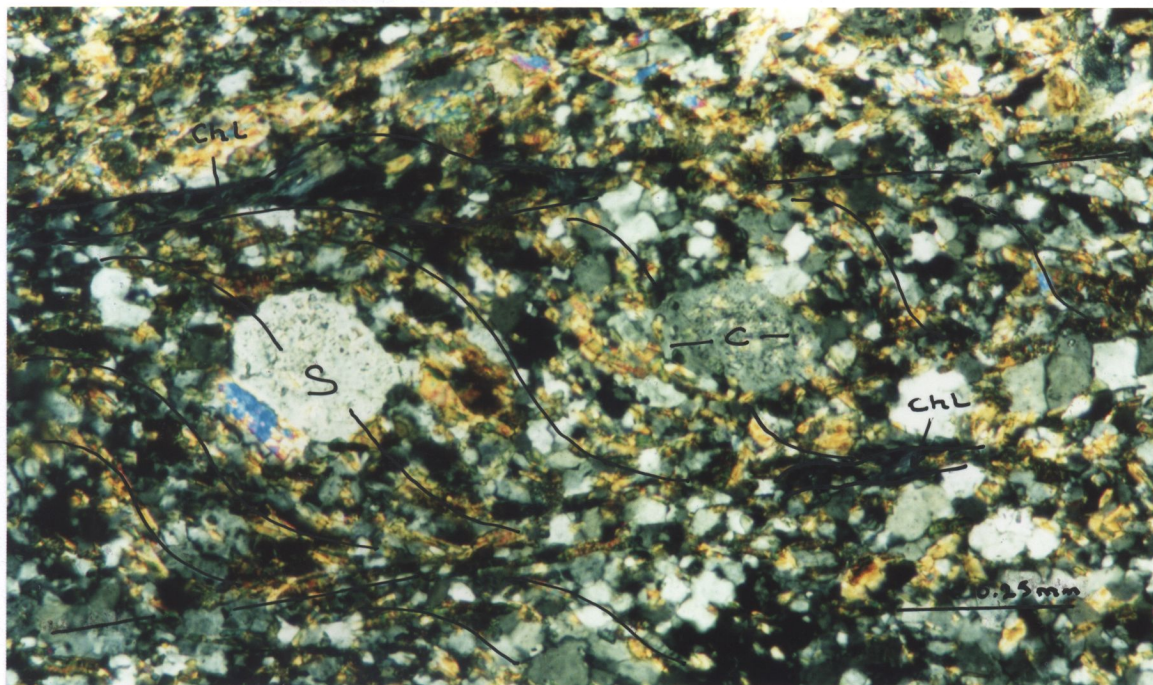


Plate 3.13: Photomicrograph of sheared quartzo-feldspathic biotite gneiss at Nankuko quarry, showing S-C fabrics. Chlorite has grown along the C-planes. Chl-chlorite. Sample CK76, x100, CPL. KB442622.

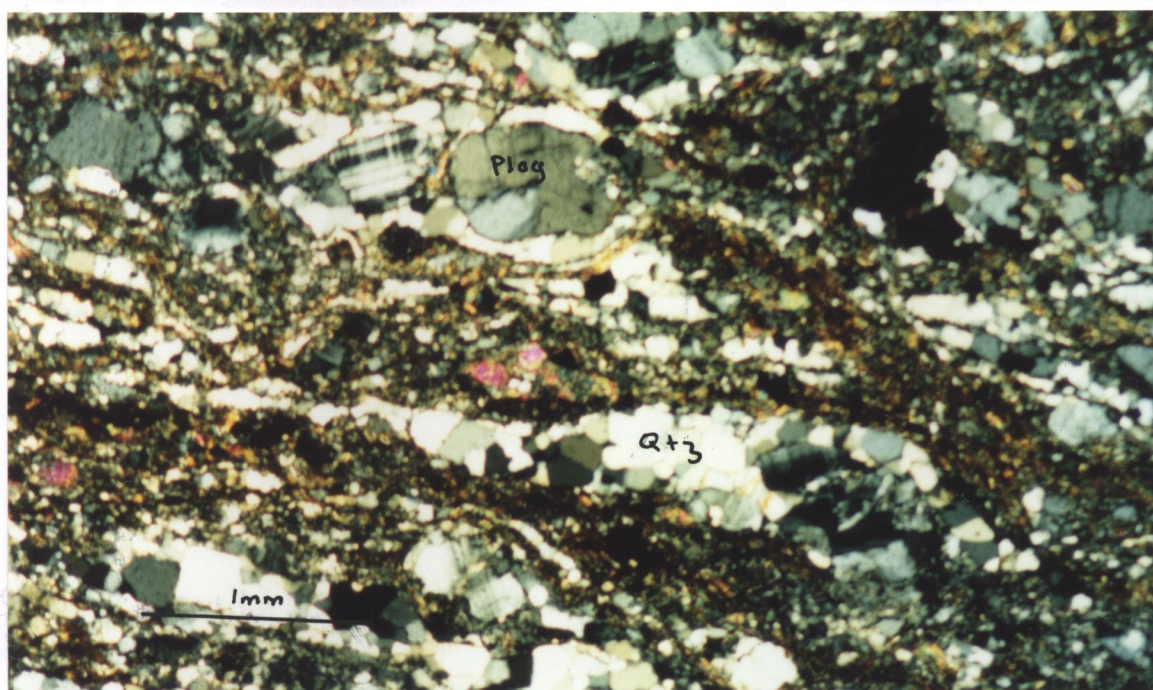


Plate 3.14: Photomicrograph of protomylonitic augen gneiss showing quartz ribbons flowing around plagioclase. Note fined-grained crushed groundmass. Sample CK58, x25, CPL. KB541695

The presence of strain free quartz suggests recovery after deformation.

Sample CK11 has two foliations defined by muscovite and subordinate green biotite. The muscovite mostly occurs in the main foliation and in discrete narrow shear zones, suggesting that the mineral grew as a result of breakdown of feldspars during shearing. Some fine-grained unstrained biotite is seen to form at the expense of muscovite, indicating a thermal event after shearing. The new biotite is aligned parallel to the main foliation. The subsequent event is considered to be accompanied by recrystallisation of quartz in the gneisses. A weak foliation wraps around microcline and deflected at low angle into the shear foliation. Fine-grained anastomosing shear zones cross-cut relatively coarse-grained gneiss (Plate 3.16). The zones consist of quartz, feldspar, muscovite and small amounts of greenish-brown biotite. Two types of greenish-brown biotite can be distinguished; randomly oriented biotite and biotite oriented parallel to the foliation. The fine-grain size in these zones is due to cataclastic deformation (Plate 3.16). Shear movement in the rock therefore took place along discrete zones.

Accessory minerals commonly include sphene, epidote, and Fe-oxides, apatite and allanite.

Stretched xenoliths occur within sheared gneiss at KB536726. The xenoliths have a fine-grained, granular texture, and are darker in colour than the host. The xenoliths consists of about 40-50% plagioclase, 25-30% biotite, 15-20% quartz and minor microcline. sparsely distributed apatite and epidote.

Most of the plagioclase is partly sericitised with some grains twinned on the albite and carlsbad twin laws. Cleavage (010) at right angles to twin laminae is discernible in some grains. Biotite and relatively finer grained quartz, showing polygonal texture, occur as interstitial minerals to plagioclase. The biotite imparts the dark colour to the rock. As in the host rock, two generations of the biotite were distinguished: an older strongly pleochroic, light brown to dark greenish-brown biotite showing kinking and 'birds eye' deformation textures, and a younger undeformed weakly pleochroic dark greenish-brown variety. The older biotite is associated with muscovite, which it appears to be replacing. Muscovite also shows deformation textures.

Relatively coarse, fractured, elongate porphyroblasts of apatite are sparsely distributed in the rock. In some places, the porphyroblasts are surrounded by crystalline quartz. Similar grains were observed in the host rock.

On the basis of modal contents of quartz-plagioclase-K-feldspar, coupled with the abundant biotite, the rock approximates the modal composition of a tonalite on the APQ classification diagram of igneous rocks.

### **3.3.1.3 Biotite-muscovite schist**

Schistose rocks occur in the Mwomboshi gneiss in narrow E-W trending zones ranging in width from 3-10m. The rocks are generally weathered. The schists are dark, strongly foliated, finer grained, and have a higher proportion of micas compared to the adjacent gneiss. They are composed of elongate felsic aggregates with few augen-shaped

porphyroclasts, set in a mica-rich groundmass. The schistosity is defined mainly by muscovite with minor biotite. Porphyroclasts of both micas are sparsely distributed throughout the rock. Coarse flakes of micas are kinked. Small biotite flakes are post-tectonic, as they seem to be forming at the expense of muscovite.

The constituent minerals exhibit microstructures, which indicate that grain size reduction was predominantly by cohesive cataclastic flow. In sample CK21, mica rich zones consist of an intergrowth of randomly oriented small micas, mainly muscovite, with subordinate amounts of brown biotite. This suggests that a later, probably second, cataclastic shear movement overprinted an earlier deformation along the foliation. Felsic bands are composed mainly of recrystallised quartz with subordinate amounts of highly sericitised plagioclase. Isolated smaller aggregates of quartz show triple junctions. Sample CK61 consists of elongate aggregates of quartz and feldspars, and augen feldspars, set in a groundmass composed chiefly of a crushed aggregate of fine-grained feldspar and subordinate quartz, with parallel orientated micas, mainly brown biotite and some muscovite. The elongate aggregates of quartz and feldspars define a lineation. Porphyroclasts of feldspars generally show deformation twins. Growth twins with straight and relatively wide twin lamellae are preserved in some grains. The felsic aggregate lineation is developed parallel to the strike, which indicates lateral shear movement. However, no shear sense indicators were observed. The feldspar porphyroclasts are strained, fractured and show strong undulatory extinction. Fine isolated grains showing strong undulose extinction indicate granulation along the margins. The matrix is made up of irregularly shaped grains, of feldspars with strong undulose extinction while quartz



grains are generally strained with few recrystallised grains meeting in triple junctions. Though some of the grains in the groundmass, particularly quartz, have recrystallised, the cataclastic texture is still retained.

Accessory minerals include sphene, opaque minerals and epidote in decreasing order of abundance.

#### **3.3.1.4 Protomylonitic fine-grained augen gneisses**

Protomylonitic gneisses are composed of ribbon-shaped felsic aggregates and augens set in a micaceous matrix, which constitutes up to 50% of the rocks. The ribbon-shaped aggregates and the fine micas in the matrix define a weakly crenulated foliation. The rocks exhibit microstructures indicative of deformation predominantly by cataclastic mechanisms. The matrix of some gneisses (samples CK58 and 55) are composed of irregularly shaped, granulated grains showing strong undulose extinction. Fine flakes of biotite and muscovite define the main foliation (Plate 3.14). Porphyroclasts of feldspars are characterized by granulation, grain-scale fractures, and deformation twins.

The ribbon-shaped aggregates define a lineation, which plunges steeply to the south, down dip. This suggests that the protomylonitic gneisses were formed during steep to vertical movement in high angle thrusts.

In handspecimen CK58, augen shaped porphyroclasts (1-2 mm), are finer than in the other samples and consists mainly of discrete clasts and aggregates of feldspar. The feldspar is mainly plagioclase with subordinate microcline. Most of the feldspars exhibit deformation twins characterized by thin tapering twin lamellae. In thin section ribbon-shaped aggregates of quartz oriented parallel to the foliation, are mostly **one or two grains** wide, and in many cases flow around relatively coarse rigid porphyroclasts (Plate 3.14), suggesting that they are syntectonic with respect to the foliation. In some cases relatively large equant, ribbon-shaped quartz aggregates constitute tails of feldspar porphyroclasts (Plate 3.14). The porphyroclast system (Passchier and Simpson, 1986) resembles  $\sigma$ -type porphyroclasts. In the studied rocks, these indicate a south over north thrust transport or reverse shear movement. The matrix, which constitutes about 50% of the rock, is composed of fine-grained felsic minerals and abundant oriented micas flowing around the porphyroclasts. The felsic grains are granulated and strained. The mica is mainly greenish brown biotite with subordinate muscovite and both show kinking and 'birds eye' textures. In some cases muscovite is evidently being replaced by the biotite.

Sample CK55 contains relatively larger porphyroclasts and less mica than CK5 (Plate 3.14). The grain size variation corresponds to the intensity of shearing. Deformation twins and kink bands are common in plagioclase and microcline respectively. Some of the untwinned clean microcline contains small irregularly shaped blebs of probably albite. Other relatively large untwinned feldspars display a patched perthitic intergrowth shown

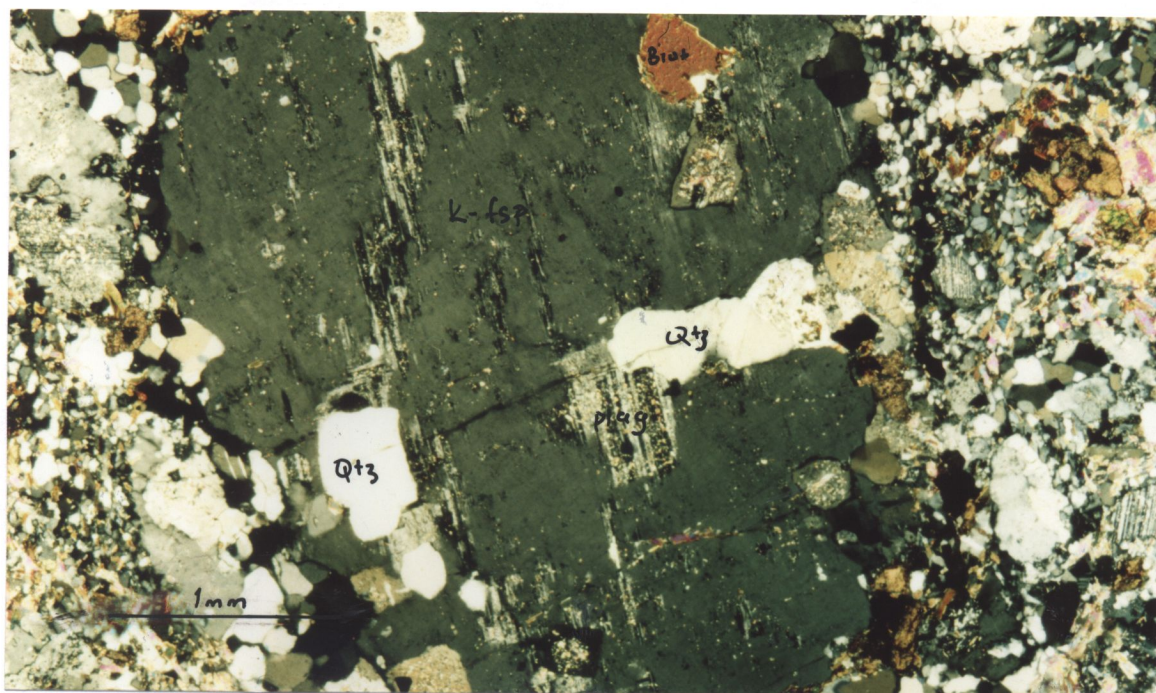


Plate 3.15: Photomicrograph of sheared biotite-muscovite gneiss showing perthitic feldspar with inclusions of quartz, biotite and exsolved twinned plagioclase. Qtz-quartz, K-fsp: K-feldspar. Sample CK17, x25, CPL. KB536726

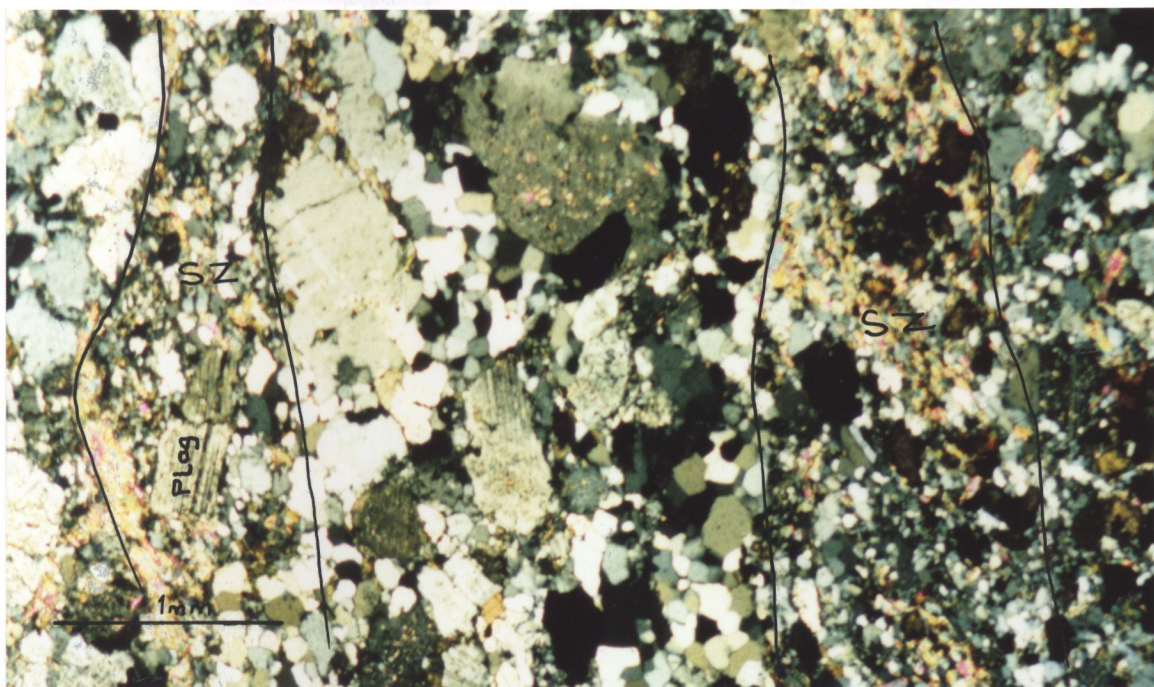


Plate 3.16: Photomicrograph of sheared biotite-muscovite gneiss showing discrete narrow shear zones separated by an unsheared portion. Note fractured plagioclase in the zone on the left side. SZ-shear zone, plag-plagioclase. Sample CK17, x25, CPL. KB536726.



by smaller twinned plagioclase enclosed in the host feldspar. The feldspars are granulated around the margins.

Sample CK66, is composed of parallel oriented elongate felsic aggregates with a few slightly coarser porphyroclasts set in a medium-grained more or less equigranular groundmass of slightly sericitised plagioclase. Micas are subordinate and lie in the foliation plane. The groundmass is composed predominantly, of medium-grained equigranular plagioclase and minor amounts of microcline. Grain boundaries between the plagioclase grains are generally lobe shaped (Plate 3.17) and in some cases, diffuse. The lobe shaped boundaries are due to grain boundary migration, which is indicative of incipient marginal recrystallisation. Some of the plagioclase show myrmekitic intergrowths along boundaries with microcline (Plate 3.17) whilst others enclose irregularly shaped blebs of quartz.

The development of myrmekite along grain boundaries parallel to foliation is probably strain-induced. In some places, abundant exsolved blebs or veins give an impression of a fine-grained matrix.

### **3.3.1.5 Laminated feldspathic quartzite**

Laminated quartzites occur in steep to vertical narrow zones with an ENE trend. The rocks have a laminated appearance due to alternation of quartz and quartzo-feldspathic laminae. The quartz laminae are slightly coarser-grained than the felsic laminae probably due to annealing.

The quartz laminar consists of a mosaic of interlocking recrystallised quartz grains with straight to slightly curved boundaries meeting in triple junctions. Occasional elongate lenses of turbid feldspars occur within the quartz laminar. Small flakes of fresh green-brown biotite are sparsely disseminated and define a foliation, which is parallel to the lamination. Relatively larger flakes of muscovite showing birds eye texture are associated with the biotite.

The finer-grained quartzo-feldspathic laminar consists of quartz and feldspar in almost equal amounts. The quartz grains are unstrained and exhibit polygonal texture. Feldspars are slightly altered and elongated parallel to the foliation. Deformation twins are evident in some plagioclase grains. Micas, mainly muscovite, are relatively more abundant in these laminae than in the quartzitic ones. Isolated small grains of epidote are common in the quartzo-feldspathic laminae. The boundaries between the quartzo-feldspathic laminae and quartzitic laminae are transitional. The abundance of muscovite in the quartzofeldspathic laminae suggests breakdown of feldspar during shear movement. The shear movement is considered to have taken place along quartzo-feldspathic laminae.

#### **3.3.1.6 Muscovite quartzite**

The rock is pinkish white in colour, and is characterized by alternating (1mm) thick quartzite and (3 mm) thick feldspathic laminae. Quartzite laminae consist of large recrystallised, interlocking, slightly flattened quartz (Plate 3.18). The feldspathic laminae are relatively finer-grained consisting of (0.5-1 mm) large quartz and occasional feldspar

and sparsely distributed small muscovite flakes aligned parallel to the long axis of the quartz.

The quartz grains exhibit serrated (Plate 3.18) boundaries and strong undulose extinction due to development of deformation bands. The deformation bands in the majority of the grains are oriented parallel to the foliation. The grains, particularly quartz, exhibit a shape-preferred orientation due to slight flattening. The grains show different colours when a gypsum plate is inserted, indicating that they have different crystallographic lattice orientation (Spry, 1969). Mica inclusions in quartz define a strong fabric. The mica inclusions suggest annealing of quartz (Plate 3.18).

Accessories include tourmaline, epidote and opaque minerals. Small subhedral-anhedral detrital grains of tourmaline are sparsely distributed through out the rock. Larger tourmaline grains are also present.

The parallel orientation of deformation bands and foliation suggest that the fabric elements are syntectonic. The grains with deformation bands oriented oblique to the foliation were unfavourably oriented during their development. Development of deformation bands indicate dislocation slip at low temperatures, whilst the formation of serrated grain boundaries are a sign of incipient marginal recrystallisation at relatively higher temperatures (Hobbs et al., 1976).

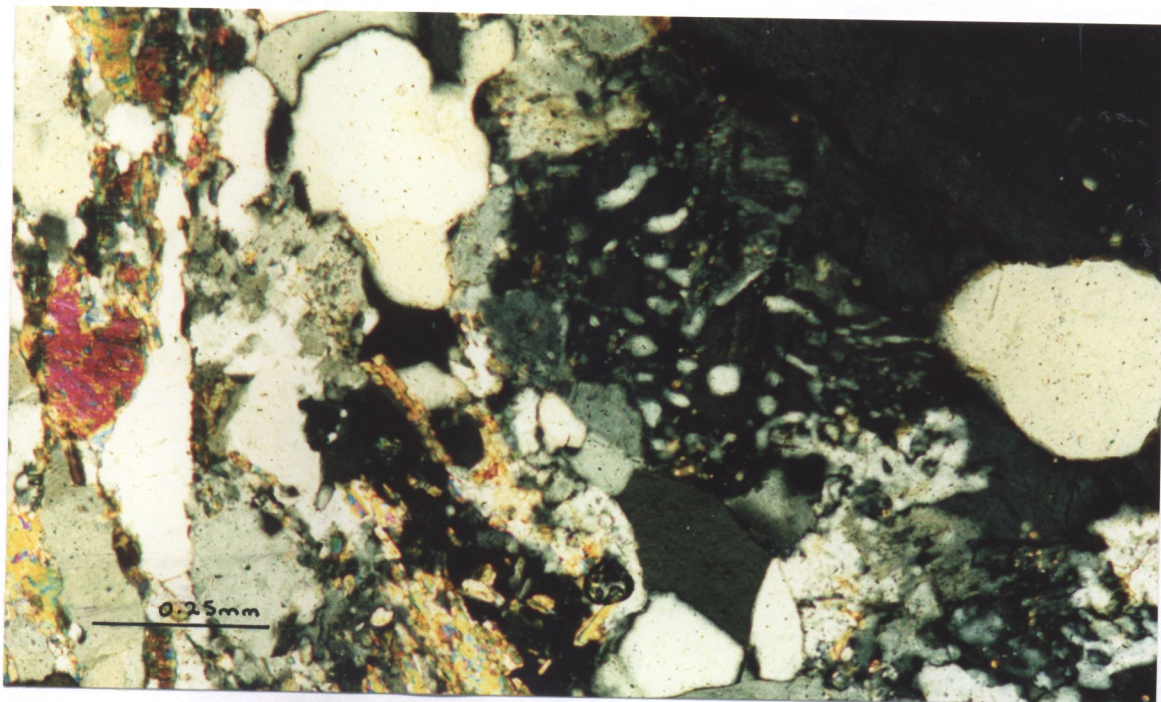


Plate 3.17: Photomicrograph of protomylonitic augen gneiss showing myrmekitic intergrowths between plagioclase and microcline on grain faces parallel to the foliation. Sample CK66, x100, CPL. KB552677.

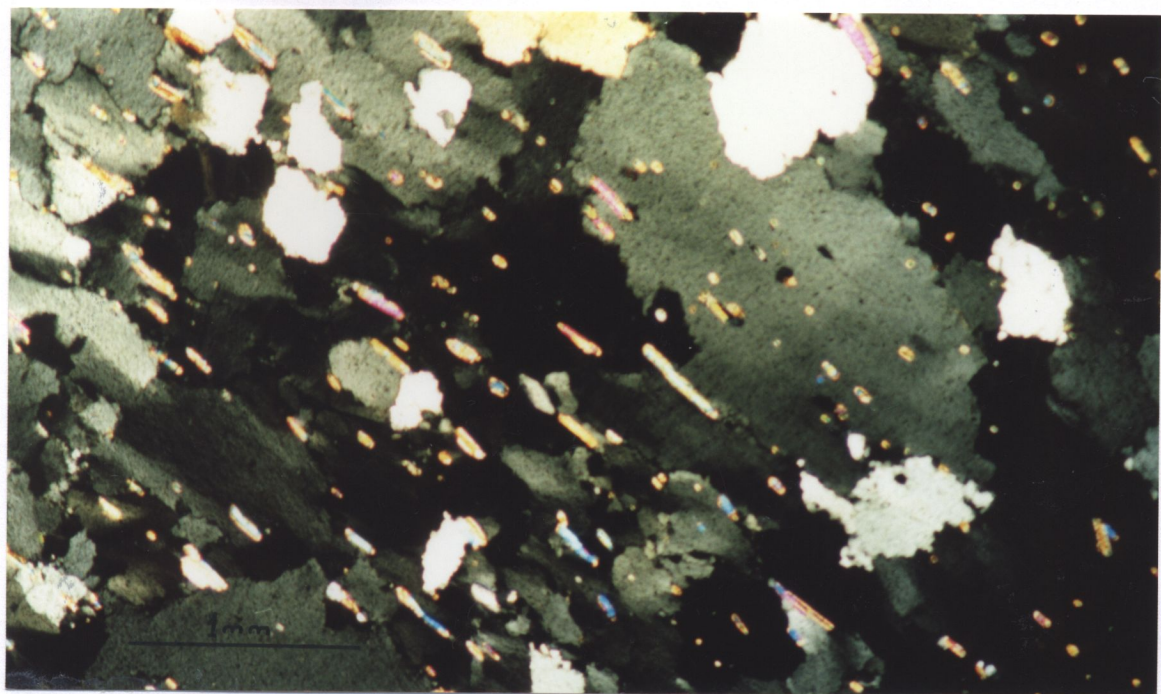


Plate 3.18: Photomicrograph of muscovite quartzite showing serrated grain boundaries and fine oriented muscovite inclusions in quartz. Sample CK90, x25, CPL. KB383496

The large tourmaline is probably post tectonic, as they are not fractured. The presence of the detrital tourmaline suggests a sedimentary origin of the quartzite rather than a product of intense shearing of the Mwomboshi gneiss.

#### **3.3.1.7 Chlorite-epidote hornblende schist**

The rock is fine to medium-grained, greenish in colour and schistose, with disseminated elongate felsic aggregates.

The rock is composed mainly of preferentially oriented bluish-green hornblende set in a fine-grained groundmass. S-C fabrics indicate west over east sinistral lateral sense of movement (Plate 3.19). Hornblende (80%) is bent, kinked and fractured indicating cataclastic deformation. Amphibole porphyroclasts are wrapped around by the foliation.

Large porphyroblasts (300  $\mu\text{m}$ ) of twinned and untwinned plagioclase constitute about 10-15% of the rock. Some of the plagioclase enclose small laths of amphiboles oriented parallel to the external foliation. This indicates that the feldspar is post or late syntectonic, whilst others are pre-tectonic as they are wrapped around by the main foliation.

Elongate clusters of sphene are distributed throughout the rock parallel to the foliation. These clusters of sphene, which in some places are associated with opaque minerals, appear to have been derived from the breakdown of another mineral (not identified), which has been completely replaced.

The C-planes are composed of fine-grained quartz, albite, zoisite, and chlorite, which formed at the expense of hornblende and plagioclase (Plate 3.19). The quartz /albite and zoisite are strained as shown by strong wavy undulose extinction, indicative of low temperature crystal plastic deformation. Chlorite is post-tectonic as it does not show deformation textures. In some C-planes, fine and coarse flakes of chlorite occur together with zoisite. The occurrence of chlorite is restricted to these zones and seems to have formed after the amphiboles and biotite. Brown biotite is minor and is noted to be replacing the amphiboles. Zoisite occurs as fine disseminations in the groundmass with the fine-grained variety being due to granulation during shear movement.

### **3.3.2 Chikonkomene Formation**

#### **3.3.2.1 Sericitic quartzite**

Sericitic quartzite constitutes the bulk of the Chikonkomene metasediments. The rock is generally thinly bedded ( $S_0=S_1$ ) varying from 5-10 cm.  $S_0$  is primary layering and  $S_1$  is a layer parallel foliation. The bedding is cross-cut by a shallow dipping fracture cleavage ( $S_2$ ) defined by copper-coloured and white micas.

The quartzites consist of sub-angular porphyroclasts of quartz set in a fine-grained matrix of recrystallised quartz intervened by trails of muscovite along the foliation,  $S_0=S_1$ .  $S_0$  is indicated by an alignment of opaque grains along  $S_1$ . Accessories include tourmaline, and sphene. The main foliation is weakly crenulated, resulting in a poorly developed



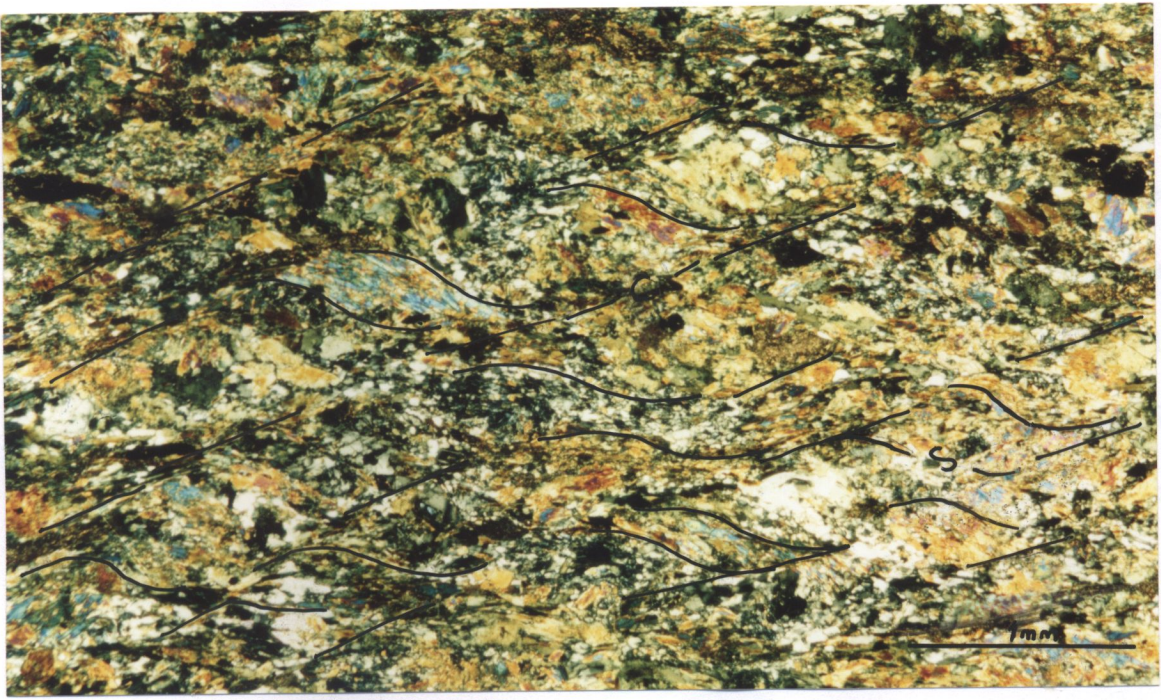


Plate 3.19: Photomicrograph of hornblende schist showing S-C fabrics indicating sinistral sense of shear. Sample CK65, x25, PPL. KB552679.

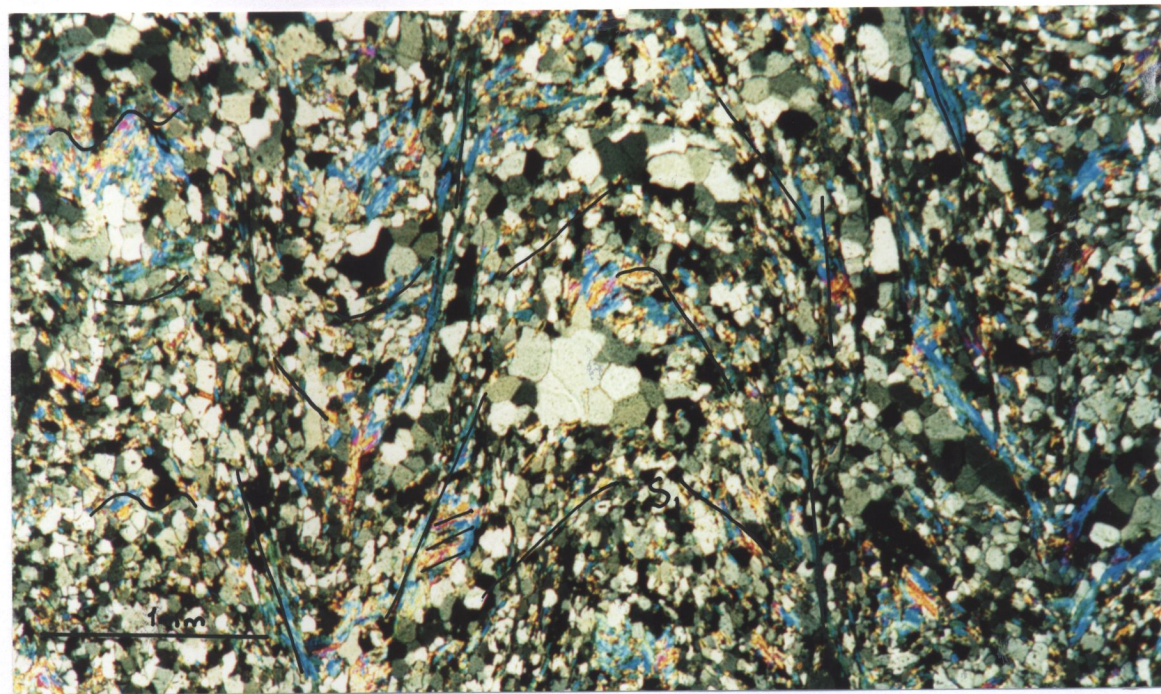


Plate 3.20: Photomicrograph of muscovite quartzite showing crenulated  $S_1$  and crenulation cleavage  $S_2$  and recrystallised clasts of quartz aggregates. Sample CK40, x25, CPL. KB562777.

crenulation cleavage,  $S_2$  (Plate 3.20). Some quartzites have a wide range of grain sizes of porphyroclasts set in a finer-grained matrix of a granoblastic mosaic of recrystallised quartz grains. The composition of rounded to elongate clasts range from quartzite, meta-siltstone with abundant opaque minerals, tourmaline-rich psammitic quartzite and single clasts of strained quartz surrounded by unstrained grains. The clasts are stretched along  $S_1$  and in some cases transposed into  $S_2$ . Trails of opaque minerals enhance the outline of microfolding. Porphyroclasts in a fine-grained matrix may also indicate an originally poorly sorted sedimentary texture, however, optically continuous quartz overgrowths are not present indicating that the rock has certainly undergone static recrystallisation. Laboratory experiments have demonstrated that fine-grained aggregates have lower strengths than their coarser grained counterparts (Tullis and Yund, 1985) and it follows therefore, that former take up more strain and undergo cyclic recrystallisation. Some quartzites have very few porphyroclasts. Samples CK32 and 34 have the same mineralogical composition, but only differ in grain size, with the latter being finer grained and containing more muscovite. Porphyroclasts, in sample CK34, are generally rounded but some are elongate in shape and comprise mainly recrystallised quartz aggregates and strained grains in some places, whilst those in CK32 exhibit strong undulose extinction. The quartzites, particularly the fine-grained variety accommodated strain predominantly by thermally activated crystal-plastic mechanisms.

In some places (e.g. KB532777) the muscovite quartzite is sheared to a fine-grained, dark phyllitic quartzite along narrow zones (Plate 4.21). The phyllitic quartzite consists mainly of fine-grained muscovite, quartzite and opaque minerals in decreasing order of



abundance. The muscovite and opaque minerals define three foliations  $S_0=S_1$ ,  $S_2$  and  $S_3$ .  $S_0=S_1$  is crenulated and occurs in the microlithons of the main  $S_2$  crenulation cleavage. Crenulation of the main foliation produced a weak  $S_3$  cleavage (Plate 3.21).

### **3.3.2.2 Iron-banded quartzite**

The sericitic quartzite grades into iron-banded quartzites with an increase in the abundance of iron oxides. The mineralogical composition and texture are the same.

At locality KB454773, kyanite pods occur within iron-banded quartzite. The pods are massive and composed of randomly oriented pale blue-green kyanite laths up to 2 cm in length, embedded in a quartzitic matrix. A network of purple veinlets of fluorite intrudes the iron-banded quartzite and kyanite.

In thin section, the pods are composed of kyanite, fluorite, quartz and iron oxides. The kyanite laths are generally randomly oriented (Plate 3.22), though some show a certain degree of alignment. The kyanite is kinked, fractured and shows undulatory extinction. In some grains, the kyanite is downgraded to sericite. Multiple simple twinning is common in the kyanite, probably related to deformation. Some large porphyroblasts of kyanite enclose small grains of quartz, and muscovite indicating their late development.

Purple coloured fluorite prisms radiate from the centre of the veinlets. The veinlets are certainly late as they cut across the rock in all directions.

Strained muscovite grains are randomly oriented in the quartzite matrix and generally occur at the grain boundaries of granoblastic quartz. In some cases, the muscovite forms a mantle around kyanite indicating retrogression.

The groundmass consists of a mosaic of unstrained granoblastic quartz. The quartz grains host sericite possessing a strong fabric. Opaque grains are closely associated with sphene and follow undefined trails. Untwinned plagioclase (albite) occurs in small amounts.

### **3.3.2.3          Tourmaline quartzite pebble**

Tourmaline quartzite cobbles-pebbles are dark and fine-grained. They consist of rounded aggregates, and elongate lenses of quartz grains set in a matrix of fine-grained granoblastic quartz and relatively finer-grained pale green pleochroic needles of tourmaline.

The rounded aggregates are composed of relatively coarse-grained quartz showing rather weak undulose extinction. Recrystallised quartz grains in elongate porphyroclasts, display a polygonal texture and are unstrained.

The matrix is composed of a pale green pleochroic aggregate of small acicular to prismatic needles of tourmaline. The tourmaline grains show a weak preferred orientation, which defines a crude foliation, however some few grains are oriented oblique to the foliation.

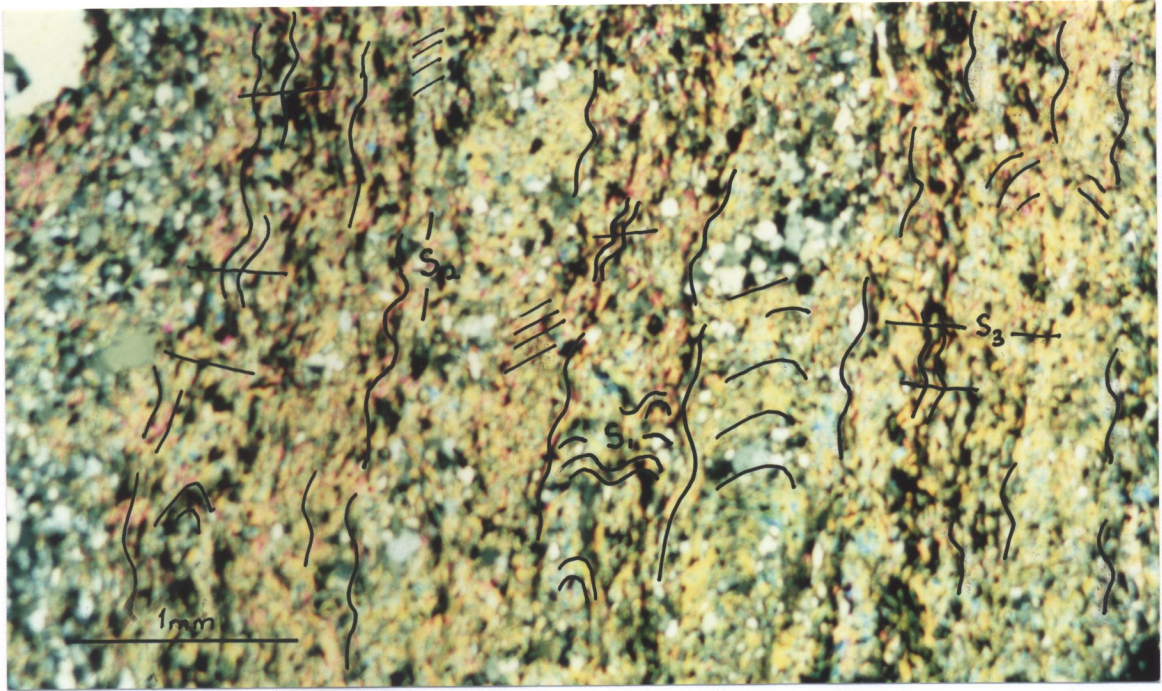


Plate 3.21: Photomicrograph of phyllitic quartzite showing three overprinting cleavages; S<sub>1</sub>, S<sub>2</sub> and S<sub>3</sub> and concentration of opaque minerals along S<sub>2</sub>. Sample CK30, x25, CPL. KB532777.

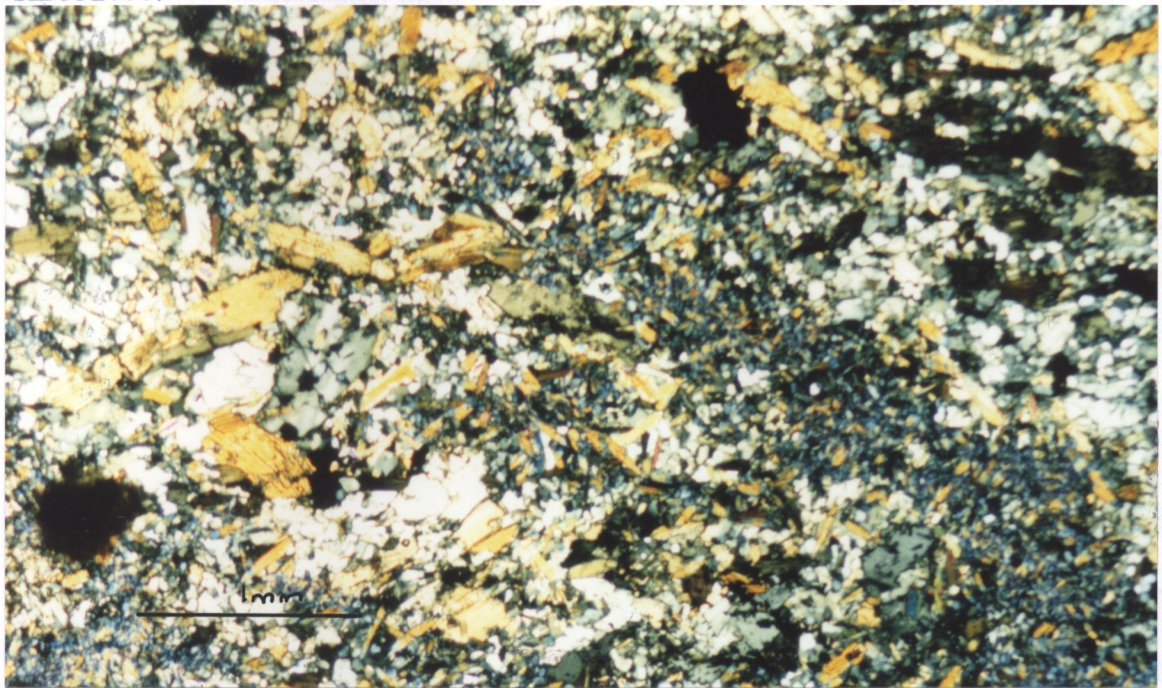


Plate 3.22: Photomicrograph of kyanite pod showing randomly oriented kyanite blades, purple fluorite and quartzitic groundmass. Ky-kyanite; Flu-fluorite. Sample CK77, x25, CPL. KB454773.

The abundance of tourmaline indicates boron-rich fluids in the source rock from which the quartzite pebble was derived. Strongly pleochroic, green to brown, rounded grains of tourmaline are sparsely distributed.

Accessories include opaque minerals, sphene and zircon.

#### **3.3.2.4 Brecciated carbonaceous meta-siltstone**

The contact between the Mwomboshi gneiss and the Chikonkomene Formation is a fault contact. A brecciated carbonaceous meta-siltstone is located along the contact at locality KB548738. An unbrecciated meta-siltstone consists of alternating white and dark bands. The white bands vary in thickness from 1-5 mm. In thin section, the white bands are composed of a mosaic of fine-grained equant quartz grains exhibiting polygonal texture. The dark bands consist of fine-grained quartz with abundant carbonaceous material, which imparts the dark colour to the rock.

Some thin quartz bands are evidently isoclinally folded, suggesting that the bands are a result of duplication by folding. The banding is therefore tectonic. The bands are cross cut at an oblique angle by fine quartz veinlets. The quartz veinlets are certainly a later feature and most of them are one grain wide. Most of the thin bands that are folded are one grain wide in thickness and were probably initially quartz veins.

In a section cut perpendicular to banding, the quartz laminae are up to 2 mm in thickness and in some cases one grain wide (0.125 mm). Some thin quartz laminae appear to be offshoots from thicker laminae, substantiating that the quartzite bands were originally quartz veinlets. Carbonaceous rafts completely enclosed in quartzite bands further support the evidence for the origin of the thin quartz laminae. The section cut perpendicular to banding shows gently folded bands in contrast to the other section where the bands are tightly interfolded (Plate 3.23).

In one carbonaceous layer, a thin quartz lamina displays minor ptigmatic folds formed during the initial shortening of the rock prior to buckling and refolding.

The brecciated rock consists of dark angular fragments, granoblastic quartz aggregates and strained clasts of quartz of various sizes set in a relatively light coloured matrix. Some fragments show similar banding noted in the unbrecciated variety. In thin section, the brecciated rock is composed of laminated angular fragments set in a very fine-grained matrix. Some fragments possess a strong crenulation fabric defined by muscovite indicating that prior to brecciation, the precursor rock had been intensely deformed. The matrix is composed of very fine-grained cryptocrystalline mixture of quartz, sericite and abundant carbonaceous material. Some clasts of quartz have irregular shapes and appear embayed.



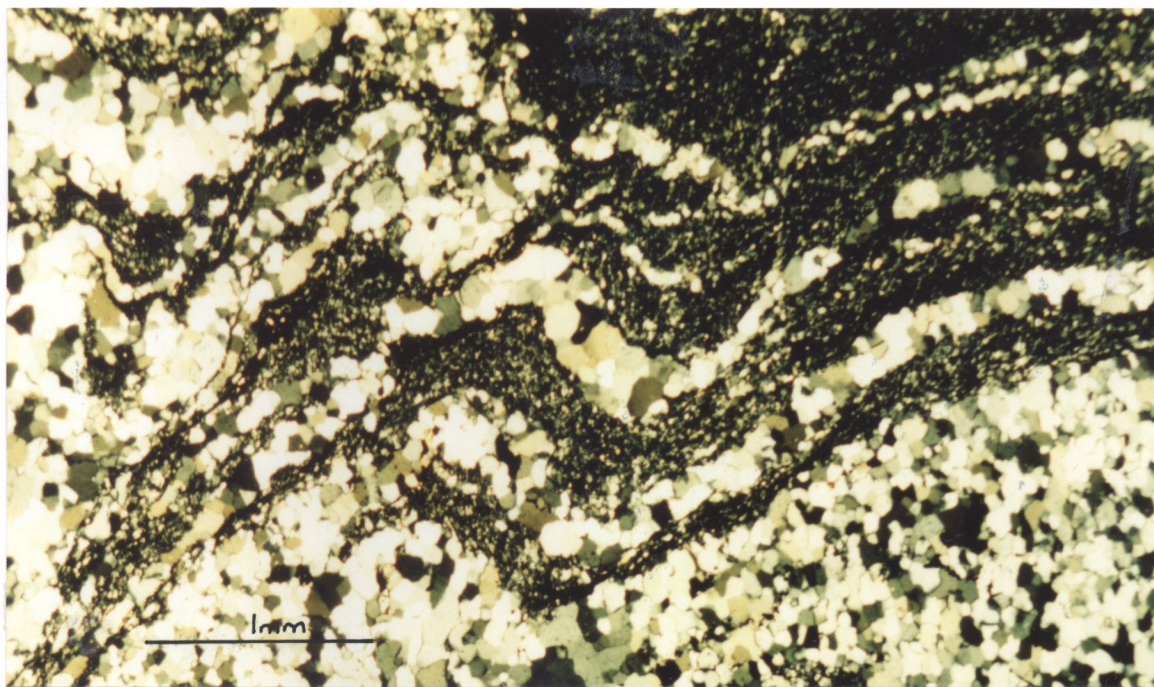


Plate 3.23: Photomicrograph of banded carbonaceous meta-siltstone showing  $F_2$  gently folded bands. Sample CK1, x25, CPL. KB548738.

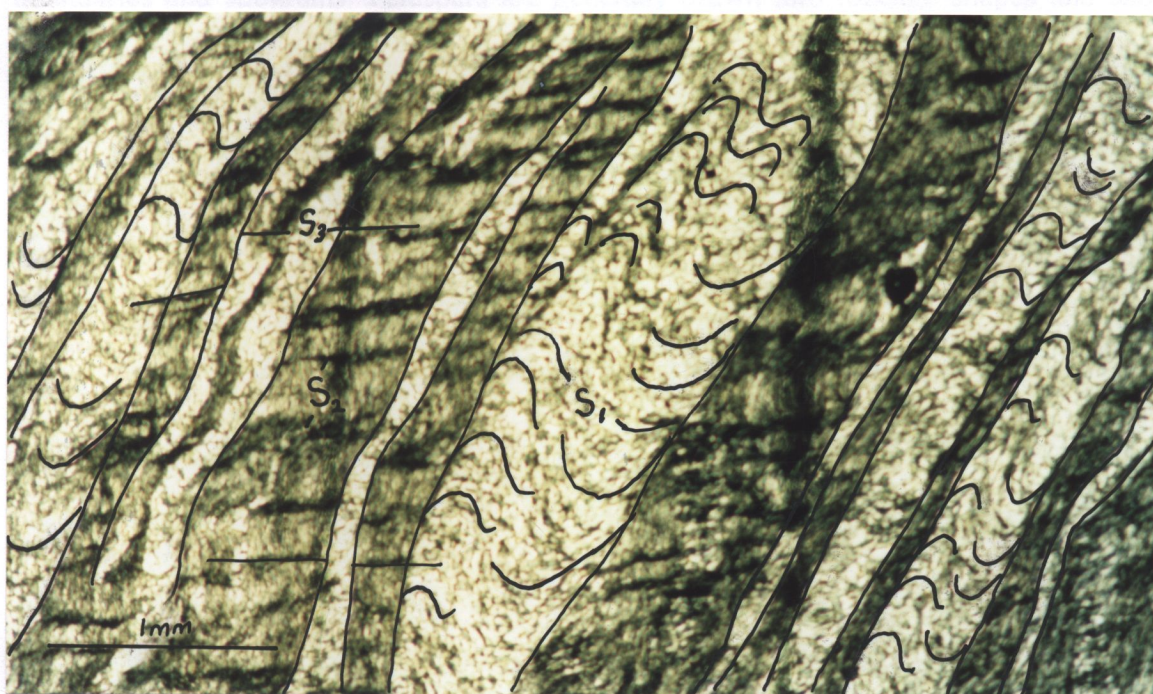


Plate 3.24: Photomicrograph of banded phyllite showing three overprinting cleavages defined by  $S_1$  in the microlithons,  $S_2$  crenulation domains and  $S_3$  crenulation of  $S_2$ . Sample CK86, x25, PPL. KB502858

### **3.4 Discussion and summary**

#### **3.4.1 Chisamba area**

Petrographic analysis of rocks from the Chisamba area show that some lithologies hitherto mapped as quartzites and dolomitic limestones are quartz mylonites and interbanded calc-silicates, scapolitic marble and amphibolites, respectively.

Shearing in the Chisamba area is partitioned along discrete shear zones shown by alternating zones of unsheared and highly sheared rocks. In quartzo-feldspathic protomylonites, quartz microstructures include undulose extinction, serrated grain boundaries and subgrains. Feldspars are generally drawn into lozenge shapes and show deformation twins, kinking and marginal granulation, indicating a certain amount of crystal-plastic deformation. Evidence for dynamic recrystallisation of feldspars does not exist. The quartz mylonites are dynamically recrystallised. Quartz microstructures in quartz mylonites range from undulose extinction, subgrains and core and mantle structures. Scapolite in the calc-silicate is dynamically recrystallised along discrete shear zones, where as diopside is granulated along the margins. All these microstructures indicate low temperature deformation consistent with greenschist facies metamorphic conditions. Some less sheared gneisses and quartzites display annealing textures reflecting a thermal event, which is probably related to the emplacement of granitoids e.g. Hook Granite Massif.

The most striking metamorphic event observed in thin section is the breakdown of garnet to plagioclase and hornblende indicating isothermal decompression (discussed in detail in chapter 5). This means that shearing along the MDZ was preceded by exhumation probably related to the Lufilian thrusting.

The gneisses in the Chisamba area, particularly the unsheared portions of calcareous gneiss, are petrolographically similar to the gneiss of the Kabwe area but differ principally in the intensity of shearing and deformation mechanisms. The intensity of shearing is related to the structural location of the area. The more sheared rocks involving predominantly crystal-plastic mechanisms are located in the Chisamba-MDZ area, whilst the less sheared and cataclastically deformed rocks are located outside or at the fringes of the MDZ, in the Kabwe area.

### **3.4.2 Kabwe area**

The Mwomboshi gneiss consists of anastomosing shear zones on a millimeter to decimeter scale showing varying intensities of shearing. The coarse-grained weakly foliated quartzofeldspathic gneiss at Nankuko quarry represents the least sheared part of the Mwomboshi gneiss, though narrow discrete shear zones also traverse it. Protomylonitic gneisses and mylonitic biotite schists represent rocks of relatively high intensities of shearing.

A study of thin sections of sheared derivatives of the Mwomboshi granite-gneiss has shown evidence for cohesive cataclastic flow at moderate temperatures and relatively high confining pressure. These include protomylonitic gneisses, and schists. Higher temperature



deformation, predominantly by crystal-plastic mechanisms, is shown by laminated feldspathic quartzites.

The sheared derivatives of the Mwomboshi gneiss occur in isolated shear zones intervened by weakly deformed gneiss. Thus the Mwomboshi gneiss is partitioned into narrow zones of intense deformation, and less deformed larger portions. This is clearly seen on thin section scale.

Grain size reduction of mainly quartz and to a lesser extent feldspars is a common feature in the protomylonitic and schistose rocks. Feldspars occur mainly as porphyroclasts, exhibiting several deformation textures, including; marginal granulation, grain-sacle fracturing, kinking, deformation twins, and undulose extinction. The feldspars thus accommodate strain by both intergranular and crystal-plastic adjustment. On the other hand, quartz occurring mainly in the groundmass is strained, but in many cases it displays annealing textures indicative of recovery.

Elongate ribbons of quartz and felsic aggregates are a prominent feature in the mylonitic rocks. The association of ribbons of recrystallised quartz aggregates with feldspar porphyroclasts may be due to extreme flattening of quartz or felsic aggregates accompanied by dynamic recrystallisation and growth of new grains.

Feldspars exhibit orientated patch perthite textures. The patched perthite is considered to have resulted from unmixing during greenschist facies deformation. The preferred orientation of perthite is controlled by crystallographic direction (Passchier and Trouw,

1996). In some cases myrmekitic intergrowths have developed between microcline and plagioclase on grain faces parallel to the foliation. The relationship between foliation and growth of myrmekite is largely strain controlled (Vernon, 1991; Simpson and Wintch, 1989). According to Simpson and Wintch (1989), deformation controlled myrmekite replacement occurs at amphibolite facies conditions. This is not consistent with retrograde metamorphism noted throughout the Mwomboshi gneiss. The myrmekite intergrowth predates the shearing and developed during regional amphibolite facies metamorphism.

Microstructures showing internal monoclinic shape symmetry (Passchier and Simpson, 1986; Simpson and Schmid, 1983) indicating sense of shear in the rocks are generally lacking or vague. The kinematic indicators noted in oriented mylonitic and schistose samples include aggregate lineations, probable pressure shadows, and crudely developed S-C fabrics.

The occurrence of xenoliths within the Mwomboshi gneiss of similar mineralogical composition suggests an igneous origin of the gneiss

It is evident that the mineralogical composition of the Mwomboshi gneiss has since been modified by secondary metamorphic processes, but is difficult to assign these processes to a specific metamorphic event. Throughout the Mwomboshi gneiss, microcline is poikiloblastic, consisting of inclusions of the same composition as matrix, indicating that it is metasomatic. In many cases it is wrapped round by the foliation and granulated.

Shear zones in the Mwomboshi gneiss trend E-W or ENE parallel to the trend of the Irumide belt, within which it is situated. The deformation textures, which are predominantly cataclastic in the shear zone rocks, differ markedly from those noted in the Chisamba-MDZ area. There are two possible explanations for this difference:

- 1) The shear deformation textures observed in the Kabwe area are Irumide in age.
- 2) The shear zones are coeval with the MDZ but formed at higher crustal level.

Annealing textures exhibited by quartz clearly post date shearing. These textures are probably related to regional igneous activities related to the MDZ.

The quartzites of the Chikonkomene Formation are recrystallised and quartz exhibit undulose extinction and, core and mantle structures. These textures are consistent with the low temperature regime of Hirth and Tullis (1992). The abundance of sericite indicates lower temperature conditions of deformation. The banded phyllite of the Neoproterozoic Kangomba Formation has three overprinting foliations. This is an important observation as it gives an indication of how many deformations events affected the older Mesoproterozoic Chikonkomene quartzites. Phyllitic quartzite in the Chikonkomene Formation records three deformation episodes.  $S_0=S_1$  have been transposed into  $S_2$ , the main shear foliation, which was in turn crenulated by a NW trending  $S_3$ . This implies that the phyllitic quartzite developed during an older orogenic event, probably of Mesoproterozoic Irumide age.

## **Chapter 4**

### **4.0 STRUCTURE**

#### **4.1 Introduction**

Results of detailed structural mapping in the study areas are presented in this chapter. Mesoscopic and microscopic shear sense indicators are used for the first time to deduce the sense of shear in the MDZ. A discussion and summary of the results is also presented.

#### **4.2 Chisamba area**

The prominent structures in the Chisamba area are ENE-WSW trending strike slip faults, and E-W trending tight to isoclinal folds most prominent in the quartzites (Fig. 4.1). Field observations have shown that the area has undergone at least two deformation phases, but the last one has overprinted all the earlier ones. Structures observed in the field include, foliations, folds, lineations, and shear zones. All the faults were inferred from aerial photographs.

##### **4.2.1 Foliations**

At least three generations of foliations were observed i.e.  $S_0$ ,  $S_1$ ,  $S_2$  and  $S_3$ . Parallel bedding is preserved in quartzites and calc-silicates. Beds range in thickness from 2-20 cm. In certain places, the quartzite appears laminated due to closely spaced (1mm) cleavage. At Mungulube hill, banded iron-quartzites show cross bedding, marked by iron-oxide laminae, which indicates sediment transport from SE to NW. However, the paleo-current

direction deduced from the cross bedding may be misleading due to the complex folding in the area.

The bedding in the quartzite is cross cut by a spaced cleavage. In some places, where bedding can not be distinguished from spaced cleavage, it is assumed that the two are parallel.

The area is divided in three domains on the basis of the general strike of the foliations.

Domain 1 represents foliations with ENE and NE trends (Fig.4.2 A), and covers the area drained by the Wangwa River and its tributaries and the northeastern part of the study area. Domain 2 represents foliations with more or less E-W trends (Fig.4.2 B) and covers the area that is drained by the Kapwilu stream. The two plots portray a swing in foliations from mostly NE-ENE in domain 1 to E-W in domain 2. The swing in foliation indicates dextral shear movement. Domain 3 covers the eastern part of the area in the vicinity of the GNR and shows foliation with NNW trends dipping west to southwesterly (Fig.4.2 C).

#### **4.2.2 Lineations**

Lineations observed in the field comprise stretching lineations, fold hinge lineations, mineral lineations, crenulation lineations, intersection lineations, boudins, and grooves and ridges. The stereographic plot of the linear fabrics shows that they are all co-linear (Fig. 4.2 D).

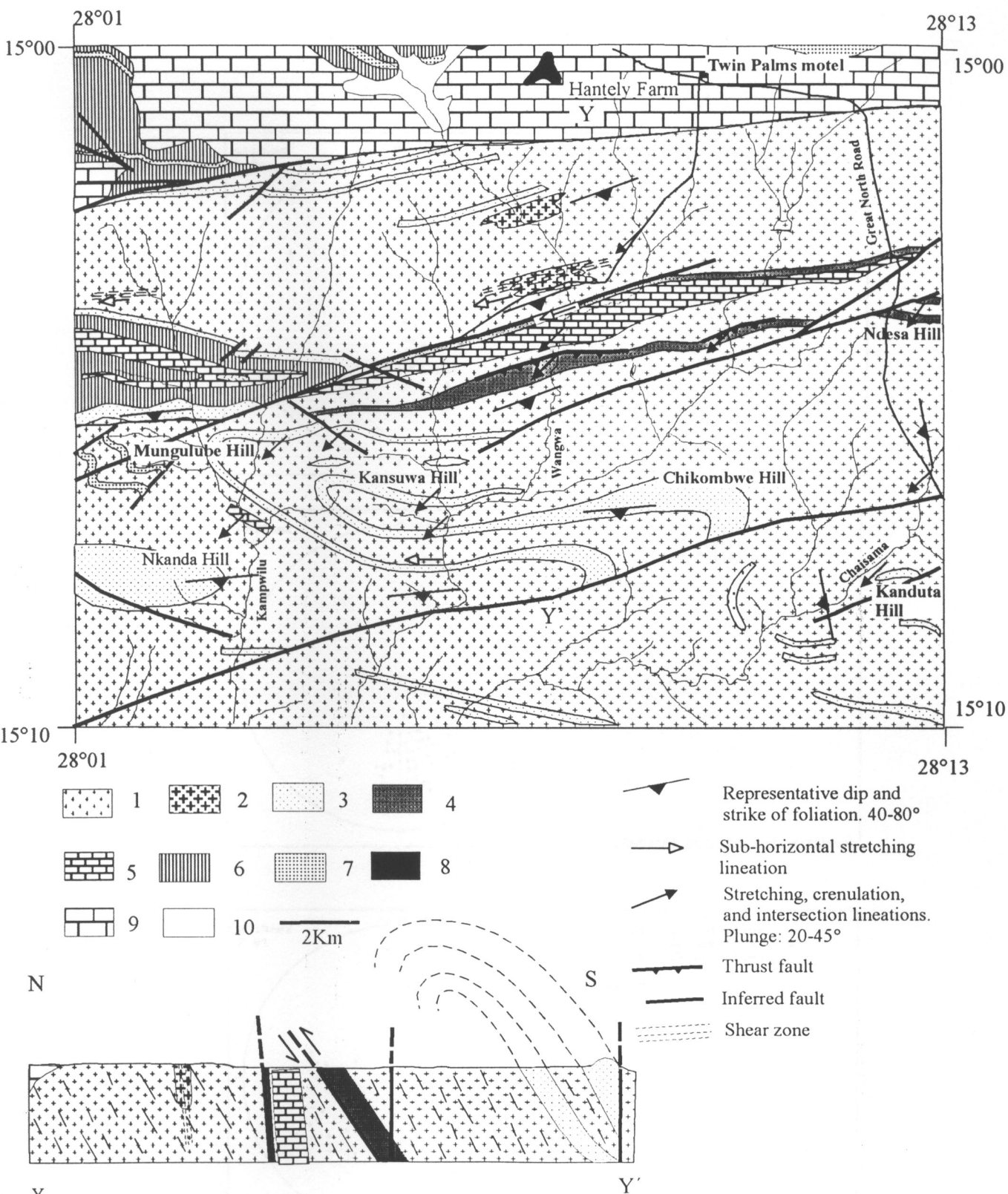


Fig.4.1: Structural map of the Chisamba area and schematic cross-section along Y-Y'.

1: Granite gneiss and sheared equivalents. 2: Calcareous gneiss. 3: Kyanite bearing quartzites. 4: Quartz mylonites. 5: Calc-silicate, scapolitic marble, and minor amphibolite. 6: Garnet schists. 7: Iron banded quartzites. 8: Olivine gabbro. 9: Dolomite. 10: Alluvium

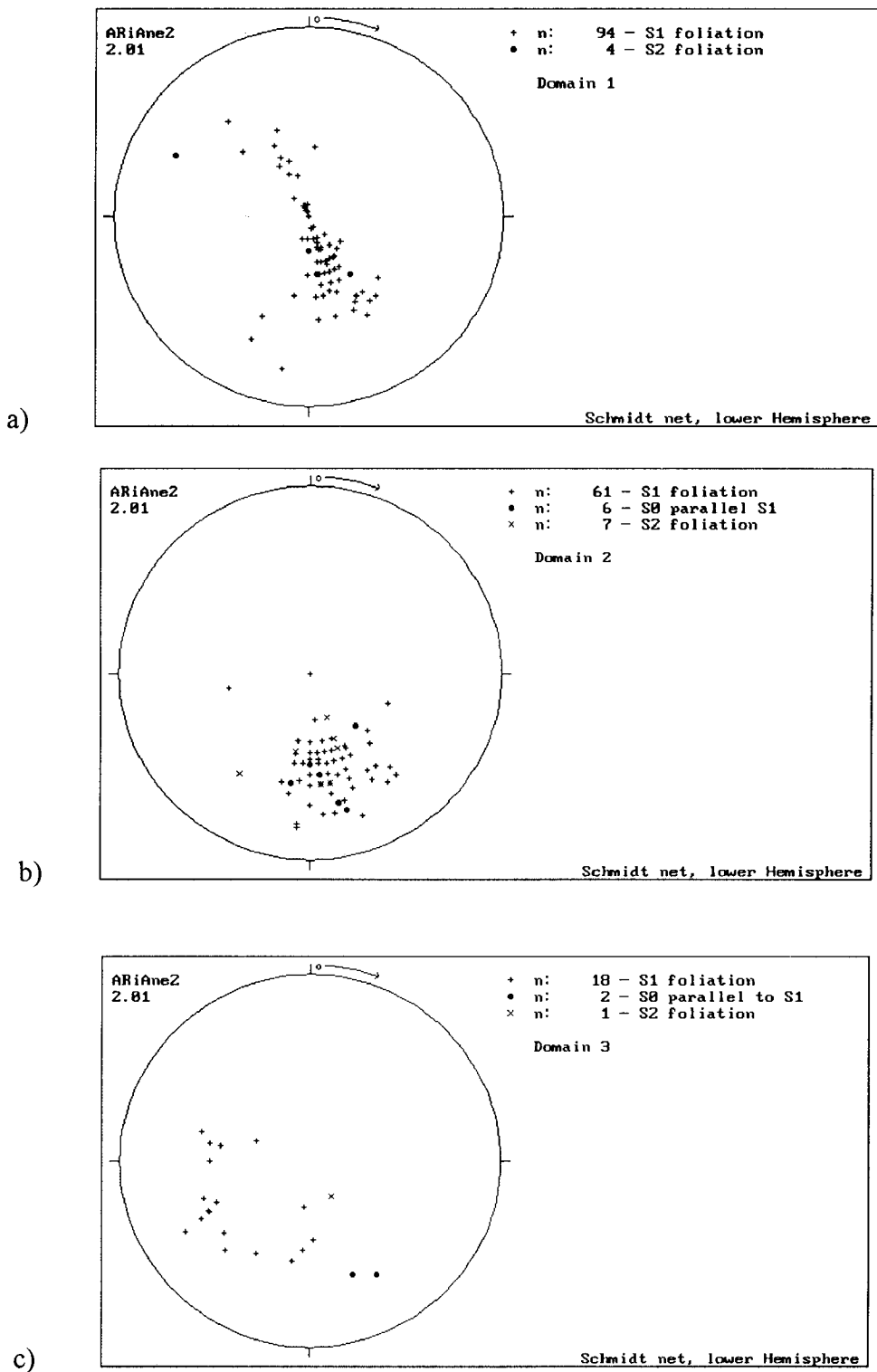


Fig. 4.2: Equal area, lower hemisphere projection. Plot of dip direction and dip (a) Domain 1 (b) Domain 2 (c) Domain 3 and (d) lineations

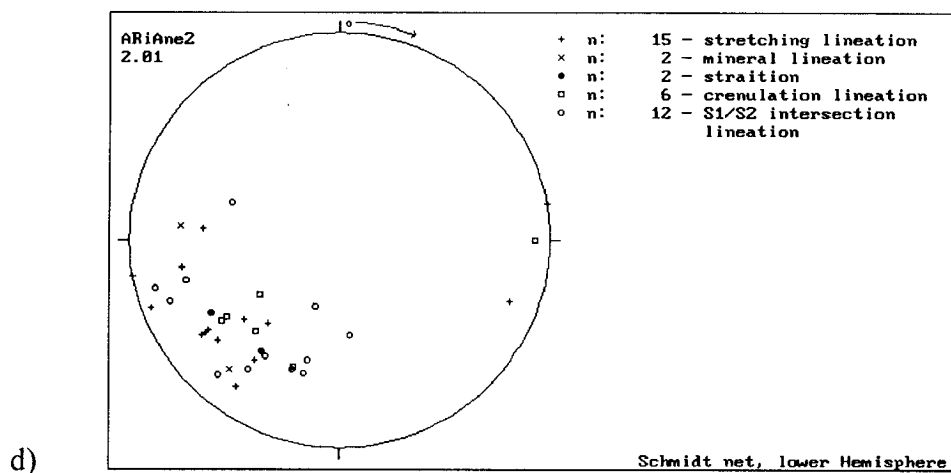


Fig. 4.2: continued

#### 4.2.2.1 Stretching lineations

Two types of stretching lineations were observed; sub-horizontal ( $5^\circ$  towards  $230^\circ$ ) and plunging lineations ( $20^\circ$ - $45^\circ$  towards  $230^\circ$ ), (Fig. 4.1). Both are defined by ribbons of quartz and felsic aggregates in quartz mylonites and protomylonitic gneisses. The sub-horizontal stretching lineation is developed on steep-vertical shear planes (Plate 4.1) whereas plunging stretching lineations occur on shallow to steeply dipping ( $30^\circ$ - $60^\circ$ ) shear planes (Plate 4.2).

The stretching lineation consistently plunges to the SW. In thin section, mica-fish indicates oblique NE-directed thrust movement, with a component of horizontal sinistral displacement. In some cases stretching lineations are associated with the development of quartz veins perpendicular to the stretching lineation. On the basis of their similarity in



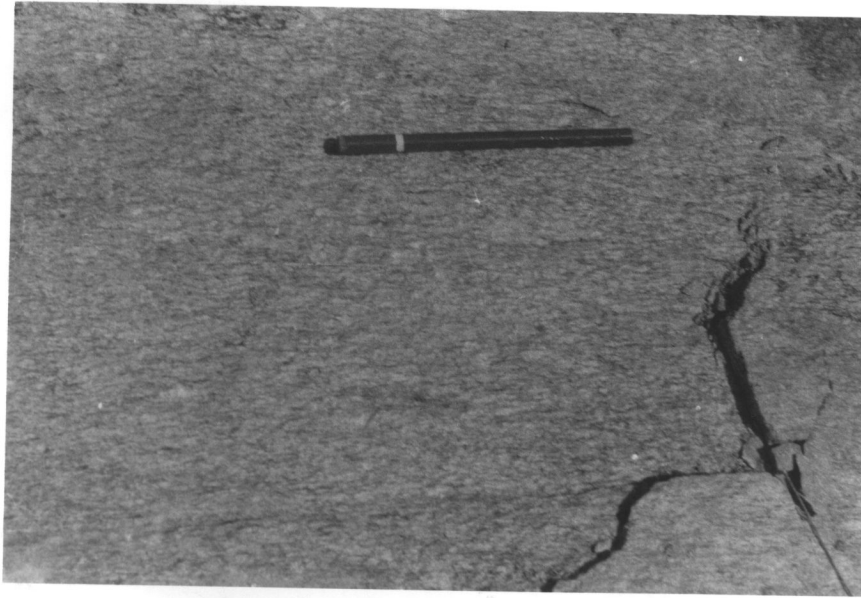


Plate 4.1: Horizontal stretching lineation in quartzo-feldspathic protomylonite. Pencil parallel to lineation. CH106351



Plate 4.2: Stretching lineation defined by stretched quartz and quartzo-feldspathic aggregates indicating SW over NE oblique thrust transport. CH308308.

attitude with the Lufilian thrust transport direction, it is suggested that they are related to the thrusting event in the Lufilian Arc to the north of the MDZ. The oblique thrust observed in the MDZ means that thrusting involved sinistral strike slip displacement.

Mesoscopic and microscopic shear indicators demonstrate that the sub-horizontal stretching lineations are associated with dextral strike slip displacement along the MDZ.

#### **4.2.2.2 Mineral lineations**

Mineral lineations plunge to the SW. They are defined by aligned hornblende in amphibolites and kyanite in quartzites.

#### **4.2.2.3 Crenulation lineation**

Crenulation lineations were observed in biotite schists and marble. Their attitude is consistent with the other lineations. The crenulation lineations are parallel to fold axes of the major folds in the area, but may have been rotated to the present attitudes during shear movement along the MDZ.

#### **4.2.2.4 Intersection lineation**

Bedding-foliation intersection lineations were measured in quartzites and all plunge to the SW. Where the intersection lineation could not be measured in the field, the attitude of the intersection line was determined on the stereogram.

#### **4.2.2.5 Grooves and ridges**

Grooves and ridges on planar surfaces define lineations with attitudes similar to the other linear fabrics. Grooves are generally not mineralised but some places are filled with a smear of black tourmaline (Plate 4.3). Ridges are shown by a parallel alignment of lines of slightly higher relief than the surrounding flat surface. Surfaces, where grooves and ridges have developed probably represent fault planes and the lineations indicate ENE-WSW slip on the fault planes.

#### **4.2.2.6 Boudins**

At CH237368, a stretching lineation in an S-L tectonite is defined by the long axis of boudins. The lineation plunges  $15^\circ$  towards  $230^\circ$ , consistent with other lineations (Plate 4.4). The attitude of the lineation indicates NE directed thrust transport.

#### **4.2.3 Folds**

Simpson et al. (1963) recognised at least three generations of major folds in the basement, but could not relate them to any specific deformation events due to inadequate exposure in the fold closures. In the Katangan sequence Simpson et al. (1963) described the folds as primary recumbents which have been re-folded at least twice.

Few mesoscopic-scale fold structures were observed in the area to enable a reasonable correlation with deformation phases. All the fold axis trends are more or less parallel. This



Plate 4.3: Tourmaline filled grooves plunging SW on a probable fault plane in quartzite. CH301345



Plate 4.4: S-L quartzitic tectonite. Lineation plunges to the SW. CH153316



Plate 4.5: Isoclinal intrafolial minor fold in muscovite quartzo-feldspathic gneiss  
CH323384



Plate 4.6: loose block of muscovite biotite quartzo-feldspathic gneiss showing tight folding. CH141275

suggests that the folding events could have been co-linear. It is therefore difficult to distinguish one generation from the other. The outcrop pattern of the quartzites and mylonites indicates large scale northerly verging, south-westerly plunging folds (Fig. 4.1). This is reflected in some mesoscopic-scale fold structures. Bedding and foliation in quartzites intersect in lines trending SW with variable plunge. The variation in plunge is likely due to later deformation phases.

An intrafolial rootless quartz vein is isoclinally folded in sheared quartzo-feldspathic gneiss (Plate 4.5). The  $S_2$  axial planar foliation indicates that the fold is  $F_2$ . A loose block of banded gneiss exhibits tight folds (Plate 4.6). The banding consists of alternating biotite gneiss and muscovite granite-gneiss. The banding is probably tectonic.

In calcareous gneisses, two types of minor fold structures were observed. The minor folds are folded about two sub-parallel spaced  $S_2$  and  $S_3$  cleavages. Isoclinally folded quartz veins,  $F_2$ , are folded about  $S_2$  and  $F_3$  are gently folded about  $S_3$ .

Calc-silicates are gently folded about an E-W trending fold axis and the folds are considered to be  $F_1$  on the basis of the development of an  $S_1$  axial planar cleavage. The folding in the calc-silicates is defined by thin iron-oxide banding probably representing bedding (Plate 4.7).



Plate 4.7: Folded diopside-scapolite calc-silicate with dark iron-oxide bands outlining folds. CH219343



Plate 4.8: Isoclinal to tight intrafolial folds in banded scapolitic marble. CH219342

Marble is disharmonically folded, the folds being outlined by white bands. Intrafolial and rootless folds (Plate 4.8) are isoclinally folded, with highly attenuated fold limbs. Fold closures indicating refolding are evident (Plate 4.8). On the basis of the folds closures, the folds are considered  $F_2$  folds. However, marble easily flows under stress and thus the fold style may not represent the true nature of the folding.

#### **4.2.4 Shear zones and kinematic indicators**

Tectonic models for the MDZ are largely based on regional structural trends and no microstructural studies have been undertaken. The understanding of the kinematic development of the MDZ is critical to the geodynamic evolution of the Pan-African belts in central-southern Africa. In view of the conflicting shear sense interpretation of the MDZ which have been proposed (De Swardt et al., 1964; Coward and Daly, 1984; Unrug, 1983; Porada, 1989; Hoffman, 1991; Ring, 1993) this section is concerned with carefully documenting the sense of shear in the Chisamba-MDZ area.

The sense of shear is always observed in the shear sense observation plane (SSOP) (Hamner and Passchier, 1991). However, the SSOP is not always presented in an outcrop. Further, some fabrics are not discernible with the naked eye or hand lens. These and many other factors, constrain mesoscopic shear sense evaluation in the field. Microstructures provide maximum shear sense information as the SSOP is fairly accurately selected in the laboratory. The convention used to describe shear sense in this report is dextral (clockwise rotation) and sinistral (anticlockwise rotation). Mesoscopic scale kinematic indicators are scarce due to poor exposure.



#### **4.2.4.1 Mesoscopic structures**

The most common kinematic indicator in the study area is stretching lineation. The orientation of the plunging stretching lineation approximates the direction of thrust movement (Daly, 1986). In the study area, the trends of plunging stretching lineations are orientated oblique ( $215^{\circ}$ - $230^{\circ}$ ) to the strike of the foliation ( $245^{\circ}$ - $260^{\circ}$ ). The attitudes of the plunging stretching lineations coupled with microstructures indicate oblique thrust movement from southwest to northeast. This also suggests that movement involved a sinistral strike-slip component. The stretching lineations are co-linear with the other linear elements in the area, indicating that either they are genetically related or were drawn into parallelism during shear movement.

At CH214355, calcareous gneiss is deformed into an L-tectonite defined by a strong sub-horizontal stretching lineation, with an attitude of  $5^{\circ}$  towards  $230^{\circ}$  (Plate 4.9). The lineation indicates strike slip movement.

At CH216356 a foliation ( $010^{\circ}/80^{\circ}$  N) is deflected into narrow near-vertical shear zones ( $065^{\circ}/86^{\circ}$  N) indicating dextral shear sense (Plate 4.10). Sub-horizontal stretching lineations on vertical shear planes suggest strike slip shear movement.

At CH216356, S-C fabrics indicate ENE over WSW dextral shear movement. Felsic augens are aligned parallel to the S-fabric.

The vergence of the folds in the area is consistent with the thrust transport direction deduced from plunging stretching lineations. Since the foliation is axial planar to the folds in the area, the former developed at the same time as the latter during thrusting.

#### **4.2.4.2 Microscopic structures**

Thin sections for evaluating sense of shear were cut perpendicular to the foliation and parallel to the stretching lineation.

A large number of thin sections are required for a reliable shear sense evaluation. However, due to limited outcrops in the study area, the evaluation is based on few thin sections.

Different types of asymmetric microstructures were used to deduce the sense of shear. These include mica-fish,  $\sigma$ -type porphyroclast systems, oblique shape fabric and S-C or C' fabrics.

##### **4.2.4.2.1 Mica-fish**

Mica-fish is a spindle shaped muscovite porphyroclast with associated tails drawn out at the tips of the fish (Lister and Snoke, 1984). Mica fish is the most widely developed shear sense indicator in the area, particularly in the quartz mylonites. The monoclinic shape symmetry and stair-stepping of the tails indicate ENE over WSW dextral sense of shear in strike-slip shear zones (Plate 3.10 and 3.11). In quartz mylonite developed in a thrust

zone, the mica fish indicates SW over NE oblique thrust transport. In the same quartz mylonite, titanite displays a fish structure with a slight obliquity to the shear plane, also indicating the same sense of thrust transport. Feldspars caught up in quartz ribbons are lozenge shaped but possess orthorhombic shape symmetry.

#### **4.2.4.2.2 S-C and C' fabrics**

S-C and C' fabrics were observed in quartzo-feldspathic protomylonites. The mylonites possess a sigmoidal S-foliation and two shear planes, C and C' planes. The curvature of the S-foliation into either the C or C' fabrics indicates dextral sense of shear. C' shears develop at a low angle to the both S and C planes. Chlorite and sericite developed in the shear planes indicating formation under greenschist facies conditions.

#### **4.2.4.2.3 Oblique grain shape fabric**

Another common shear sense indicator in the protomylonites is the oblique grain shape fabric. In some polycrystalline quartz ribbons oriented parallel to the shear plane, an internal oblique shape fabric is defined by elongate quartz grains. The obliquity of the fabric to the shear plane indicates dextral sense of shear (Plate 3.8). The shape fabric is strain insensitive, as it does not track the finite strain ellipsoid closely (Hamner and Passchier, 1991).



Plate 4.9: Sub-horizontal stretching lineation in calcareous quartzo-feldspathic gneiss.  
CH229358



Plate 4.10: Deflection of foliation into narrow shear zone (SZ) indicating dextral sense of shear in quartzo-feldspathic protomylonite. CH216356

#### 4.2.4.2.4 $\sigma$ -type porphyroclast

$\sigma$ -type porphyroclasts are developed in protomylonites. It is not easy to distinguish asymmetric porphyroclasts in the protomylonites due to the small amount of matrix.  $\sigma$ -type porphyroclasts consists of plagioclase with short asymmetric wings. The porphyroclast system may be classified as  $\sigma_b$ -type (Passchier and Simpson, 1986) since they posses short wings which curve in the C or C'-planes. The asymmetry and stair-stepping direction of the wings indicate ENE over WSW dextral sense of shear.

#### 4.2.5 Faults

All the faults were inferred from aerial photographs. Simpson et al. (1963) deduced dextral strike-slip movement on inferred faults on the basis of displacement of quartzite bands. At locality CH220348, a steep to vertical garnet-quartz mylonite coincides with the position of an inferred fault. A stretching lineation defined by quartz has a horizontal ENE attitude indicating a large component of strike-slip displacement. The quartz mylonite indicates ductile deformation in contrast to the inferred brittle deformation.

In the northern section of the study area, a major ENE trending inferred fault follows the contact between Neoproterozoic Lusaka Dolomite to the north and Palaeoproterozoic? basement gneiss to the south. The presumed faulted contact is indicated as a dip-slip fault, which has juxtaposed younger Lusaka Dolomite with older basement gneiss. In some places, an inlier of Chunga Formation schists is in contact with older basement gneiss. The contact is curved in a few places but is generally straight. The curved contacts are not

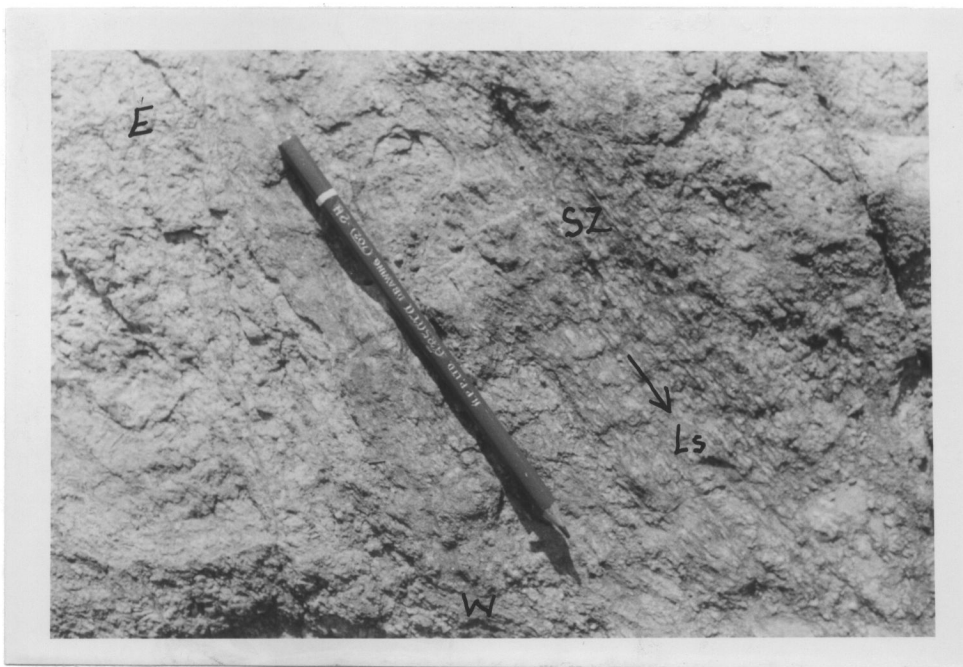


Plate 4.11: Sub-horizontal stretching lineation defined by quartz aggregates in quartzofeldspathic gneiss. Lineation plunges to the west. KB537736

shown to be faulted. In view of the curved contacts, the contact may have been initially an unconformity between overlapping dolomite and gneiss, and subsequently faulted during movements along the MDZ.

### 4.3 Kabwe area

The area is characterized by an E-W trending fault zone known as the Nyama dislocation zone. The general structural trend is E-W in the Mwomboshi gneiss and ENE in the overlying Chikonkomene Formation (Fig. 4.3). At least three deformation phases were recognised in the area, the last one being fault movement along the Nyama dislocation zone, coeval with that of the MDZ. Several mesoscopic structures, both primary and

secondary, were observed in the area. These include planar and cross-bedding, convolute bedding, foliations, lineations, folds and faults.

#### **4.3.1 Foliations**

The general structural trend in the Mwomboshi gneiss is E-W with southerly directed dips (Fig. 4.4 A). The foliation in the gneisses is expressed as a crude gneissic foliation defined by micas. In some places the gneisses are compositionally banded. The banding is defined by alternating fine to medium grained quartz-feldspar-biotite and quartz-feldspar bands. Muscovite occurs in minor amounts in both bands. The foliation in the gneisses is an  $S_2$  axial planar foliation, with an average attitude of  $260^\circ/60^\circ$  S, shown by tightly to isoclinally folded bands, representing  $S_1$ .

The structural trend in the Chikonkomene Formation is generally E-W with shallow to moderate, steep northwest and southwest dip (Fig. 4.4 B). Three distinct foliations were noted in the Chikonkomene Formation metasedimentary rocks; bedding  $S_0=S_1$ , ( $075^\circ/45^\circ$  N), and crenulation cleavage  $S_2$  ( $070^\circ/30^\circ$  N). A third weakly developed crenulation cleavage,  $S_3$ , was observed in thin section in sheared phyllitic quartzite.

Bedding,, which occurs either as plane bedding or cross bedding is defined by thin iron-oxide bands. The plane bedding ranges in size from a few mm up to 5cm thick. Stretched

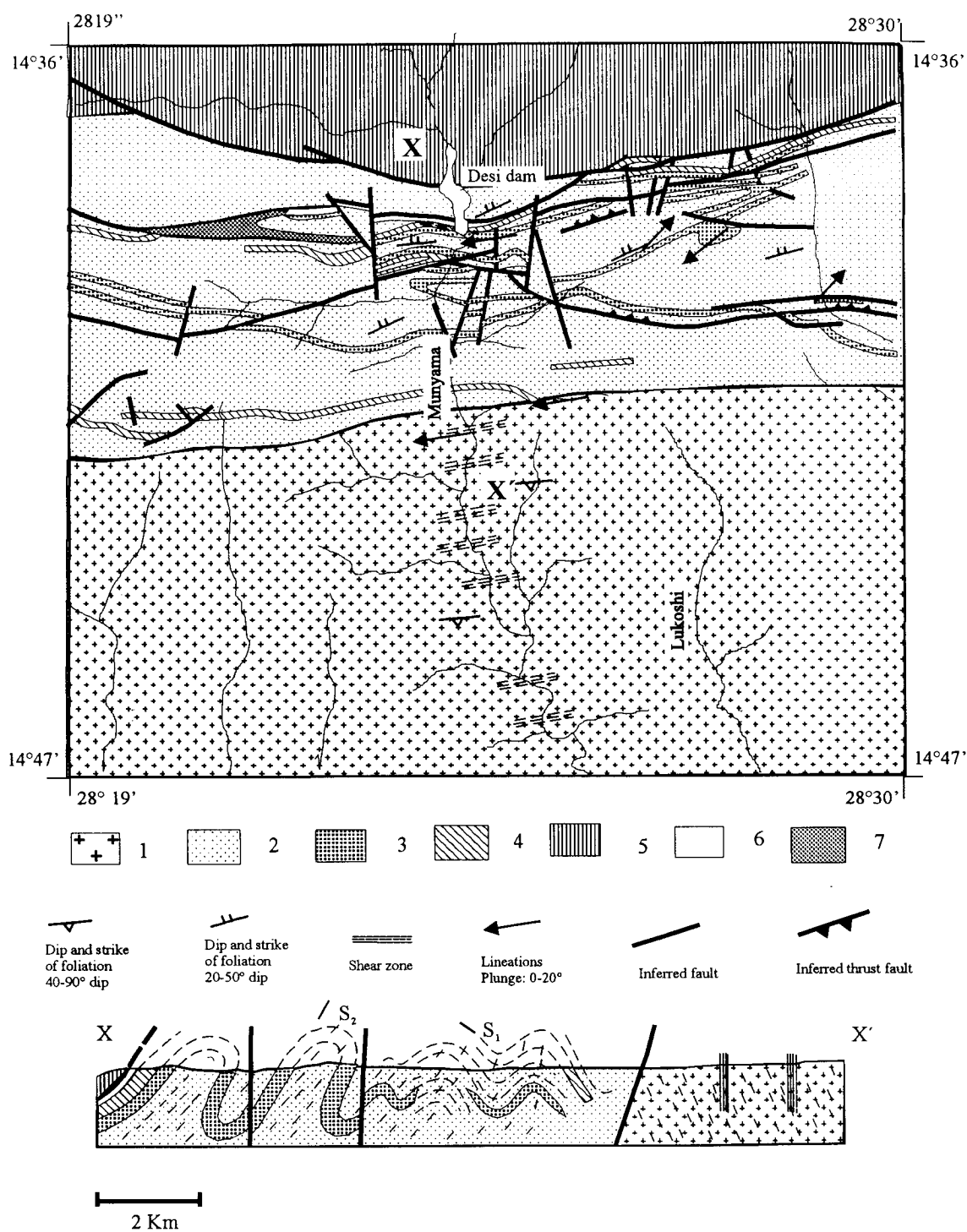


Fig. 4.3: Structural map of the Kabwe area and schematic cross section along X-X'.  
 1: Mwomboshi gneiss. 2: Sericitic quartzite. 3: Polymictic meta-conglomerate.  
 4: Iron banded quartzite. 5: Gritty quartzite. 6: Phyllite, slate and arkoses. 7: Quartzite



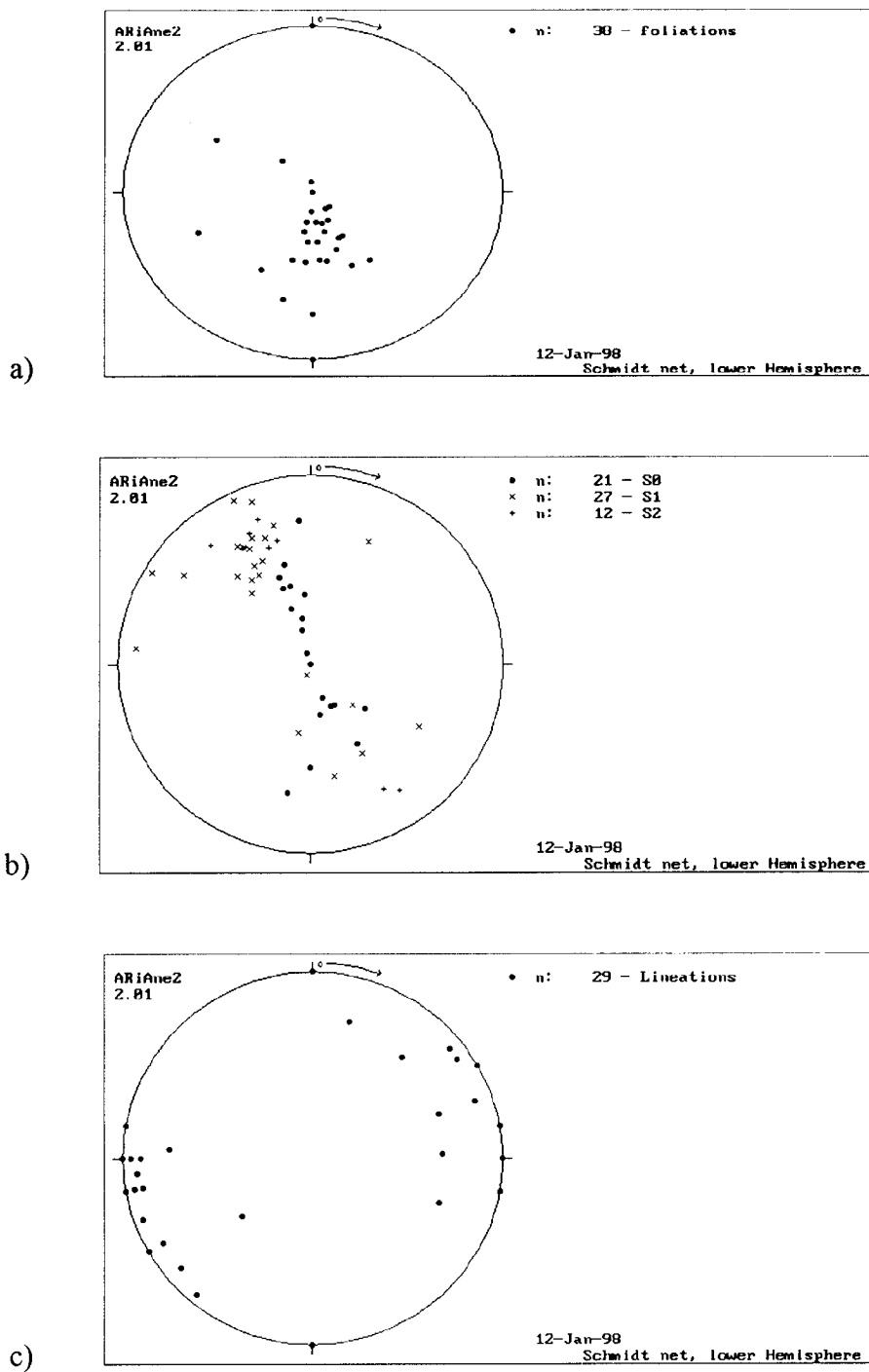


Fig. 4.4: Equal area, lower hemisphere projection. Plot of dip-direction and dip (a) Mwomboshi Formation (b) Chikonkomene Formation and (c) Lineations comprising; crenulation and stretching lineations

pebbles and cobbles represent bedding in polymictic meta-conglomerates. In some places, the pebbles and cobbles are flattened and stretched in a foliation plane, which is parallel to  $S_0$ .  $S_1$  is defined by fine muscovite, which in many instances is parallel to the iron oxide banding or alignment of pebbles and cobbles. In many places,  $S_1$  is crenulated along with the iron-oxide bands and pebbles, resulting in a strongly developed  $S_2$  crenulation cleavage ( $060^\circ/30^\circ$  N). Very fine micas (sericite) which, in some places, are pink coloured define  $S_2$ . The plot of foliations coupled with field observations reflects a normal overturned fold structure with a southerly vergence (Fig. 4.3: Fig. 4.4).

#### **4.3.2 Lineations**

Lineations observed in the area are mineral stretching lineations, striations, elongation of pebbles and xenoliths, boudins, crenulation lineations and  $S_0=S_1/S_2$  intersection lineation.

##### **4.3.2.1 Stretching lineations**

Sub-horizontal elongate quartz grains define a stretching lineation, in a narrow discrete shear zone in granite-gneiss (Plate 4.11). The lineation plunges  $5^\circ$  towards  $260^\circ$  indicating a large component of strike slip movement. Deflection of foliation and displacement of feldspar along cleavage indicate east over west strike slip dextral shear movement. The shear sense movement in the shear zone probably reflects displacement on a major fault boundary between the gneisses and metasediments (Fig. 4.3).

At KB536726, stretched xenoliths within a sheared biotite granite-gneiss define a stretching lineation. The xenoliths are horizontal with a trend of  $080^{\circ}$  and are stretched parallel to the fold axis on the limb of a fold and therefore define a 'b' lineation. At the same locality shear extension fractures are shown by cross-cutting feldspathic veins (Plate 4.12). The stretching of the xenoliths may be related to the extension shears.

Elongated pebbles define stretching lineation. Strain of pebbles plotted on a Flinn diagram from one locality indicates a deformation with more flattening than stretching (discussed under section 4.3.6). However, the long axis of the flattened pebbles defines an elongation lineation in a foliation plane. The elongated pebbles plunge towards northeast. The trend of the pebbles, coupled with southerly vergence of the structures in the metasediments, indicate thrust transport to the southwest.

#### **4.3.2.2        Striations**

Striations on a fault plane were observed along the major fault boundary between the gneisses and metasediments at KB548738. The striations plunge  $5^{\circ}$  towards  $260^{\circ}$ , indicating the same sense of movement given by the mineral stretching lineation above. The presence of fault breccia and other features discussed elsewhere at the same locality supports the existence of a major fault in the area.

#### **4.3.2.3 Boudins**

In the Mwomboshi gneiss, feldspathic bands sometimes occur as boudins floating in relatively dark gneiss. The boudins are stretched in the  $S_2$  foliation plane and are horizontal. In the Chikonkomene Formation, some of the white pebbles and cobbles in the conglomeratic horizons are derived from boudinage of quartz veins (Plate 4.13). The boudins are also stretched in the foliation plane and are horizontal.

#### **4.3.2.4 Crenulation lineation**

The development of the crenulation cleavage  $S_2$  was accompanied by crenulation of the pebbles and cobbles in the polymictic meta-conglomerates. The hinges of crests of these folded pebbles define a crenulation lineation parallel to the fold axis of the associated major fold. The fold axes plunge between  $0^\circ$  and  $15^\circ$  towards NE or SW (Fig. 4.2 C). Prior to crenulation, the pebbles and cobbles were flattened, stretched and probably defined a lineation on an  $S_1$  foliation. The crenulated pebbles and cobbles are considered to represent a folded  $S_1$  lineation.

#### **4.3.2.5 Intersection lineation**

Intersection lineations were determined on a stereogram from the attitudes of intersecting  $S_1$  and  $S_2$ . The attitudes of fold axes defined by intersection lineations are parallel to the



Plate 4.12: Stretched dark xenoliths and cross-cutting feldspathic extension veins in sheared quartzo-feldspathic gneiss. KB536726

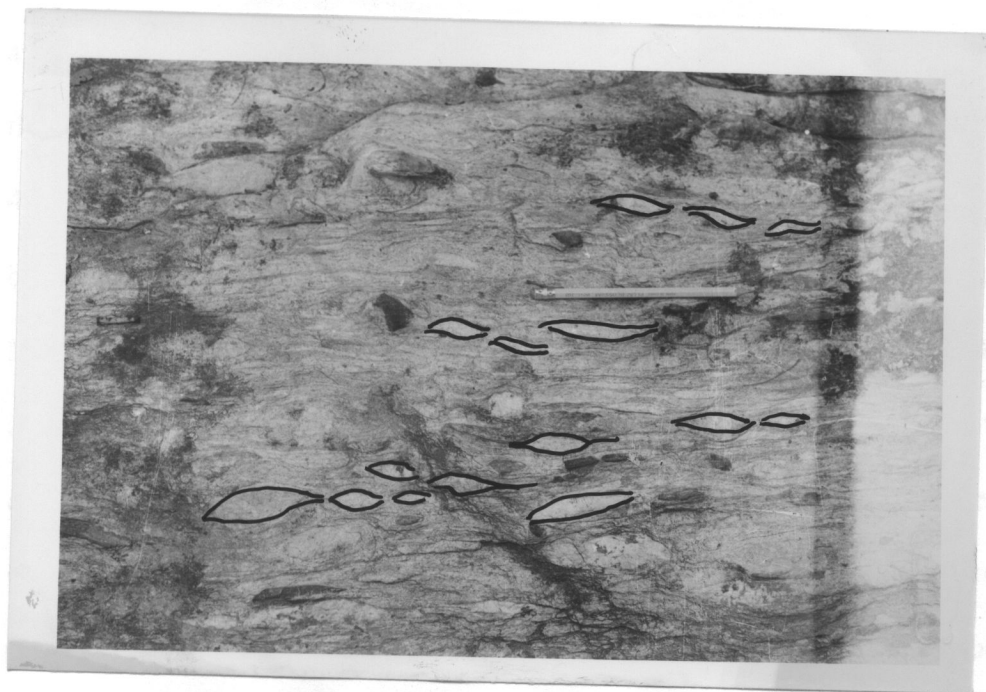


Plate 4.13: Pseudo-conglomerate formed by boudinage of quartz veins in muscovite quartzite. KB563771

fold axes determined from crenulation lineation.

#### **4.3.3 Folds**

Folding is evident throughout the study area, particularly in the Chikonkomene Formation. The Mwomboshi gneiss forms the core of a westerly closing anticlinorium in the Chisamba area (Moore, 1964). Meta-conglomeratic and iron-banded members of the Chikonkomene Formation occur as intercalations throughout the area.

Mesoscopic fold structures are not uncommon in the Mwomboshi gneiss. The fold structures are outlined by leucocratic bands in compositionally banded gneiss. The folds are tight to isoclinal and are folded about an  $S_2$  axial planar shear foliation. This means that folds in the gneisses are of  $F_2$  generation. At KB536726, a normal tight fold (Plate 4.14) is associated with stretched xenoliths defining a 'b' lineation. The fold axis defined by the lineation is horizontal and trends parallel to the foliation. A plot of foliations in the Mwomboshi gneiss indicates a northerly verging fold structure. Further south of the study area within the Mwomboshi gneiss, Moore (1964) mapped thrust faults with northerly directed transport in contrast with the southerly thrust transport deduced in the Chikonkomene Formation. Thrusting in the Mwomboshi gneiss is considered to be older than that in the Chikonkomene Formation. The folding in the gneiss is probably related to thrusting that is why there is repetition of strata.

The Chikonkomene metasedimentary rocks have suffered at least three folding events. The parallelism of  $S_0$  and  $S_1$  indicating isoclinal folding is considered to be the first event.  $F_1$  folds are preserved in some places where quartz veins are isoclinally folded in muscovite quartzite resulting in tectonic banding (Plate 4.15). The bands exhibit pinch and swell structures due to subsequent deformations.  $F_2$  folds find expression in crenulated cobbles accompanied by the development of strong crenulation cleavage (Plate 4.16). The third folding event is associated with crenulation of  $S_2$  to produce  $S_3$ . In the Chikonkomene Formation  $S_3$  was not observed in the field but was noted in thin section in phyllitic quartzite.

In the Kangomba Formation located to the north of the Chikonkomene Formation, folded phyllite is exposed at Munyama settlement school (KB502857). The phyllite recorded three folding events, which are also observed in isolated places in the Chikonkomene Formation. The phyllite is composed of alternating light and dark coloured thin bands. The banding is crenulated resulting in a strongly developed crenulation cleavage. Fine details of the nature of banding were revealed on a flat surface of a handspecimen and in thin section. Fine-grained micas define a crenulation in the light bands, which is deflected in the dark bands. This means that the crenulation in the light bands is an  $F_1$  micro-folding which was also crenulated to produce  $F_2$  micro-folds and accompanying  $S_2$  represented by dark bands (Plate 3.24). Folding of the banding i.e.  $S_1$  and  $S_2$  gave rise to a strong, third generation crenulation cleavage, which is axial planar to  $F_3$  micro-folds.

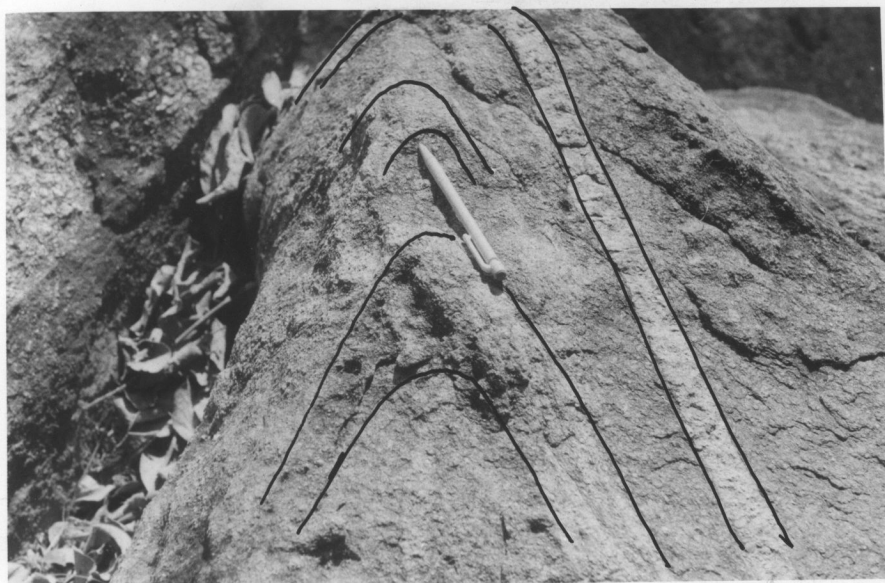


Plate 4.14: Folding in sheared quartzo-feldspathic gneiss outlined by feldspathic veins  
KB536726



Plate 4.15: Isoclinally folded quartz veins in muscovite quartzite. KB543764



A profile of a ridge of sericitic quartzite exposed at Desi-dam bridge, shows geometries indicative of a sequence of stretching, followed by folding of quartz veins (Plate 4.17). The section is perpendicular to the trend of the fold axis in the area. The asymmetry of the folds indicating north over south thrust transport. In the same section, boudins are completely detached and have a sigmoid geometry, which indicates the same sense of shear. The shear sense indicated by these fold geometries is not consistent with stress patterns responsible for the other structures in the area. Boudins in polymictic metaconglomerates are stretched along ENE trends, whereas stretching and folding is along NW and SE trends, in this particular situation.

At KB558779, minor fold structure indicates a completely different fold style (Plate 4.18). The fold geometry indicates anticlockwise rolling of a quartz vein i.e. north over south rolling, through  $90^\circ$ . This implies southerly directed thrusting which is consistent with the vergence of the structures in the area. The vein occurs in the plane of  $S_2$  foliation in sericitic quartzite suggesting that rolling is synchronous with the development of  $S_2$ .

Along the major fault boundary between the gneisses and metasediments, quartz veins are intricately folded in a dark fine-grained rock (Plate 4.19). The nappe-like fold geometries are related to movement along the fault.



Plate 4.16: Highly stretched and folded cobbles in polymictic meta-conglomerate.  
KB543778



Plate 4.17: S-type folds outlined by quartz veins in conglomeratic muscovite quartzite.  
Vertical height is 6m. Desi Dam Bridge. KB533774

#### **4.3.4 Faults**

The majority of the faults in the study area were inferred from aerial photographs and a few were observed in the field.

Striations on a fault surface of the dark banded rock plunge  $5^{\circ}$  towards  $260^{\circ}$  indicating a large component of east over west dextral strike slip displacement. The same sense of shear is exhibited from a brittle-ductile shear zone along the same fault zone (Plate 4.23). At KB383496 outside the study area, striations on a southward dipping foliation plane ( $095^{\circ}/54^{\circ}$  N) in quartzite occurring within the Mwomboshi gneiss plunge  $55^{\circ}$  towards  $210^{\circ}$  indicating northeasterly or southwesterly directed thrust transport.

Pale-blue kyanite pods are brecciated, and invaded by purple veinlets of fluorite. The pods are located along a fault mapped by Moore (1964).

#### **4.3.5 Shear zones and kinematic indicators**

Shear zones have developed in many places within the Mwomboshi gneiss, and to a lesser extent in the Chikonkomene Formation. They are characterised by marked grain size reduction and strong shear foliation compared to the adjacent rocks. The shear zones are developed parallel to the foliation in the adjacent unsheared rock.

#### 4.3.5.1 Mwomboshi gneiss Formation

The Mwomboshi gneiss comprises areas of localised intense shearing intervened by areas, which have suffered very little shearing or none.

Granite gneiss at Nankuko quarry (KB442622) is affected by narrow, 4-10 cm wide, steep to vertical shear zones. The shear zones are easily recognised by a marked grain size reduction and strong shear foliation defined by biotite and stretched felsic aggregates. The stretched felsic aggregates define a horizontal lineation. Boundaries with the adjacent unsheared rock are sharp indicating that they probably represent slip planes. There are two cross-cutting foliations in unsheared gneiss. One of the foliations ( $080^{\circ}/70^{\circ}$  N) is parallel to the shear zone boundary and the other ( $110^{\circ}/65^{\circ}$  S) is deflected into the shear zone. The sense of deflection of foliation, coupled with the horizontal lineation ( $080^{\circ}$ ), indicates west over east sinistral strike slip shear movement (Plate 4.20). S-C and C' fabrics in thin section indicate the same sense of shear (Plate 3.13). Shearing involved granulation of feldspar and quartz. Breakdown of feldspars to sericite and epidote; and biotite to chlorite along shear planes, indicates shearing under greenschist facies conditions.

Close to the fault contact between metasediments and gneisses, narrow (5 cm wide) parallel shear zones have developed in weakly foliated granite gneiss (Plate 4.11). The unsheared portion of the gneiss between the shear zones is relatively coarse-grained and the mineral constituents are aligned parallel to the foliation. The foliation is deflected into the shear zones with a dextral sense of rotation. Stretched quartz grains in the shear zones

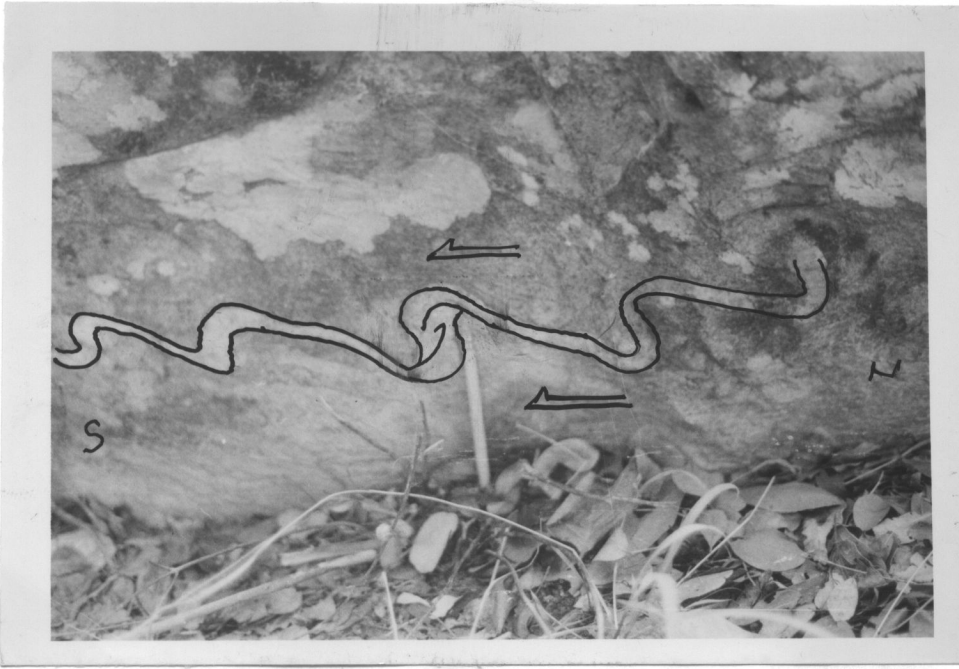


Plate 4.18: Rolled quartz vein in muscovite quartzite indicating S over N thrust transport. KB558779



Plate 4.19: Intricately folded quartz veins in a carbonaceous meta-siltstone at a major fault contact. KB547738

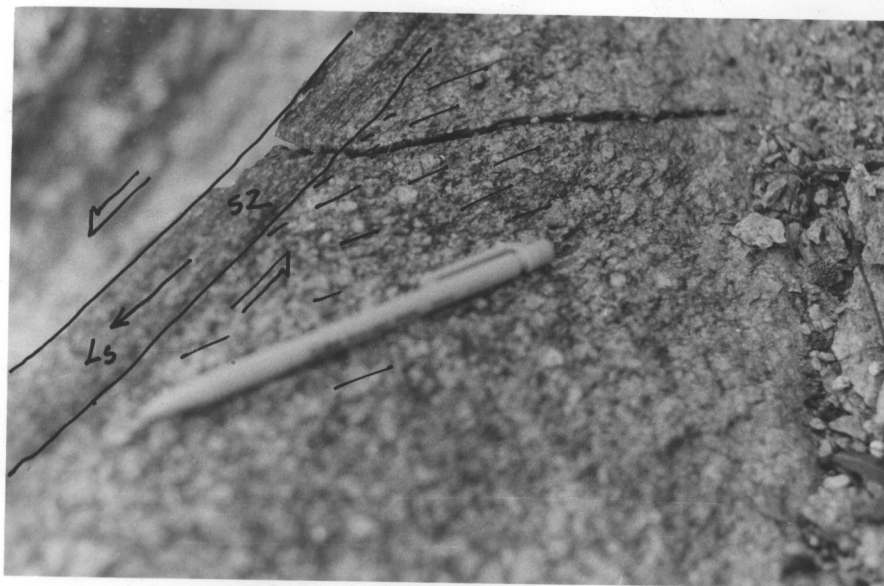


Plate 4.20: Narrow shear zone (SZ) transecting relatively coarse grained quartzofeldspathic biotite gneiss at Nankuko quarry. Deflection of foliation into shear zone indicates sinistral sense of shear. KB442622

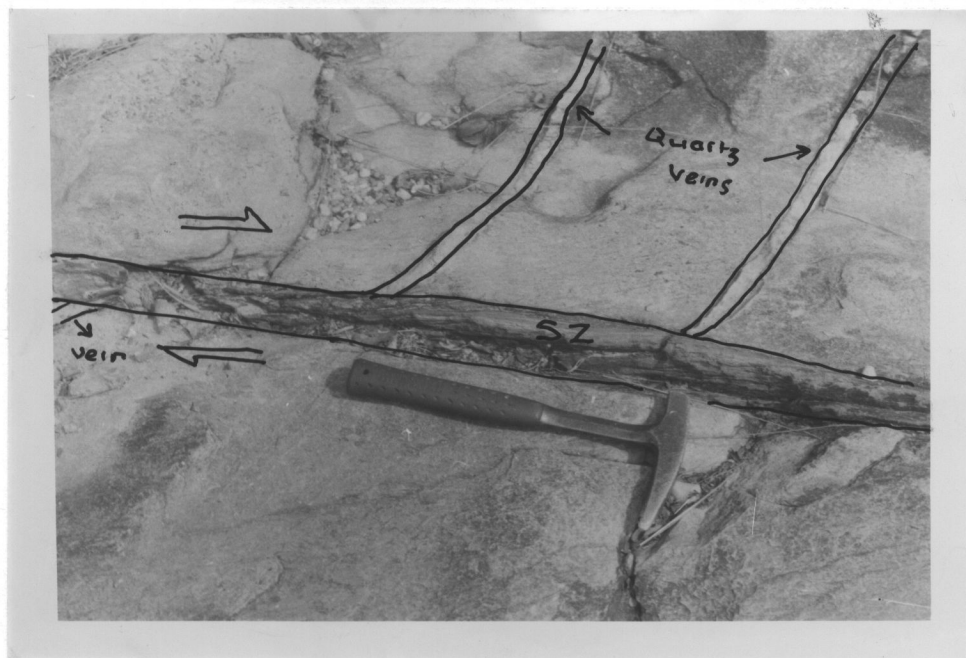


Plate 4.21: Phyllitic quartzite marking shear zone. Displacement of quartz veins on opposite sides of zone indicates dextral sense of shear. KB532777

define a strong sub-horizontal stretching lineation plunging  $5^{\circ}$  towards  $260^{\circ}$ . The similarity of transport direction to that deduced in the fault contact located slightly to the north suggests that these shear zones are probably related to the fault displacement. Development of muscovite along shear planes indicates low grade metamorphism.

Localised intense shearing in the Mwomboshi gneiss is also indicated by schistose zones ranging in size from 10-20 m wide. Grain size reduces from the unsheared gneiss to the shear zone and is accompanied by an increase in biotite content. The shear foliation is defined by alternating biotite rich and felsic layers. Stretched felsic aggregates define a lineation. In some zones the lineation indicates horizontal displacement indicating strike-slip shear, whilst high angle thrusting is evident in others. The stretching lineation in one zone has a large pitch and plunge  $60^{\circ}$  towards  $140^{\circ}$  indicating a NW directed high angle thrust or reverse shear with a large component of vertical displacement. Quartz in schistose zones is statically recrystallised and unstrained. Fresh biotite has formed in shear planes at the expense of muscovite indicating a thermal event post-dating shearing. It is suggested that the schistose shear zones developed during an older deformation event probably during the Irumide deformation.

Other zones of intense shearing in the gneisses are marked by east-north-east striking vertical laminated quartzitic or silicified zones. As in the schistose zones, both intensity of shearing and grain size reduction can be followed from the surrounding gneiss to the centre of the shear zone. The lamination defining a strong shear foliation is composed of alternating quartzitic and feldspathic layers. In thin section the feldspars are stretched in

the foliation planes and slightly altered to sericite whilst the quartz grains are statically recrystallised and have over grown a strong fabric defined by fine muscovite and rutile. Undulose extinction and deformation bands in quartz grains indicate another post-recrystallisation deformation, which is probably related to the incipient sericitisation of the feldspar. The quartz grains are also slightly flattened in the foliation plane. There are no shear sense indicators. Recrystallisation of quartz and stretched feldspar indicate shearing at high temperatures.

#### **4.3.5.2 Chikonkomene Formation**

Shear zones are not common or easily recognised in the metasediments. They are marked by narrow (4-6 cm wide) reddish brown, fine-grained phyllitic bands and occur parallel to the foliation. The foliation is defined by fine aligned sericite, opaque minerals and elongate quartz aggregates of a low grade assemblage. At KB532777, a shear zone with an attitude of 065°/45° SE displaces quartz veins in a dextral shear movement (Plate 4.21). The shear sense provides direct evidence for dextral displacement in the Nyama dislocation.

In sericitic quartzite a cobble wrapped around by an  $S_2$  foliation exhibits anticlockwise rotation indicating sinistral movement, i.e. northern side westward and southern side eastward (Plate 4.22).

*En echelon* tensional fractures across a shear zone in a vein along the area of the fault contact indicate dextral shear (Plate 4.23).



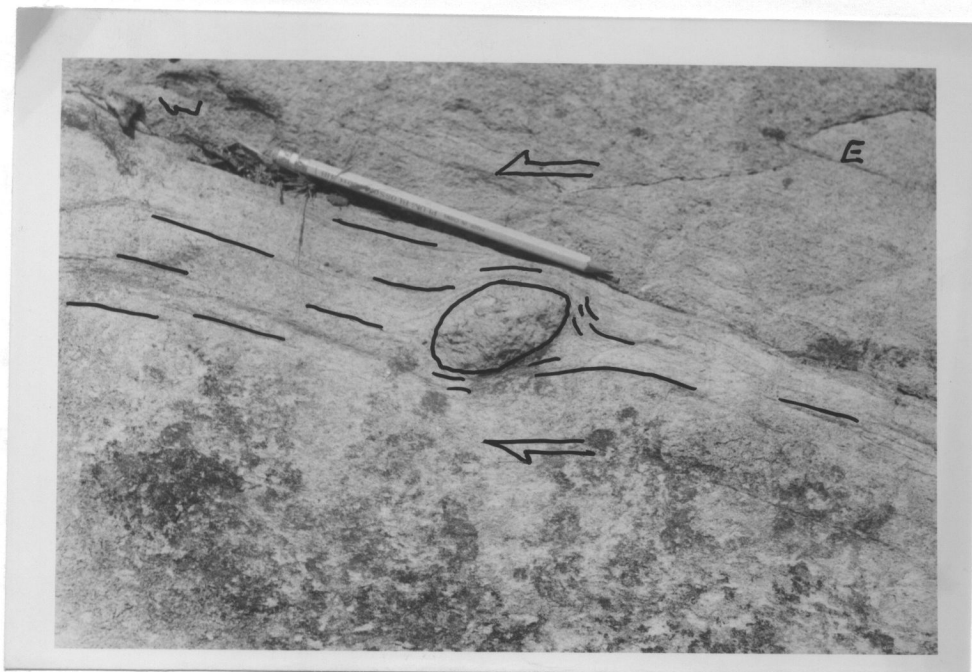


Plate 4.22: Rotated cobble in sericitic quartzite indicating sinistral sense of shear.  
KB543764



Plate 4.23: Brittle ductile shear zone indicating dextral sense of shear along a major fault contact. KB547738

The sense of shear is consistent with that deduced at another locality along the same fault. The tensional fractures indicate brittle ductile shear deformation.

**4.3.6 Strain analysis**

Strain analysis was not conducted in the Chisamba area due to the absence of strain markers. This account is based on results of strain analysis conducted in the Kabwe area at two localities in the Mwomboshi gneiss and Chikonkomene Formation.

**4.3.6.1 The Mwomboshi gneiss**

Xenoliths in the Mwomboshi gneiss are stretched in the foliation plane and define a horizontal stretching lineation. The principal strain axes (X, Y, Z) were measured and the type of strain was determined using the Flinn diagram. It was not always possible to obtain all the three axes in one xenolith. Measurements of the strain axes are presented in Table 4.1. The average lengths, of the principal axes obtained are X=17.5 cm, Y=3.5 cm, and Z=3.0 cm. The ratios of the principal planes given by a=X/Y and b=Y/Z were calculated and plotted on the Flinn diagram (Fig. 5.1). The xenoliths plot in the apparent constriction field (Ramsay and Huber, 1983). The type of strain is determined from the K value define as:

$$K = (a-1) / (b-1) .....(1)$$

The value K=20 indicates that strain makers are prolate ellipsoids (Fig. 4.5).

**4.3.6.2            The Chikonkomene Formation**

The cobbles in the meta-conglomerate are either flattened in the plane of the foliation or folded.

At KB543762, pebbles and cobbles are flattened in the plane of the foliation and the long axis X defines a dimensional lineation. Lengths of principal strain axes of deformed cobbles; X, Y and Z are presented (Table 4.1). The mean values of the principal axes are; X = 8.8 cm, Y = 4.3 cm and Z = 1 cm. The ratios of the principal axes plotted in the apparent flattening field on the Flinn diagram. The value of K=0.3 obtained from equation (1) indicates an oblate strain ellipsoid (Fig. 4.5).

The contrasting strains in the Mwomboshi gneiss and Chikonkomene Formations indicate deformation under different stress patterns. The stretching strain in the gneiss is associated with pre- or early Irumide deformation, while the flattening is associated with Lufilian deformation events.

A sufficiently long stretched and flattened cobble in polymictic meta-conglomerate is crenulated about an S<sub>2</sub> axial planar cleavage. Its original length, L<sub>0</sub> = 28cm, before folding and final length, L<sub>1</sub> = 17cm, after folding were measured and the shortening strain (e) determined. The strain ‘e’ is defined by:

$$e=(L_1-L_0)/L_1.....(2)$$

Table 4.1: Measurements of principal strain axes and strain parameters of (a) xenoliths and (b) pebbles and cobbles, X, Y, and Z cm

	(a) xenoliths				(b) cobbles and pebbles							
	X	Y		Z	X			Y			Z	
	20.0	1.1	1.0	2.0	10.0	5.5	4.5	3.0	3.0	0.5	2.0	1.0
	13.0	5.0	5.0	6.0	5.0	16.0	9.0	4.0	4.5	0.5	1.5	1.0
	6.0	2.0	1.0	3.5	6.0	7.5	12.5	2.0	5.5	0.5	2.5	1.0
	7.0	2.0	2.5	4.5	7.0	9.0	15.0	3.0	7.0	1.0	1.0	0.5
	35.0	1.0	1.5	4.0	5.5	18.0	5.0	8.0	6.0	1.5	0.5	1.2
	6.0	1.5	7.0	1.0	8.0	10.0	5.0	3.5	3.5	0.7	0.5	1.0
	10.0	1.0	1.5	2.0	8.5	8.5	10.0	3.5	5.5	0.5	1.0	1.0
	22.0	1.0	10.0		10.0	6.5	10.0	4.0	2.0	0.4	1.5	0.3
	35.0	2.0			4.0	8.0	11.0	4.0	5.0	0.4	1.5	0.8
	20.0	1.0			10.0	5.0	4.0	3.5	3.0	1.0	2.5	0.6
					14.0	17.0	10.0	4.5	4.5	1.0	1.0	0.4
					12.0	5.0	2.5	5.0	3.5	1.5	1.5	1.5
					9.0	6.5	5.0	5.0	4.5	1.5	0.6	1.8
					13.0	14.0	10.0	3.0	3.0	1.5	0.8	0.8
					8.5			5.0	5.0	1.0	1.0	0.8
								2.5	5.5	0.5	0.7	0.3
								4.0	2.5	0.8	0.5	0.4
								4.5		2.0		0.5
								8.0		1.5		
								6.0		1.0		
								4.0		0.7		
										0.6		
										1.0		
										1.5		
										1.0		
										1.0		
X/Y	5.0				2.0							
Y/Z	1.1				4.3							
K	20.0				0.3							

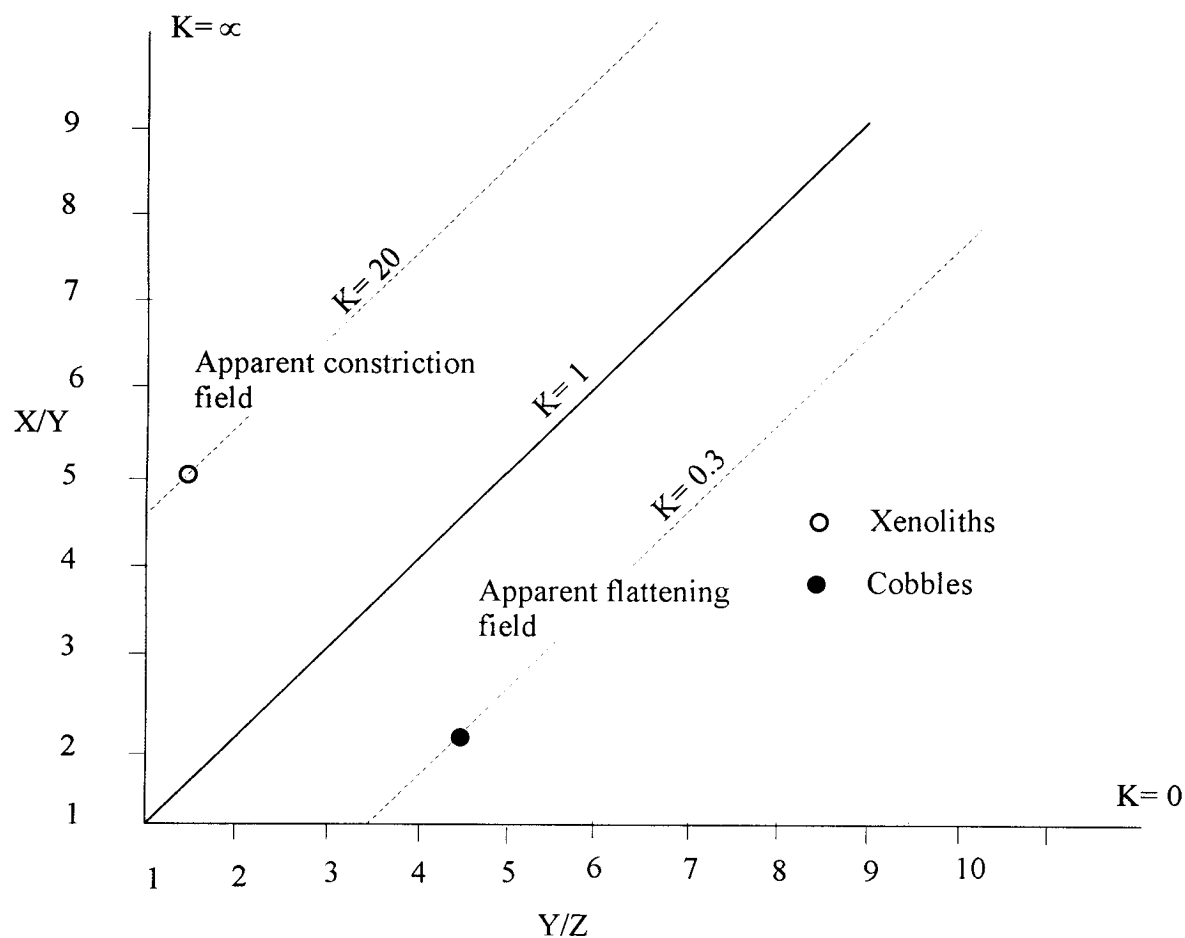


Fig.4.5: Flinn diagram plot of strain of stretched xenoliths in the Mwomboshi gneiss and cobbles in the Chikonkomene Formation.

Equation (2) yields 0.39. The amount of shortening is considered as the minimum strain as most of the strain was taken up in the schistose matrix. The development of a strong cleavage, which wraps around the folded cobbles, indicates that the maximum strain was concentrated in the matrix. This indicates strain partitioning (Ramsay and Huber, 1983; Price and Cosgrove, 1990).

#### **4.4 Discussion and summary**

##### **4.4.1 Chisamba area**

The northeasterly structural vergence in the Chisamba area is consistent with the thrust transport in the Lufilian Arc, but is in contrast with the southwesterly-directed thrust transport of the Zambezi Belt.

Two types of stretching lineations are distinguished on the basis of the amount of plunge; ENE-NE sub-horizontal ( $0-5^\circ$ ) lineation on steep to vertical shear planes and plunging ( $25-40^\circ$ ) lineation on moderately dipping shear planes. All the shear sense indicators associated with sub-horizontal stretching lineations provide a consistent pattern of dextral transcurrent shear in the MDZ in the Chisamba area. The oblique stretching lineation and associated

shear foliation indicate sinistral strike-slip movement. On the basis of parallelism with and similarity with Lufilian thrust transport, the oblique stretching lineation is considered to have developed during the major thrusting event of the Lufilian orogeny. The occurrence of both sub-horizontal and oblique plunging stretching lineations is considered to be a

result of successive deformation events. The strike-slip event is envisaged to be later than the thrust event.

Meso-and microstructural shear sense indicators in the Chisamba area possess asymmetric shapes indicating that deformation in the MDZ was non-coaxial. In contrast, asymmetric shear sense indicators in the Kabwe area suggest that shear deformation in the Kabwe area was predominantly coaxial.

All the faults were inferred from aerial photographs and were not observed in the field. The coincidence of an inferred fault with quartz mylonite suggests that the inferred faults represent narrow shear zones. This also indicates that deformation in the Chisamba area was predominantly ductile.

#### **4.4.2 Kabwe area**

Despite being located outside the MDZ, the Kabwe area displays similar structural trends to those observed in the Chisamba area. However, mesoscopic structures suggest different deformation mechanisms. The ENE-WSW trends are attributed to deformation during the Irumide orogeny and probably accentuated by later movement along the MDZ. Sub-horizontal stretching lineations in the Mwomboshi gneiss are associated with east over west dextral strike-slip movement. Plunging stretching lineations and vergence of structures in the Mwomboshi gneiss indicate northward directed thrusting. In the Chikonkomene Formation plunging stretching lineations, structural vergence and minor

fold geometries indicate southward directed thrusting. It is suggested that the two thrust transport directions correspond to the southeasterly and northwesterly structural zones of the Irumide belt of Daly (1984).

Both dextral and sinistral shear sense indicators were observed in the Kabwe area. A sinistral sense of shear is more common than dextral suggesting a predominantly sinistral regime. The dextral shear sense associated with the Nyama Dislocation Zone (NDZ), was observed mainly in the Chikonkomene meta-sediments. The sinistral shear movement noted mainly in the Mwomboshi gneiss is considered to be an older shear deformation, probably associated with Irumide orogeny.

Unlike in the Chisamba area, faults were easily recognised in the field by the presence of fault breccia. This indicates that deformation in the Kabwe area was predominantly cataclastic.



## Chapter 5

### 5.0 METAMORPHISM

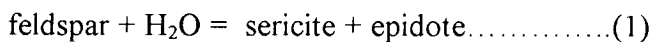
#### 5.1 Introduction

Interpretation of metamorphic conditions prevailing during shear deformation in the Chisamba and Kabwe areas are largely based on petrographic analysis. One sample from the Chisamba area was analysed using an electron microprobe. Analyses of garnet and hornblende are used in the garnet-amphibole geothermometer to estimate the pre-shearing metamorphic grade of some rock types found in the MDZ.

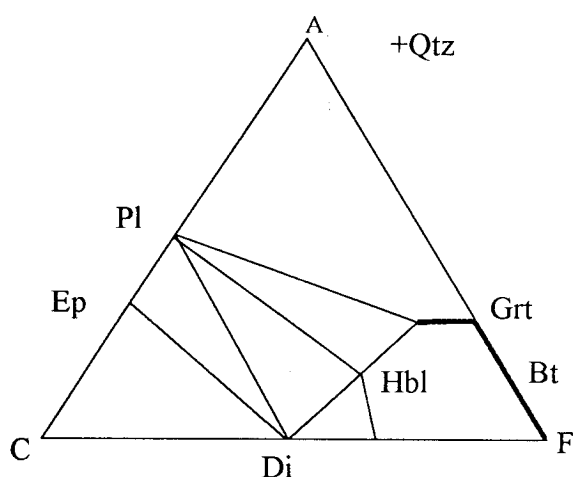
#### 5.2 Chisamba area

##### 5.2.1 Quartzo-feldspathic gneisses

Quartzo-feldspathic Gneisses have undergone various intensities of shearing to produce relatively finer-grained equivalents. The gneiss consists of the assemblage; quartz+microcline+plagioclase+muscovite+biotite (Fig. 5.1 C). Sericite is quite abundant in sheared portions of the gneisses along shear planes. The sericite is a product of retrograde metamorphism and formed from the breakdown of feldspars according to the hydration reaction:

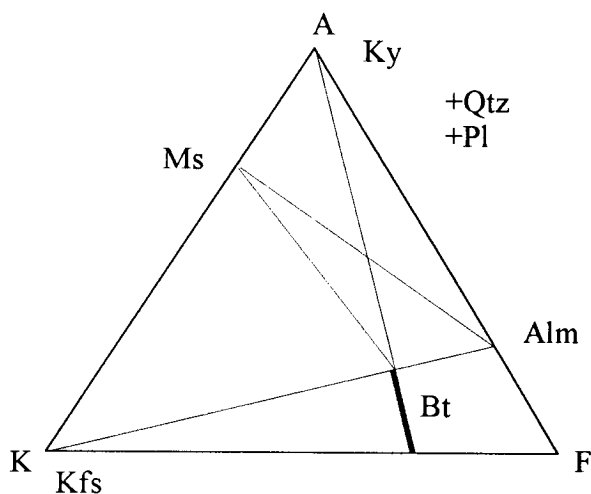


Biotite is also replaced by chlorite along shear planes.



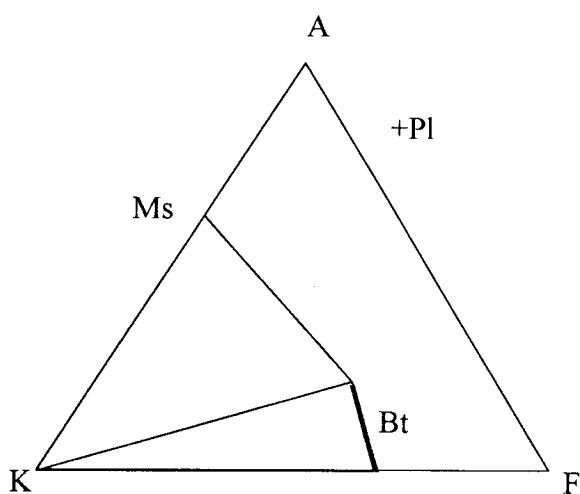
A: Mineral assemblages:

- Grt+Hbl+Pl+Bt+Scp
- Scp+Di+Pl+Ep+Cal



B: Mineral assemblages:

- Alm+Ms+Bt+Kfs
- Ky+Ms



C: Mineral assemblage:

- Qtz+Pl+Kfs+Ms+Bt

#### Mineral abbreviations

Alm	-	almandine
Bt	-	biotite
Cal	-	calcite
Di	-	diopside
Ep	-	epidote
Grt	-	garnet
Hbl	-	hornblende
Kfs	-	K-felspar
Ky	-	kyanite
Ms	-	muscovite
Pl	-	plagioclase
Qtz	-	quartz
Scp	-	scapolite

Fig.5.1: A-ACF diagram for mineral assemblages in calc-silicate rock and garnet amphibolite  
B-AKF diagram for garnet-quartz mylonite and kyanite-muscovite quartzite. C- AKF diagram for quartzo-feldspathic gneisses

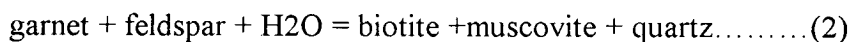
The breakdown of feldspar and biotite to the assemblage of chlorite and sericite is indicative of greenschist facies metamorphism.

### 5.2.2 Garnet-biotite-muscovite quartzo-feldspathic gneiss

The rock has a mineral assemblage; garnet+biotite+muscovite+quartz+plagioclase (Fig. 5.1 B). The minerals in the matrix are in stable equilibrium and exhibit straight boundaries and are coarser-grained than inclusions in garnet. The assemblage; biotite+muscovite+quartz +plagioclase, represents the first metamorphic event,  $M_1$ . This assemblage is stable from greenschist to amphibolite facies conditions. However the coexistence of amphibolite facies assemblages in the area suggest that it is also indicative of almandine amphibolite facies.

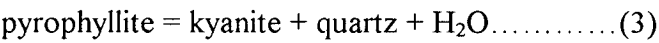
Porphyroblasts of garnet host fine-grained inclusions of quartz and biotite, of the groundmass, indicating static growth during a thermal event,  $M_2$ . The granoblastic textures and unstrained nature of the grains indicates annealing during the thermal event (Plate 3.1). The garnet is replaced by green biotite along fractures during a later metamorphic,  $M_3$

according the reaction given by:



**5.2.3 Kyanite-muscovite quartzite**

The rock has the assemblage kyanite + muscovite + quartz (Fig. 5.1 B). The absence of K-feldspar in the rock suggests that kyanite formed by dehydration of pyrophyllite during M<sub>1</sub>, according to the reaction:



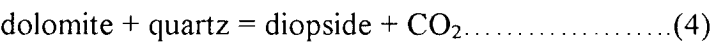
This implies that the rock was high in aliminium and was metamorphosed at relatively high pressures and low temperatures.

Quartz grains are strained and host inclusions of muscovite, and kyanite indicating static recrystallisation during M<sub>2</sub>.

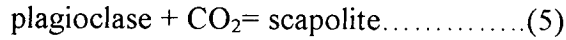
Kyanite laths are mantled by fine mica indicating uplift during a later metamorphic event, M<sub>3</sub> (Plate 3.3). Kyanite inclusions in quartz are not retrograded suggesting that the retrogression post-dated static growth of quartz.

**5.2.4 Scapolite-diopside rock**

The calc-silicate rock is represented by the assemblage diopside+scapolite+plagioclase (Fig. 5.1 A), which is stable in the amphibolite facies. The absence of tremolite in the assemblage indicates that diopside formed according to the reaction;

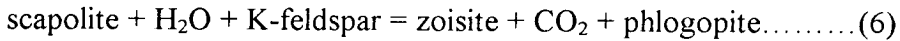


The CO<sub>2</sub> available from the above reaction combined with plagioclase to form scapolite by the reaction:



The composition of scapolite in the Lusaka dolomite is sodic mizzonite  $\text{Me}_{55}$  (Drysdall and Smith, 1966) which is stable at greenschist facies conditions. This indicates that scapolite composition and conditions of formation in the calc-silicate lithology are different from those reported in Lusaka dolomite.

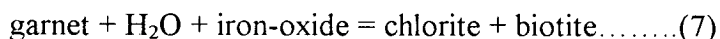
Along narrow shear zones, where there is fluid circulation, scapolite breaks down to deep blue zoisite and phlogopite by the reaction:



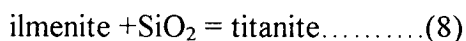
### 5.2.5 Garnet amphibolites

Garnet amphibolites are associated with marble and gneisses. The garnet amphibolite in the marble contains scapolite, whereas that in the gneiss does not. This may be explained by the availability of a fluid phase ( $\text{CO}_2$ , Cl), that stabilises scapolite relative to plagioclase.

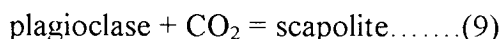
Peak metamorphism,  $M_1$ , in the amphibolites is given by the assemblage, hornblende I + plagioclase I + garnet + quartz  $\pm$  biotite (Fig. 5.1 A). In both types of amphibolites, garnet is surrounded by a moat of plagioclase II, euhedral hornblende II, epidote, sphene and  $\pm$  biotite. The breakdown of garnet to plagioclase II and hornblende II indicates isothermal decompression,  $M_2$  (Plate 3.6). Garnet is further replaced along fractures by biotite and chlorite indicating greenschist facies metamorphism,  $M_3$  given by the reaction:



In the decompression assemblage epidote occurs as inclusions in plagioclase which is partly replaced by scapolite indicating high Ca compositions of the plagioclase. Complete replacement of plagioclase is displayed by epidote inclusions in scapolite. Titanite in the decompression sites is associated with ilmenite after which it formed by the reaction:

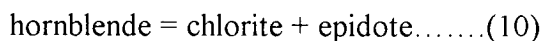


Scapolite forms at the expense of plagioclase according to the reaction:



Hornblende is seen to be retrograded to chlorite and epidote along kink bands in the rock.

The breakdown of hornblende may be represented by the reaction:

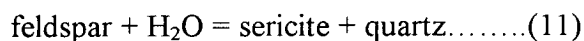


In some hornblende porphyroblasts, chlorite preferentially develops along one set of cleavage.

### 5.2.6 Mylonitic rocks

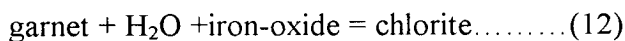
Metamorphism in shear zones is often retrogressive because the mineral assemblages produced are usually more hydrated and formed at lower P-T than the preexisting rocks that the shear zone traverses (Beach, 1980). Mylonitic rocks have mineral assemblages characteristic of retrograde metamorphism in shear zones. Shear planes in quartzo-feldspathic protomylonites are defined by the assemblage: chlorite+sericite, which formed from the breakdown of biotite and plagioclase, respectively. In some instances, retrogression has gone to completion with entire plagioclase and biotite being completely

pseudomorphed. The breakdown of feldspar to sericite proceeds according to the reaction:

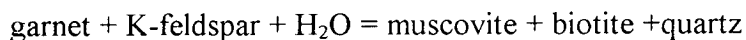


Rutile ( $\text{TiO}_2$ ) is known to be accommodated in the crystal lattice of biotite and hornblende at high temperature conditions (Spear, 1993). The formation of chlorite after biotite is accompanied by release of rutile, which was accommodated in the biotite lattice at higher temperatures.

The quartz mylonite with an original assemblage; garnet+quartz+feldspar+muscovite, has been partly retrograded. The garnet is retrograded along fractures to chlorite according to the hydration reaction:



In some instances, garnet breaks down to biotite and muscovite indicating a different chemical potential. Small inclusions of quartz in garnet reflects that it formed from the reverse reaction indicated by its retrograde assemblage; biotite+muscovite+quartz. The breakdown of garnet may be represented by the reaction:



Rounded masses of fine-grained sericite with inclusions of quartz probably indicate the breakdown of plagioclase.

### 5.2.7 Mineral chemistry

Microprobe analysis of one garnet-amphibolite sample was performed at the Goettingen University, Germany, by Dr Tembo. A Jelscan microprobe was used with an operating voltage of 15 KV and a probe current of 12  $\mu$ A.

The computer program Minfile was used to calculate the structural formulae of garnet, plagioclase and amphibole.

#### 5.2.7.1 Garnet

All the garnet grains in thin section show evidence of equilibration at lower Pressure and Temperature. The analyses of the rim and core of the garnet show insignificant chemical variation (Table 5.1). The structural formula of garnet was determined on the basis of 24 oxygen ions per unit cell (Deer et al., 1966). Fe <sup>+3</sup> is insignificant so that the total Fe is taken as Fe <sup>+2</sup>. The analysis show that the garnets are largely a solid solution of almandine (Fe<sub>3</sub>Al<sub>2</sub>Si<sub>3</sub>O<sub>12</sub>), and grossular (Ca<sub>3</sub>Al<sub>2</sub>Si<sub>3</sub>O<sub>12</sub>) components with minor amounts of pyrope (Mg<sub>3</sub>Al<sub>2</sub>Si<sub>3</sub>O<sub>12</sub>) and spessartine (Mn<sub>3</sub>Al<sub>2</sub>Si<sub>3</sub>O<sub>12</sub>) components.

#### 5.2.7.2 Plagioclase

The structural formula was determined on the basis of 16 oxygen per structural formula unit (p.f.u) and yields an average plagioclase composition of (Ca 0.35 Na 0.65 ) Al 1.35 Si 2.65 O<sub>8</sub>. The anorthite content ((Ca/(Ca+Na+K))x100) of An<sub>35</sub>, indicates that the plagioclase is andesine (An<sub>30-50</sub>) (Table 5.2.)



### **5.2.7.3 Hornblende**

Two types of hornblende were identified; hornblende in the foliation (hbl I) and euhedral hornblende (hbl II) in the corona of garnet (Plate 3.6). Microprobe analyses were conducted on both. The chemical variation between hbl II and hbl I is insignificant. The structural formula of the hornblende was determined on the basis of 24 oxygens (Table 5.3).

The hornblendes have  $\text{Na} < 0.67$  and  $(\text{Ca} + \text{Na}) > 1.34$  p.f.u, in the M4 site. The hornblendes therefore belong to the calcic-amphibole group according to the classification of Leake (1978).

### **5.2.8 Geothermobarometry**

The P-T conditions determined are those associated with the breakdown of garnet indicating decompression. The computer program, Ptmfic (Soto, 1993) was used in geothermobarometry calculations.

#### **5.2.8.1 Geothermometry**

The garnet-amphibole geothermometer (Graham and Powell, 1984; Perchuk et al., 1985) was used to calculate temperature conditions. The garnet-amphibole geothermometer is

Table 5.1: Analyses of garnet. Seven (7) grain analysed

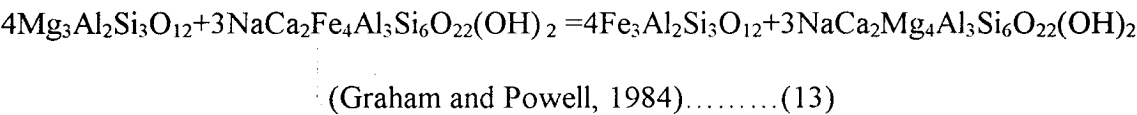
	1	2rim	2core	3rim	3core	4rim	4core	5rim	5core	6rim	6core	7rim	7core
SiO <sub>2</sub>	39.02	38.54	38.45	38.7	38.59	38.71	38.96	38.58	38.31	38.58	38.31	38.91	38.5
TiO <sub>2</sub>	0.095	0.092	0.086	0.056	0.091	0.043	0.026	0.01	0.015	0.01	0.015	0.152	0.146
Al <sub>2</sub> O <sub>3</sub>	21.63	21.59	21.6	21.69	21.81	21.62	21.45	21.56	21.77	21.56	21.77	21.59	21.77
Cr <sub>2</sub> O <sub>3</sub>	0	0.027	0.055	0	0.017	0.049	0.032	0.027	0.045	0.027	0.045	0	0.066
FeO	22.8	23.49	23.57	22.97	23.16	22.91	22.92	23.1	23.27	23.1	23.27	23.02	22.73
MnO	1.81	2.33	1.54	1.44	2.09	1.9	2.07	2.32	2.76	2.32	2.76	2.63	2.71
MgO	3.09	2.97	3.12	3.02	3.11	3.14	3.05	3.12	3.16	3.12	3.16	3.05	3.11
CaO	12.97	12.17	12.87	13.1	12.63	12.87	12.89	12.47	11.89	12.47	11.89	12.24	12.14
Total	101.45	101.21	101.32	100.99	101.51	101.28	101.41	101.20	101.22	101.20	101.22	101.62	101.17
#Si+4	6.02	5.99	5.97	6.00	5.97	6.00	6.04	5.99	6.00	5.99	5.96	6.01	5.97
#Ti+4	0.01	0.01	0.01	0.01	0.01	0.01	0.00	0.00	0.00	0.00	0.00	0.01	0.01
#Al+3	3.94	3.95	3.95	3.96	3.98	3.95	3.91	3.94	3.99	3.94	3.99	3.94	3.98
#Fe+3	0	0	0	0	0	0	0	0	0	0	0	0	0
#Fe+2	2.94	3.05	3.06	2.98	2.99	2.97	2.96	3.00	3.02	3.00	3.02	2.97	2.95
#Mn+2	0.24	0.31	0.20	0.19	0.27	0.25	0.27	0.31	0.36	0.30	0.36	0.34	0.36
#Mg+2	0.71	0.69	0.72	0.70	0.72	0.72	0.70	0.72	0.73	0.73	0.73	0.70	0.72
#Ca+2	2.14	2.03	2.14	2.18	2.09	2.13	2.14	2.07	1.98	2.07	1.98	2.04	2.02
# cations	16.00	16.03	16.05	16.02	16.03	16.03	16.02	16.03	16.08	16.03	16.04	16.01	16.01
charge	48	48	48	48	48	48	48	48	48	48	48	48	48

Table 5.2: Analyses of plagioclase. Seven (7) grains analysed

	1*	2	3	4	5	6	7
<b>SiO<sub>2</sub></b>	64.96	59.35	59.16	49.64	59.08	59.58	60.40
<b>Al<sub>2</sub>O<sub>3</sub></b>	18.08	25.12	25.21	25.35	25.26	25.40	24.52
<b>FeO</b>	0.16	0.06	0	0	0.28	0.19	0.20
<b>CaO</b>	0.01	7.34	7.47	14.54	7.56	7.28	6.53
<b>Na<sub>2</sub>O</b>	0.34	7.65	7.38	5.41	7.56	7.58	7.92
<b>K<sub>2</sub>O</b>	16.23	0.07	0.04	0.22	0.08	0.06	0.07
<b>Total</b>	99.78	99.64	99.26	95.16	99.82	100.09	99.64
<b>#Si+4</b>	3.01	2.66	2.66	2.41	2.65	2.66	2.70
<b>#Al+3</b>	0.99	1.33	1.33	1.45	1.34	1.34	1.29
<b>#Ca+2</b>	0.00	0.35	0.36	0.76	0.36	0.35	0.31
<b>#Na+1</b>	0.03	0.66	0.64	0.51	0.66	0.65	0.69
<b>#K+1</b>	0.96	0.00	0.00	0.01	0	0	0
<b># cations</b>	4.99	5.00	4.99	5.14	5.01	5.00	4.99
<b>Charge</b>	16	16	16	16	16	16	16

\*-K-feldspar

based on the Fe<sup>+2</sup>-Mg exchange between garnet and calcic amphibole according to the reaction:



The garnet-amphibole geothermometer (Graham and Powell, 1984) gives average temperatures of ≈580 °C and ≈565 °C using core and rim compositions of garnet, respectively (Table 5.4), indicating a slight fall in temperature from core to rim, due to compositional zoning. The compositional zoning reflect retrograde zonation during decreasing temperatures.

Table 5.3: Analyses of hornblende

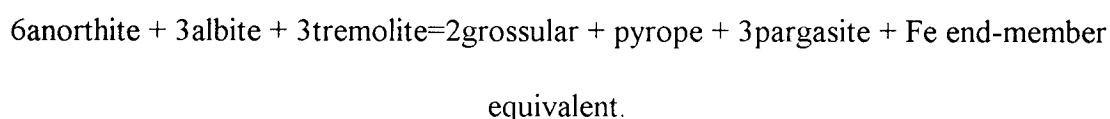
	1	2	3	4	5	6	7	8	9
	HbII	HbIII	HbII	HbII	HbII	HbII	HbII	HbIII	HbII
<b>SiO<sub>2</sub></b>	42.78	43.24	43.31	42.98	43.30	41.15	42.72	43.17	43.10
<b>TiO<sub>2</sub></b>	0.89	0.85	0.95	0.83	0.84	0.68	0.92	0.67	0.81
<b>Al<sub>2</sub>O<sub>3</sub></b>	14.06	13.61	14.26	14.07	13.08	15.52	13.82	14.36	13.67
<b>FeO</b>	15.44	16.25	14.93	15.81	15.29	16.68	15.74	15.85	15.49
<b>MnO</b>	0.32	0.29	0.17	0.28	0.22	0.23	0.25	0.25	0.21
<b>MgO</b>	9.75	9.54	9.85	9.61	9.96	8.28	9.81	9.56	10.00
<b>CaO</b>	11.78	11.75	11.62	11.81	11.85	11.75	11.67	11.83	11.55
<b>Na<sub>2</sub>O</b>	1.46	1.44	1.63	1.42	1.26	1.34	1.38	1.34	1.28
<b>K<sub>2</sub>O</b>	0.98	1.25	1.06	1.07	1.24	1.47	1.03	1.24	1.11
<b>Total</b>	97.46	98.22	97.78	97.94	97.04	97.10	97.34	98.27	97.22
<b>#Si+4</b>	6.66	6.71	6.69	6.67	6.78	6.49	6.67	6.68	6.72
<b>#Ti+4</b>	0.10	0.10	0.11	0.10	0.10	0.08	0.11	0.08	0.10
<b>#Al+3</b>	2.58	2.49	2.60	2.57	2.41	2.89	2.54	2.62	2.51
<b>#Cr+3</b>	0	0	0	0	0	0	0	0	0
<b>#Fe+3</b>	0	0	0	0	0	0	0	0	0
<b>#Fe+2</b>	2.01	2.11	1.93	2.05	2.00	2.20	2.05	2.05	2.02
<b>#Mn+2</b>	0.04	0.04	0.02	0.04	0.03	0.03	0.03	0.03	0.03
<b>#Mg+2</b>	2.26	2.21	2.27	2.22	2.32	1.95	2.28	2.20	2.32
<b>#Ca+2</b>	1.96	1.95	1.92	1.96	1.98	1.99	1.95	1.96	1.93
<b>#Na+1</b>	0.44	0.43	0.49	0.43	0.38	0.41	0.45	0.40	0.39
<b>#K+1</b>	0.19	0.25	0.21	0.21	0.25	0.30	0.20	0.25	0.22
<b>#H+1</b>	0	0	0	0	0	0	0	0	0
<b>#F</b>	0	0	0	0	0	0	0	0	0
<b>#Cl</b>	0	0	0	0	0	0	0	0	0
<b># cations</b>	16.24	16.29	16.24	16.25	16.25	16.34	16.28	16.27	16.24
<b>Charge</b>	48	48	48	48	48	48	48	48	48

The garnet-amphibole calibration of Perchuk et al., (1985) gives lower values, probably due to temperature corrections applied. The results also indicate that there are no significant temperature variations obtained from hornblende II, and I suggesting isothermal decompression.

The amphibole-plagioclase geothermometer (Blundy and Holland, 1990) gives unrealistically high temperatures ranging from 800-900 °C, and therefore not suitable a geothermometer.

#### **5.2.8.2 Geobarometry**

The garnet-amphibole-plagioclase-quartz geobarometer (Kohn and Spear, 1989) was used to calculate pressure conditions. The geobarometer is calibrated on the basis of the equilibrium:



Some pressures calculated using Fe end-member calibrations are unrealistically low. For this reason, pressures that are calculated with Mg end-member calibrations are preferred. The pressures range from 7-10 Kbars (Table 5.5).

The P-T conditions occur within the kyanite stability field; consistent with the widespread occurrence of kyanite in the study areas.

Table 5.4: Garnet-amphibole geothermometers

Graham and Powell (1984)		Perchuk et al., (1985)	
Amphibole I -T °C			
Garnet-rim	Garnet-core	Garnet-rim	Garnet-core
521.59	543.27	403.36	411.67
558.93	582.11	441.90	435.77
603.46	628.40	474.50	484.66
552.61	575.53	430.28	439.29
524.04	545.38	405.48	413.85
543.83	566.38	422.65	431.40
547.79	545.79	412.47	414.72
586.76	584.76	448.48	445.78
633.05	631.34	488.65	485.64
529.58	532.23	409.64	415.26
567.65	570.63	442.62	446.61
613.10	616.50	482.18	486.61
T <sub>AV</sub> /565.20	576.86	438.52	442.65
Amphibole II -T °C			
563.27	586.40	439.35	449.56
565.28	588.72	441.29	450.56
538.70	561.06	418.20	426.88
590.55	589.07	452.19	449.59
571.86	574.88	446.32	450.34
T <sub>AV</sub> /565.93	580.02	439.47	445.38

T<sub>AV</sub> - Average Temperature

Table 5.5: Garnet-amphibole-plagioclase-quartz geobarometer (Kohn and Spear, 1989)

T =400 °C		T=550 °C		T=NS	
Mg	Fe	Mg	Fe	Mg	Fe
9.06	7.03	9.10	5.77	8.96	10.42
9.03	8.48	9.64	10.17	7.37	3.91
6.36	0	6.42	0	6.18	1.18
9.11	8.90	9.74	10.68	7.40	4.08
9.04	7.00	9.07	5.73	8.95	10.41
7.25	0.98	7.51	0.51	6.55	1.70
9.23	2.85	3.89	-2.33	5.34	0.69
9.57	7.69	8.45	4.92	8.74	10.14
8.98	8.47	10.22	10.35	7.57	3.97
9.51	7.45	3.53	-2.66	5.22	0.58
8.19	1.71	8.64	1.61	6.98	1.99
9.51	7.45	9.63	6.29	9.17	10.59
8.86	8.46	9.45	10.14	7.26	3.91

NS - Not Specified

### **5.3 Kabwe area**

#### **5.3.1 Mwomboshi gneiss**

Mineral assemblages in the Mwomboshi gneiss and its sheared equivalents consisting of plagioclase+microcline+quartz+biotite+muscovite (Fig. 5.1C), are stable over a wide range of P-T conditions and give no indication of metamorphic grade (Bucher and Frey, 1994).

The plagioclase in many cases is sericitised and granulated along shear zones indicating greenschist facies conditions.

Fine-grained, unstrained greenish brown biotite forms at the expense of muscovite in shear zones indicating an increase in temperature post-dating shearing.

#### **5.3.2 Quartzites**

Quartzites have a simple mineral assemblage; quartz+muscovite, and not indicative of metamorphic grade. Temperature conditions are reflected by the quartz microtextures, such as undulose extinction, deformation bands and serrated boundaries. These microtextures reflect deformation mechanisms that operate at low temperatures consistent with greenschist facies conditions of metamorphism.

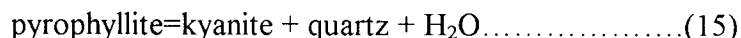
### 5.3.3 Chlorite-epidote hornblende schists

The occurrence of amphibolite schists, consisting of hornblende+plagioclase+quartz indicates amphibolite facies, M<sub>1</sub> (Fig. 5.1 A). The M<sub>1</sub> assemblage breaks down along C-planes are to an M<sub>2</sub> greenschist facies assemblage of chlorite+zoisite+albite+calcite-sphene according to the reaction of the form:



### 5.3.4 Chikonkomene Formation

The mineral assemblage of the Chikonkomene Formation metasediments consists of quartz+muscovite+iron-oxide±kyanite. Sericite occurs along foliations indicating deformation under greenschist facies conditions. Kyanite in the pods probably formed according the reaction:



during an M<sub>1</sub> event, probably Irumide orogeny. Its general absence in the metasediments suggests that it has completely been retrograded to muscovite.

Kyanite pods and iron-banded quartzites are cross-cut by purple fluorite veinlets. Although evaporite sequences are not reported in the area, the fluorite fluids may have been derived from now eroded evaporite deposit. The fluorite is probably related to the regional scapolitisation reported in the southern, central and Copperbelt areas.



## Chapter 6

### 6.0 FLUID INCLUSION COMPOSITIONS

#### 6.1 Introduction

The MDZ is economically significant as it forms the locus of gold deposits in central Zambia. Gold mineralisation associated with the MDZ occurs in second and third order structures (Kasolo, 1992). However, Simpson et al. (1963) also reported gold mineralisation within the main shear zone in the Lusaka area.

The NDZ is a relatively small zone, extending for approximately 50 Km and is believed to be coeval with the MDZ.

Fluid inclusions in vein-quartz from the MDZ and NDZ were studied in order to characterise fluid compositions and further constrain the P-T conditions that prevailed during shearing along the MDZ.

Fluid inclusions from the Matala, Dunrobin, Sasare, and Chumbwe gold deposits associated with the MDZ consist of  $\text{H}_2\text{O}-\text{CO}_2 \pm \text{Halite}$ ,  $\text{H}_2\text{O}-\text{Halite}$ , and low saline  $\text{H}_2\text{O}$  inclusions, with salinities and Th ranging between 1.7-12 Wt% NaCl Equivalent (EQ) and 213-443 °C, respectively (Kasolo, 1992).

Microthermometry of fluid inclusions from carbonate hosted Kabwe Pb-Zn deposit, located 25 Km north of study area A, indicate  $\text{H}_2\text{O}-\text{NaCl}-\text{CaCl}_2$  and  $\text{H}_2\text{O}-\text{MgCl}_2-\text{CaCl}_2$  compositions, of salinities and Th ranging from 11 to 31 Wt% NaCl EQ and 257 °C to 305 °C, respectively (Kamona, 1993).

This study presents fluid inclusion compositions, P-T trapping conditions and fluid evolution of vein-quartz in the Chisamba and Kabwe areas.

## **6.2 Sampling for fluid inclusion studies**

Oriented samples for fluid inclusion studies, one from each area, were taken from a foliation-parallel vein intrusive in the gneisses and from boudinaged quartz-vein in the Chisamba and Kabwe areas, respectively

## **6.3 Petrographic description of vein-quartz samples**

### **6.3.1 Chisamba area**

The sample was taken from a quartz vein intrusive in biotite-muscovite gneiss. The vein measures 4 m wide and trends parallel to the main foliation. It is composed of medium crystalline quartz grains, which are slightly elongated parallel to the trend of the vein and foliation.

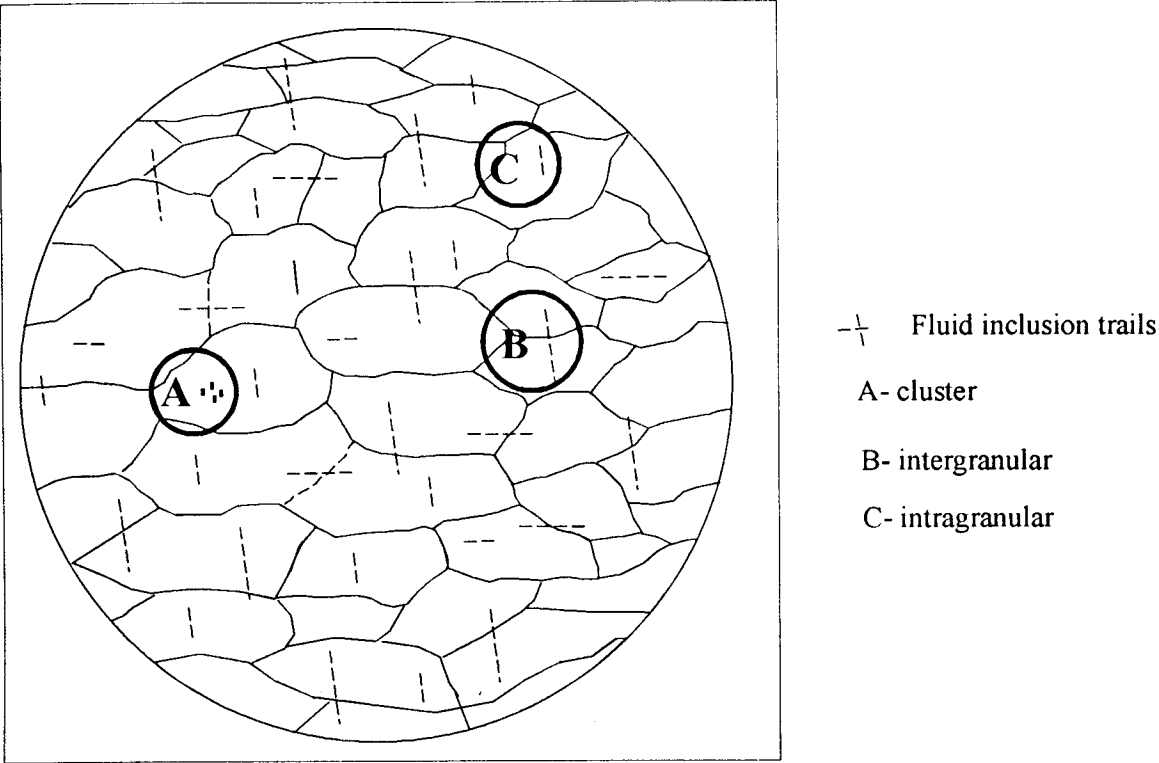
In thin section, the vein is composed of an intergrowth of medium crystalline quartz grains exhibiting serrated and irregular grain boundaries indicating strain-induced recrystallisation. Patchy extinction is characteristic of the quartz. Small subgrains exhibit straight boundaries meeting at triple junctions.

Quartz grains are affected by both healed intergranular and intragranular micro-fractures. Two sets of micro-fractures are distinguished. One set is defined by fluid inclusion trails oriented at a high angle (85-90°) to the stretching direction (Fig. 6.1). Another set of inclusion trails is oriented parallel to the direction of stretching. Isolated fluid inclusions and clusters, of probable primary origin, are also present.

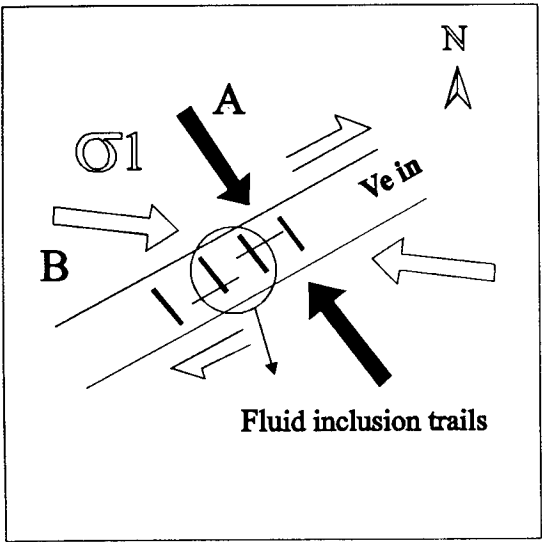
### **6.3.2 Kabwe area**

The vein is composed of milky white, medium-grained crystalline quartz with abundant specular hematite. As in many other quartz veins in this area, opaque minerals are oriented at a low angle to the trend of the vein, and foliation in the sericitic quartzite. The vein is stretched and boudinaged parallel to the foliation. Elongation of quartz grains is not apparent in hand specimen.

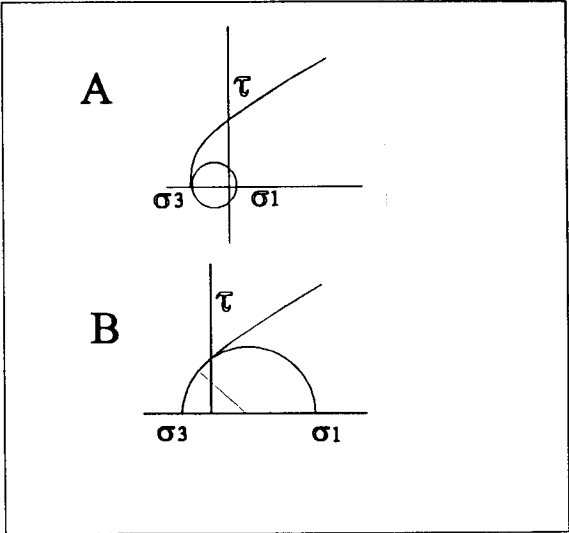
In thin section, the vein consists of a recrystallised mosaic of predominantly unstrained medium grained quartz displaying a granoblastic texture. Clusters of hematite, possessing a preferred orientation are sparsely distributed in the section.



Microscopic schematic sketch of flattened quartz grains showing the orientation of fluid inclusion trails



Stress patterns associated with fluid inclusions. Solid arrow A : extension fracture, open arrow B :shear extension



Mohr stress circle for fluid inclusion trails.  $\tau$  = shear stress,  $\sigma$  = normal stress.

Fig.6.1: Geometry of fluid inclusion trails: Chisamba area

Inclusion trails along healed fractures in this sample have no preferred orientation. They occur as intergranular to intragranular cross cutting microfractures.

#### **6.4 Geometry of fluid inclusion trails**

In the Chisamba sample, two sets of fluid inclusion trails are related to pure extension and shear extension fractures (Fig. 6.1). The shear extension is correlated with dextral movement along the MDZ. Field evidence for deformation related to pure extension was not observed.

Inclusion trails in the Kabwe sample are randomly oriented despite the presence of an external stress field exemplified by a strong fabric in the host rock.

#### **6.5 Microthermometry abbreviations**

<b>T<sub>m</sub></b>	-	Temperature of melting
<b>Th<sub>L</sub></b>	-	Temperature of homogenisation to liquid state
<b>Th<sub>V</sub></b>	-	Temperature of homogenisation to vapour state
<b>Th<sub>tot</sub></b>	-	Temperature of total homogenisation
<b>T<sub>s</sub></b>	-	Temperature of dissolution of halite
<b>T<sub>d</sub></b>	-	Temperature of decrepitation
<b>LVS</b>	-	Liquid Vapour Solid classification of inclusions
<b>DF</b>	-	Degree of fill
<b>d</b>	-	Density

## 6.6 Analytical equipment

Fluid inclusion analyses were conducted at the University of Zimbabwe, Geology Department. Fluid compositions and densities are based solely on microthermometry data (Appendix). Microthermometry was conducted using a binocular Olympus microscope (BH-2) with maximum magnification of 400; and a Linkam THM600 heating and freezing stage provided with a thermal control unit (TMS-90, TP91). Liquid Nitrogen and a thermal resistor are used for cooling and heating, respectively. The lower and upper temperature limits of the stage are -199 °C and 600 °C. Pure CO<sub>2</sub> in fluid inclusions from the Umwindsi shear zone, Zimbabwe, distilled water and synthetic standards TM135 and TM180, were used for calibration at -56.6 °C, 0 °C, 135 °C and 180 °C, respectively.

The computer program COHFLUID was employed to calculate XCO<sub>2</sub>, XH<sub>2</sub>O, d, and TMV for H<sub>2</sub>O-CO<sub>2</sub> inclusions. The same program was used to calculate isochores for the inclusions.

The subprogram SALTY was used to calculate Wt% NaCl EQ in highly saline H<sub>2</sub>O-Halite inclusions from T<sub>s</sub> and T<sub>h</sub>.

## **6.7 Fluid inclusions**

### **6.7.1 Chisamba area**

Four inclusion populations were identified in the sample: intergranular trails, intragranular trails, clusters and isolated inclusions. Fluid inclusions consist of H<sub>2</sub>O-CO<sub>2</sub> ±Halite, H<sub>2</sub>O-Halite and low saline inclusions.

#### **6.7.1.1 H<sub>2</sub>O - CO<sub>2</sub> ±halite inclusions**

H<sub>2</sub>O-CO<sub>2</sub> inclusions occur in intragranular and clustered bands. They are thus considered to be early inclusions but not necessarily primary. The inclusions generally consist of three to four phases at room temperature. The phases include (1) Liquid H<sub>2</sub>O (2) Liquid CO<sub>2</sub> (3) vapour CO<sub>2</sub> and (4) ± daughter halite crystal(s), (Fig. 6.2). DF varies between 0.1 and 0.9. DF was visually estimated for both irregular and negative shapes. Standard charts from Shepherd et al (1985) were used for the latter.

Th CO<sub>2</sub> to liquid ranges from 7 °C - 30 °C (Fig. 6.3 A). The Th CO<sub>2</sub> to liquid suggests high densities for the CO<sub>2</sub> portion of the fluid. The degree of fill ranges from 0.1- 0.6. Th<sub>tot</sub> H<sub>2</sub>O-CO<sub>2</sub> ranged between 250 °C and 400 °C (Fig. 6.3 B).

#### **6.7.1.2 H<sub>2</sub>O-halite inclusions**

H<sub>2</sub>O-halite inclusions occur both in intragranular and intergranular trails. They occur in irregular and negative shapes. H<sub>2</sub>O-halite inclusions contain three phases; liquid H<sub>2</sub>O,

# H<sub>2</sub>O-Halite AND H<sub>2</sub>O-CO<sub>2</sub> FLUID INCLUSIONS-MDZ

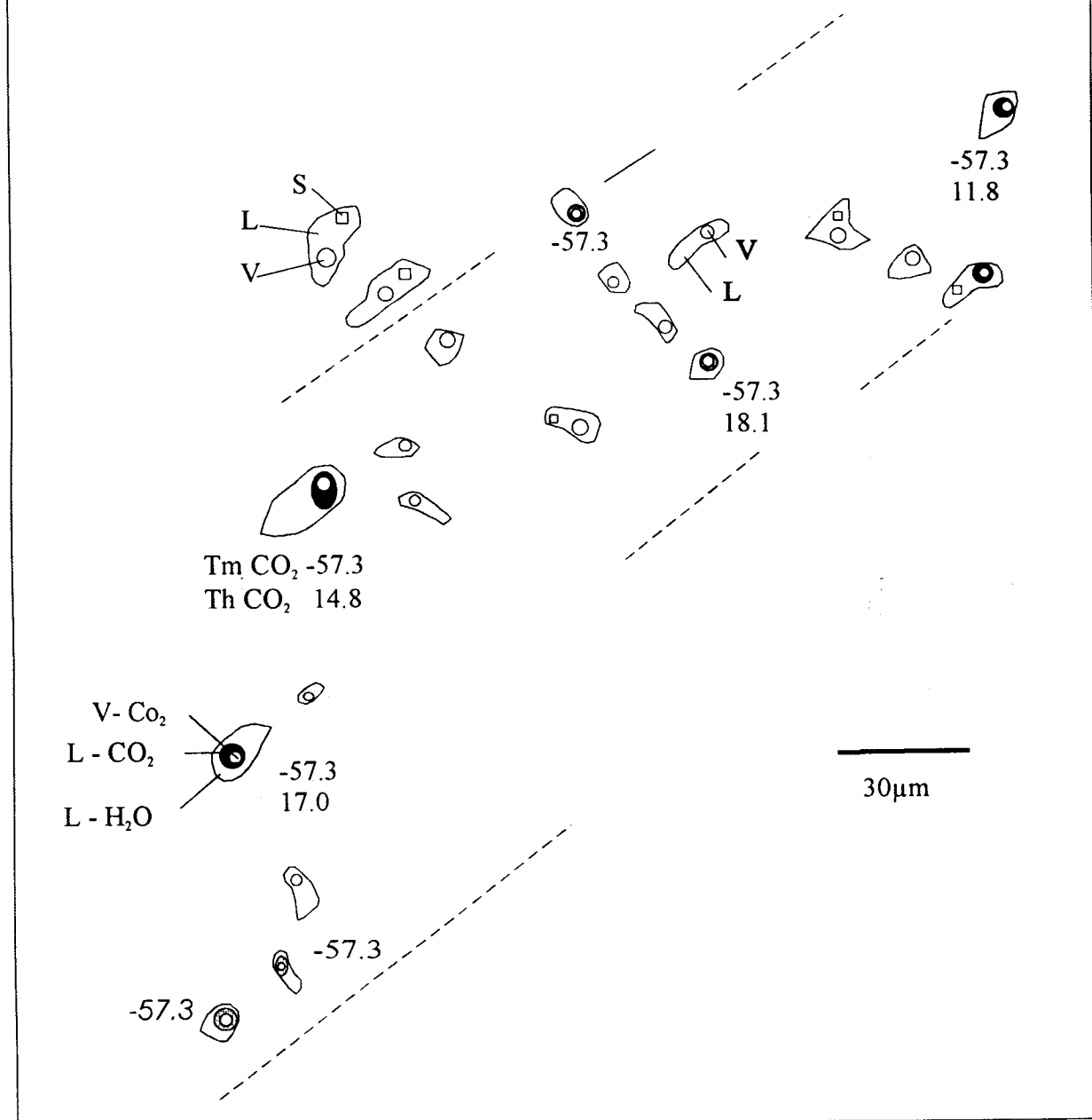


Fig.6.2: Intragranular trail of H<sub>2</sub>O-CO<sub>2</sub>, H<sub>2</sub>O-halite and low saline fluid inclusions. L-liquid V-vapour, S-daughter halite crystal



vapour H<sub>2</sub>O and one or two daughter halite crystals. Ts ranges from 250-350°C (Fig. 6.3 C). The presence of daughter crystals indicates that the fluids are oversaturated. Three phase transitions were noted (1) homogenisation to liquid (2) homogenisation to vapour and (3) dissolution of the halite. The frequency distribution ThV reflects three populations with highest peak values at 350 °C (Fig. 6.3 D).

The higher values are attributed to leaking and decrepitation. ThL and ThV occurred in the same temperature range indicating trapping from a boiling fluid (Shepherd et al., 1985).

Th<sub>tot</sub> took two forms; (1) homogenisation to vapour or liquid before dissolution of halite, implying that Ts is equal to Th<sub>tot</sub>. (2) homogenisation of aqueous phase to vapour or liquid after dissolution of halite.

Salinities calculated using subprogram salty range from 34-44 Wt% NaCl EQ. A plot of Ts against salinity shows a few points close to and along the saturation curve but most plot along vertical trends probably indicating decrepitation (Fig. 6.4).

### **6.7.2 Kabwe area**

Similarly four inclusion populations were identified; intergranular trails, intragranular trails, clusters and isolated inclusions. Fluid inclusions comprise; H<sub>2</sub>O-Halite, low saline H<sub>2</sub>O-NaCl-CaCl<sub>2</sub> and low saline H<sub>2</sub>O-complex salt.

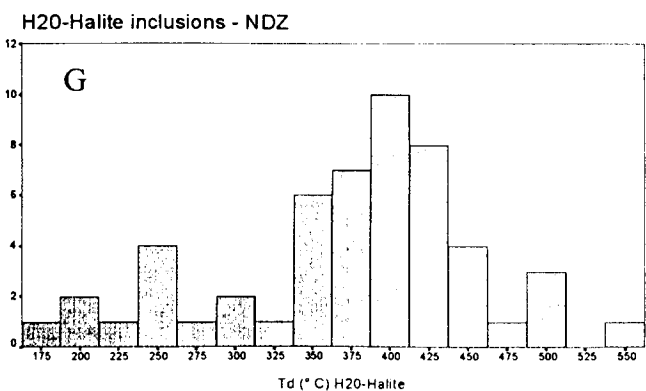
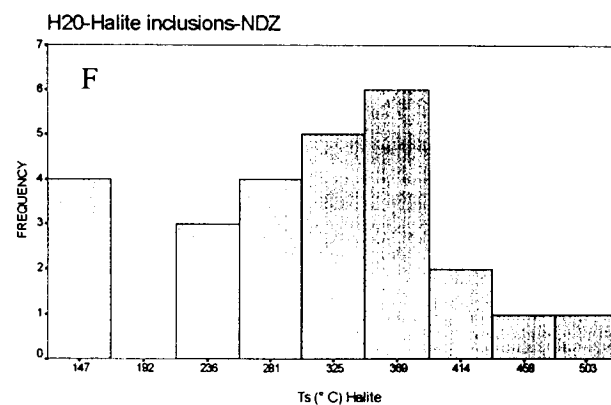
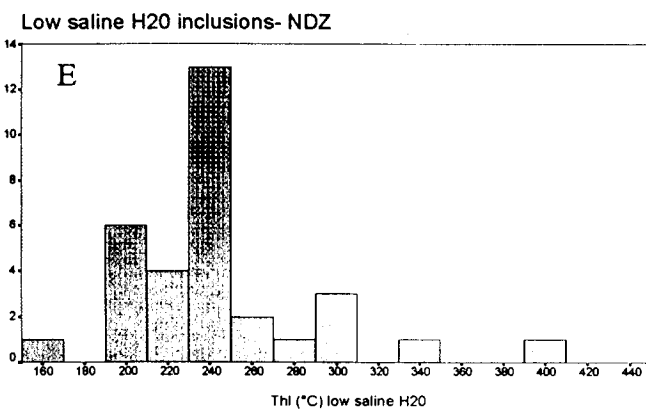
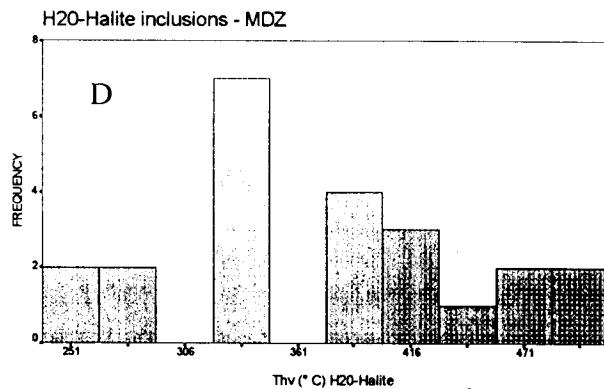
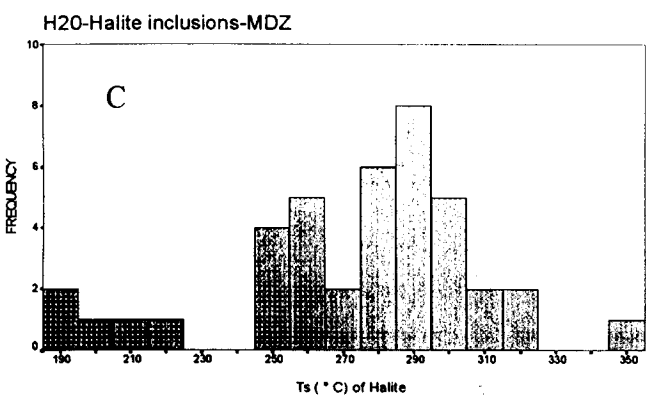
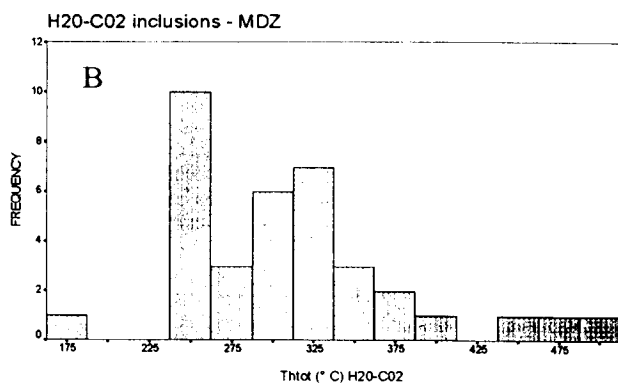
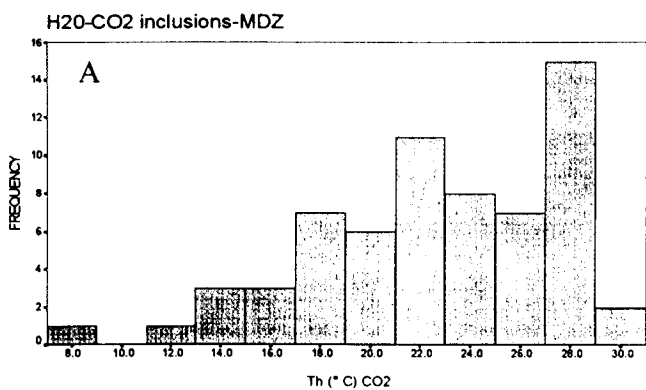


Fig. 6.3: Microthermometry histograms.  
A) Th (°C) CO<sub>2</sub>-MDZ.  
B) Thtot (°C) H<sub>2</sub>O-CO<sub>2</sub>-MDZ.  
C) Ts (°C) Halite-MDZ.  
D) Thv (°C) H<sub>2</sub>O-Halite-MDZ  
E) Thl (°C) Low saline H<sub>2</sub>O-NDZ.  
F) Ts (°C) Halite-NDZ.  
G) Td (°C) H<sub>2</sub>O-Halite-NDZ

#### **6.7.2.1 H<sub>2</sub>O-halite inclusions**

Inclusion trails do not show preferred orientation and cross-cut one another. At room temperature, the inclusions consist of three phases; liquid saline H<sub>2</sub>O, vapour and one or two daughter crystals of halite (Fig. 6.5).

The frequency distribution ThL shows peak values at 240 °C (Fig. 6.3 E). The histogram for Ts shows a wide range with higher values up to 500 °C (Fig. 6.3 F). The higher temperature range probably represents leaking which is not always easy to detect. A plot of Td shows a single peak distribution at 400 °C (Fig. 6.3 G).

#### **6.7.2.1 Low saline H<sub>2</sub>O inclusions**

Low saline inclusions contain no daughter halite crystals. They consist of two phases; vapour H<sub>2</sub>O and saline liquid. Some low saline inclusions occur in clusters (Fig. 6.5).

The first melting of the crystals occurs at -52 °C and final melting occurs at -48.4 °C indicating that the inclusions belong to the H<sub>2</sub>O-NaCl-CaCl<sub>2</sub> ternary system.

The other population of low saline inclusions behaved differently at low temperature. The T<sub>m</sub> ranged from -34 °C to -48 °C, with the highest frequency occurring in the range -38 °C to -48 °C.

## H<sub>2</sub>O-HALITE FLUID INCLUSIONS

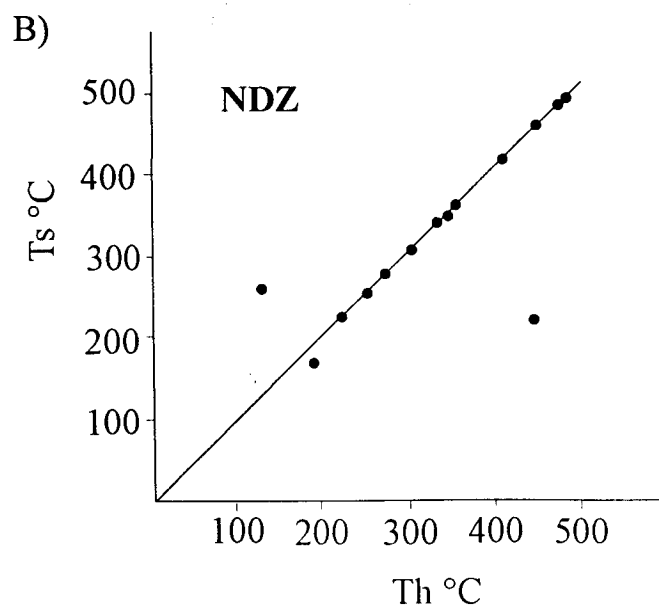
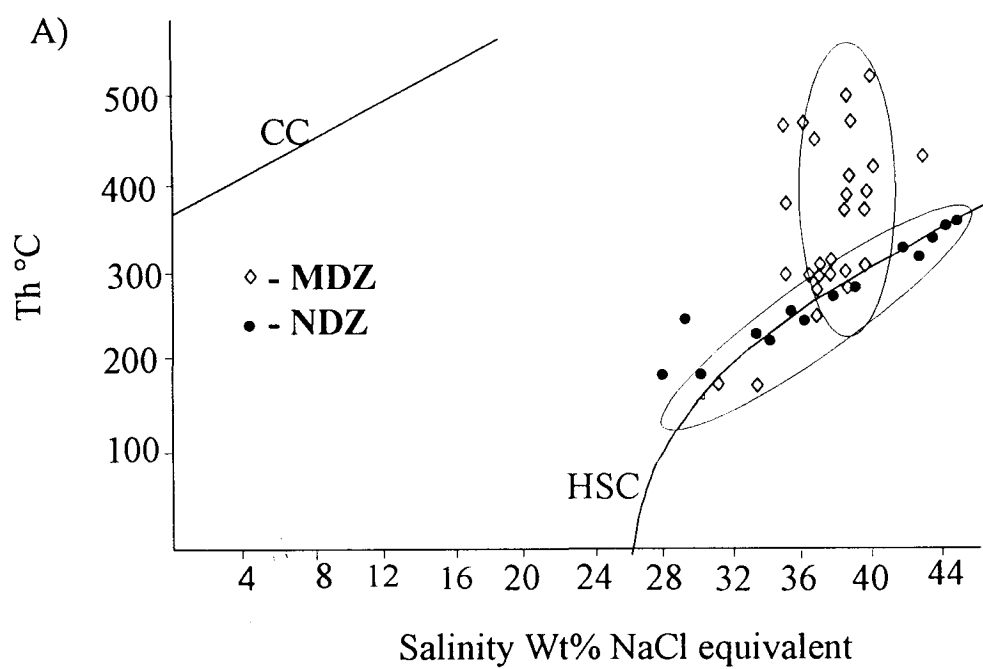


Fig.6.4: A) plot of Th against salinity (W%t NaCl) of H<sub>2</sub>O-halite inclusions from the MDZ and NDZ. B) Plot of Ts and Th of H<sub>2</sub>O-halite inclusions from the NDZ. CC: critical curve, HSC: halite saturation curve (after Shepherd et al., 1985)

## 6.8 Fluid evolution

The occurrence of  $\text{H}_2\text{O}-\text{CO}_2$  and  $\text{H}_2\text{O}$ -Halite inclusions is explained by mixing of two different fluids; a highly saline aqueous and low saline aqueous fluid at high temperatures. On cooling the homogeneous fluid unmixed into  $\text{H}_2\text{O}-\text{CO}_2$  and  $\text{H}_2\text{O}$ -Halite fluids. Thus the fluid inclusions from the Chisamba area resulted from fluid trapping at conditions of immiscibility. This is further indicated by the high salinity of the  $\text{H}_2\text{O}$ -Halite inclusions which range from 34 -38 % Wt NaCl EQ.

In the Kabwe area, the fluid inclusions are highly saline. The plot of Th vs salinity and homogenisation of fluid inclusions (Fig. 6.4) to both liquid and vapour in the same temperature range, indicates unmixing from a boiling fluid.

## 6.9 P-T conditions of trapping

The fundamental assumption in the study of fluid inclusions to determine the P-T conditions of trapping is that the volume of the inclusions has not changed or the fluid inclusion has not leaked since entrapment (Roedder, 1984). Some fluid inclusions in the samples studied exhibit implosion and decrepitation textures, and these were not analysed.

Intersection of isochores for  $\text{H}_2\text{O}-\text{CO}_2$  inclusions and the field of dissolution of halite, which corresponds to Th, were used to estimate the conditions of trapping. Isochores converge in the P-T field of trapping region between 200 °C and 350 °C corresponding to

# H<sub>2</sub>O-HALITE AND LOW SALINE FLUID INCLUSIONS - NDZ

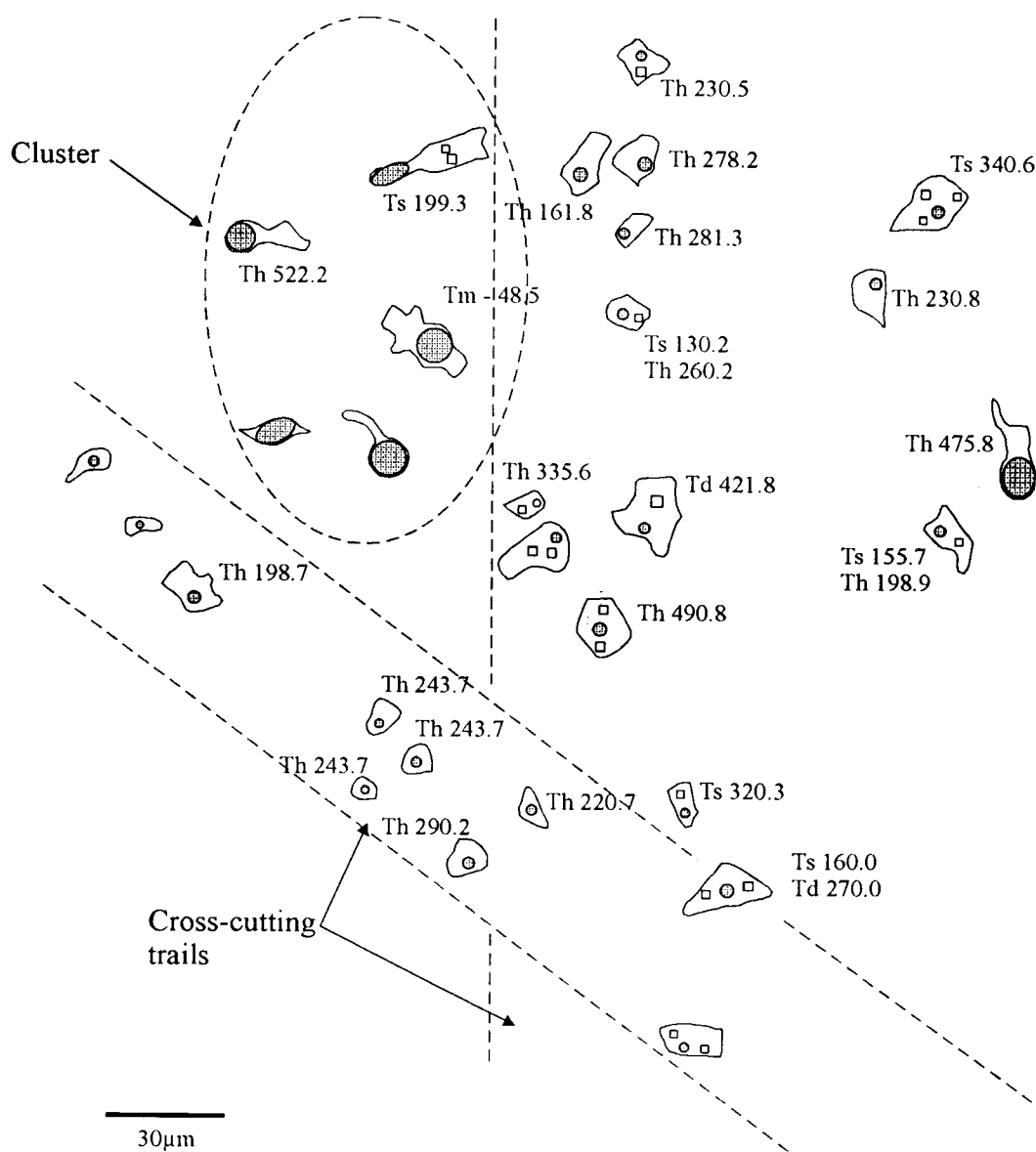


Fig. 6.5. Cross-cutting intragranular trails and clusters of H<sub>2</sub>O-halite and low saline inclusions. Some inclusions contain up to three daughter crystals

pressures between 2 and 3 Kbar (Fig. 6.6). The P-T conditions are conformable with greenschist facies grade of metamorphism.

#### **6.10 Discussion and summary**

Fluid inclusion data suggest that the fluids present during shearing along the MDZ and NDZ were highly saline brines. Salinities of H<sub>2</sub>O-CO<sub>2</sub> fluid inclusions from Matala, Dunrobin, Sasare and Chumbwe gold deposits are far much lower than those determined in the barren vein from the Chisamba area. This implies that salinity of fluid inclusions can be used as one of the criterion to distinguish between barren and gold bearing veins associated with the MDZ.

Scapolite and fluorite are widespread in the Chisamba and Kabwe areas respectively. The influx of brines is probably associated with the formation of these minerals. Fluorite veins affecting the kyanite pods suggest that the metamorphic event related to the influx of brines was later than peak metamorphism in the area. In the Chisamba area the scapolite-diopside assemblage indicates amphibolite facies conditions whilst late scapolite consuming calcic plagioclase indicates lower P-T. Microthermometry in the Chisamba area indicates greenschist facies conditions. This means that there were two episodes of fluid influx associated with brines under different metamorphic conditions.

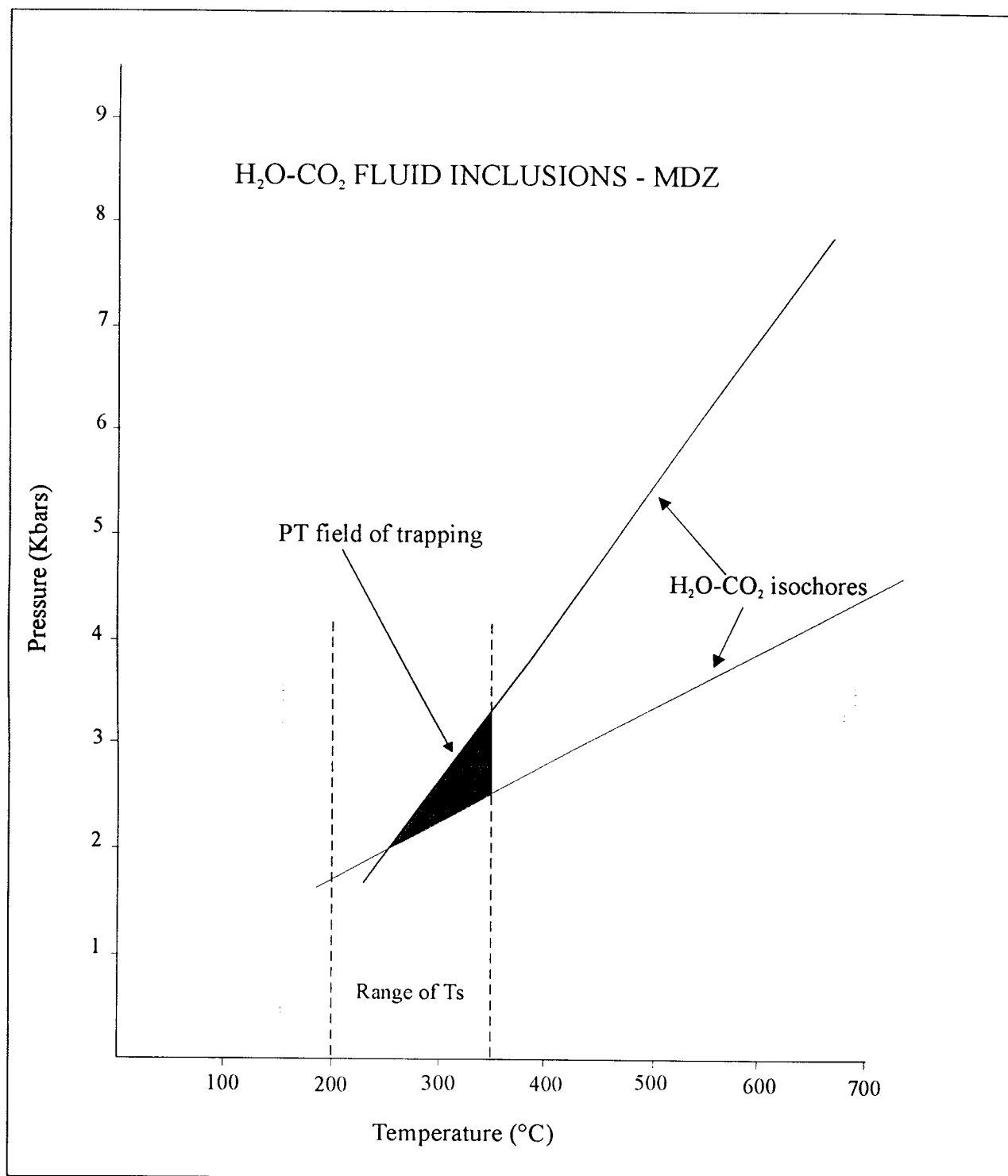


Fig. 6.6: Plot of isochores for  $\text{H}_2\text{O}-\text{CO}_2$  inclusions showing PT trapping conditions:MDZ-Chisamba



## Chapter 7

### 7.0 DEFORMATION HISTORY

#### 7.1 Chisamba area

The area consists of interfolded quartzites, biotite muscovite gneisses, calcareous gneiss, scapolitic marble, calc-silicates, and minor amphibolites. The structural trend in the area is a strong ENE-EW shear foliation, which has transposed all the earlier structures. In some areas, however, earlier NW trends are preserved. The interfolding of the lithologies, coupled with the parallelism of the lithological boundaries with the main foliation trend, indicates a structural rather than a stratigraphic sequence. At least five overprinting deformation events can be deciphered in the basement.

##### **D<sub>1</sub> event**

NW trends parallel to Lufilian Arc /Zambezi belt trends are considered to be S<sub>1</sub> due to an early D<sub>1</sub> event. D<sub>1</sub> structures are preserved in gneiss west of the Wangwa river. S<sub>1</sub> is overprinted by an ENE trending shear foliation, which is designated S<sub>2</sub>. On the eastern side of the Chaisama river, the foliation trends NW in a fold nose of a quartzite lens. The foliation wraps around the fold indicating refolding on ENE axis.

##### **D<sub>2</sub> event**

ENE trending S<sub>2</sub> is axial planar to isoclinally folded quartz veins in gneisses and banding in carbonates. In calcareous gneiss, green amphibole veins are aligned in the S<sub>2</sub> foliation

plane, indicating amphibolite facies conditions,  $M_2$  during  $D_2$ . Amphibolite facies metamorphism is also indicated by kyanite along  $S_2$  in quartzites.

### **$D_3$ event**

Calcareous gneiss in some places is affected by two ENE axial planar sub-parallel foliations with southerly dip directions. The foliation associated with isoclinal intrafolial folds is considered to be  $S_2$  and  $S_3$  is axial planar to gentle small scale folds.  $S_2$  and  $S_3$  are not always easy to distinguish in an outcrop since they are sub-parallel.

### **$D_4$ event**

Oblique stretching lineations,  $L_4$ , are developed in  $S_4$  thrust planes, which are parallel to  $S_2$  in the central part of the area. The plunge and pitch of the stretching lineation, coupled with microstructures, indicate NE directed thrusting consistent with Lufilian thrust transport. The thrust direction is the same as the vergence of structures in the basement. The deformation event related to thrusting is ambiguous. The thrusting event may be attributed to the  $D_4$  event since lineations developed on  $S_2$  or  $S_3$  foliation planes. A stretching lineation is developed on NW trending foliation in gneisses along the Chaisama stream. This indicates that thrusting was related to the Lufilian thrusting event. Thrusting is accompanied by the breakdown of amphibolite facies assemblages to greenschist facies assemblages,  $M_3$

## D<sub>5</sub> event

Shearing on narrow discrete steep to vertical S<sub>5</sub> shear planes is the last deformation event identified in the area. Sub-horizontal stretching lineations, L<sub>5</sub>, developed during D<sub>5</sub>. Although fault trends are discernible on aerial photographs, they were not detected in the field. Instead, discrete shear zones were mapped which, in some instances coincided, with inferred faults. It is suggested that D<sub>5</sub> involved predominantly ductile deformation along discrete shear zones and probably to a lesser extent brittle deformation (faulting). The D<sub>5</sub> event is associated with shear movement along the MDZ. Mesoscopic and microscopic shear sense criteria indicate ENE over WSW dextral shear displacement under greenschist facies conditions, M<sub>3</sub>.

Table 7.1 (a): Summary of the deformation history in the Chisamba area

Deformation event	Structure	Metamorphic event
D <sub>5</sub>	S <sub>5</sub> -Discrete shear zones  L <sub>5</sub> -Subhorizontal stretching lineations	M <sub>3</sub> -Greenschist facies
D <sub>4</sub>	S <sub>4</sub> -thrust planes  L <sub>4</sub> -Plunging stretching lineation indicating NE thrust transport.	M <sub>3</sub> -Greenschist facies Metamorphism
D <sub>3</sub>	S <sub>3</sub> -ENE axial planar Foliation  F <sub>3</sub> -ENE trending gentral Folds	M <sub>2</sub> -Amphibolite facise Metamorphism
D <sub>2</sub>	S <sub>2</sub> -ENE foliation trends  F <sub>2</sub> -ENE trending isoclinal folds	M <sub>2</sub> -Amphibolite facies Metamorphism
D <sub>1</sub>	S <sub>1</sub> -NW Lufilian trend	M <sub>1</sub> ?

## 7.2 Kabwe area

The study area is structurally located in the northeast trending Irumide belt. Although the foliation in the area is parallel to east-north-east to northeast trends of probable Irumide origin, Moore (1964) ascribes the main foliation in the area to Lufilian deformation but later rotated to the present orientation by sinistral drag during movement along the MDZ. Northwest trends believed to be Lufilian trends are restricted to the western margin of the basement but swing into the east-north-east trends close to the MDZ to the south. This trend is not preserved in the central part of the basement and further north away from the MDZ. It is suggested that northwest and east-north-east trends represent different orogenic events and the MDZ has accentuated the ENE trends.

The Irumide belt consists of three structural zones, namely northwesterly, upward and southeasterly facing zones (Daly et al., 1984). The study area is characterized by southward verging structures in the northern part and northward verging structures in the southern part, corresponding to the southeasterly and northwesterly structural zones of Daly et al. (1984).

The area has suffered a long and complex history of deformation. At least three overprinting deformation events are recognisable in Kabwe area.

### **7.2.1 Mwomboshi gneiss**

#### **D<sub>1</sub> and D<sub>2</sub> events: Palaeoproterozoic?**

The two deformation events recognised in the Mwomboshi gneiss are considered to be pre- and syn-Irumide deformation events, D<sub>1</sub> and D<sub>2</sub>, respectively. Compositional layering in the gneisses probably representing an S<sub>1</sub> foliation which has been tightly to isoclinally folded by D<sub>2</sub> about an east-west trending S<sub>2</sub> axial planar shear foliation. The compositional layering is considered to be an early, probably Palaeoproterozoic, fabric in the gneisses, but there could have been older fabrics which have been obliterated. The Mwomboshi gneiss is sheared to various degrees resulting in E-W trending narrow schistose and quartzitic shear zones. These are probably related to D<sub>2</sub>.

The foliation in the gneisses is sub-parallel to the foliation in the overlying metasediments but dips southwards in the opposite direction suggesting that the two foliations are developed from different deformation phases.

### **7.2.2 Chikonkomene Formation**

#### **D<sub>1</sub>-D<sub>3</sub>: Irumide deformation events**

##### **D<sub>1</sub> event**

The Irumide deformation affected both the gneisses and metasediments. The metasediments are considered to belong to the Muva Supergroup on the basis of regional correlation, and as they were deformed for the first time during the Irumide orogeny. This implies that the penetrative foliation in the gneiss is also an Irumide structure. The

parallelism of foliation with bedding, which is represented by iron-oxide banding and strained cobbles, indicates tight to isoclinal folding during  $D_1$ .

### **$D_2$ event**

The second deformation event produced a strong  $S_2$  crenulation cleavage accompanied by tight folding of flattened cobbles and pebbles in the meta-sediments on ENE axes. Where  $D_1$  structures are not affected by crenulation, they are sub-parallel to  $D_2$  structures, indicating folding on almost coincident axes.

### **$D_3$ event**

$D_2$  structures are folded to produce a weak microscopic crenulation cleavage  $S_3$ , which was observed in fine-grained mica-rich phyllitic quartzites.

## **7.2.3 Kangomba Formation**

### **$D_1$ - $D_3$ : Lufilian deformation events**

Three overprinting foliations are observed in phyllite in the Kangomba Formation (Plate 3.24). The Kangomba Formation correlates well with lower Katangan in the region (Moore, 1964). Therefore the first deformation in the Kangomba Formation is of Lufilian age.  $D_1$  is shown by a finely crenulated  $S_1$  foliation in microlithons.  $S_2$  is the main foliation, which resulted from crenulation of  $S_1$ , during  $D_2$ . Fine muscovite and abundant opaque minerals define  $S_2$ . This suggests that solution transfer accompanied the development of

Table 7.1 (b): Summary of the deformation history in the Kabwe area

Age	Deformation event	Structure	Metamorphic event
Post-Lufilian	D <sub>4</sub>	Faults and shear zones -NDZ	M <sub>2</sub> -cataclastic greenschist metamorphism
Neoproterozoic (Lufilian events)	D <sub>3</sub>	S <sub>3</sub> -crenulation cleavage	M <sub>2</sub> -greenschist Facies metamorphism,
	----- D <sub>2</sub> -----	----- S <sub>2</sub> -crenulation cleavage -----	
	D <sub>1</sub>	S <sub>1</sub> -cleavage	
Mesoproterozoic (Irumide events)	D <sub>3</sub>	S <sub>3</sub> -microscopic crenulation cleavage	M <sub>2</sub> -greenschist facies Metamorphism
	----- D <sub>2</sub> -----	----- S <sub>2</sub> -ENE crenulation Cleavage Crenulation of Pebbles -----	
	D <sub>1</sub>	S <sub>1</sub> -layer parallel Foliation Flattening and Streching of pebbles in the meta-conglomerate F <sub>1</sub> isoclinal folding	M <sub>1</sub> -amphibolite facies Metamorphism
Palaeproterozoic	D <sub>2</sub>	S <sub>2</sub> - E-W axial planar foliation F <sub>2</sub> -E-W trending tight to isoclinal folding	M <sub>2</sub> -amphibolite facies Metamorphism
	----- D <sub>1</sub>	----- S <sub>1</sub> -compositinal layering in the Mwomboshi gneiss	M <sub>1</sub> ?

S<sub>2</sub>. S<sub>2</sub> was in turn crenulated to produce weak S<sub>3</sub>, during D<sub>3</sub>. All the foliations are defined by low grade mineral assemblages indicting greenschist facies condntions.

**D<sub>4</sub> event: Post-Lufilian event**

This is the last deformation recorded in the area. It involved dextral shearing and faulting associated with the Nyama dislocation zone.



## Chapter 8

### 8.0 DISCUSSION AND CONCLUSIONS

Microstructures of quartz and feldspar in mylonitic rocks in the Chisamba and Kabwe areas reflect different deformation mechanisms. In the Chisamba area quartz generally occurs as ribbons and lens shaped aggregates showing deformation textures ranging from undulose extinction, deformation bands, serrated grain boundaries, subgrains and core and mantle textures. Feldspar exhibits deformation twins, marginal granulation, kinking and to a lesser extent grain-scale fracturing. In some instances, the feldspar that is caught up in quartz ribbons is lozenge shaped with smooth grain boundaries indicating crystal-plastic deformation. The micro-textures in both quartz and feldspar indicate low to medium temperature crystal-plastic, deformation mechanisms consistent with greenschist facies metamorphic grades. In the Kabwe area, quartz and feldspar accommodated strain differently. The quartz in the mylonitic schists is generally unstrained with straight grain boundaries indicating static recrystallisation. This implies that mylonitic textures have been partly overprinted by annealing textures. The mylonitisation in the Kabwe area, particularly in the Mwomboshi gneiss is considered to be an older event, probably related to the Irumide orogenic event. Feldspar deformed mainly by marginal granulation, though crystal-plastic deformation is indicated by deformation twins, undulose extinction and kinking. The microstructures shown by feldspar, the main constituent mineral, suggests that deformation in the Kabwe area mainly involved cataclastic and to a lesser extent crystal-plastic mechanisms.

The absence of fault rocks in the Chisamba area, widespread development of mylonitic rocks and the coincidence of an inferred fault with a mylonite zone indicate that deformation in the Chisamba area was predominantly by ductile crystal-plastic mechanisms. In the Kabwe area, faults are easily detected by the presence of fault breccia at a number of localities. This substantiates the conclusion from microtextural evidence that deformation was mainly by cataclastic mechanisms.

Metamorphic changes that accompanied deformation in both areas are similar. Amphibolite facies assemblages were downgraded to greenschist facies assemblages during shearing.

An episode of static recrystallisation shown by annealing textures is recorded in both areas. A thermal episode indicated by the emplacement of large syntectonic granitoids associated with the MDZ, e.g. Hook Granite Massif, may be related to the annealing textures observed in the Chisamba area. Metamorphic textures such as plagioclase and hornblende moats around garnet and breakdown of kyanite indicating decompression suggest that the region underwent exhumation. Deeply sourced eclogitic bodies in the Lufilian and Zambezi Belts indicate uplift in the area. The association of transcurrent movement along the SMC in general and MDZ in particular, magmatism and uplift suggests transpressive push-up or flower structure.

Fluid inclusion studies indicate different fluid compositions in the Chisamba and Kabwe areas. The fluid inclusions in the quartz vein from the Chisamba area consist of  $\text{H}_2\text{O}-\text{CO}_2$

±Halite, H<sub>2</sub>O-Halite, and low saline inclusions, whilst those from the Kabwe area comprise H<sub>2</sub>O-halite and low saline complex inclusions. P-T trapping of fluids in the Chisamba area occurred at temperatures ranging from 200 °C to 350 °C and pressures between 2-3 Kbars, consistent with greenschist facies conditions. Fluid inclusion studies of mineralised veins at Matala gold mine show similar P-T conditions. Fluid inclusions from the Kabwe area were trapped at relatively higher temperatures ranging from 350 °C to 500 °C. Although gold mineralisation has been reported within the Chisamba-MDZ area, most of the economic deposits occur in second and third order structures.

The Damaran belt strike-slip faulting along the Schleisen zone commenced between 530-510 Ma and ceased about 491-483 Ma (De Kock, 1996). Shear movement along the MDZ has been dated to have occurred at 551±19 Ma (Hanson et al., 1993) while movement in the Chimarilo zone occurred relatively early about 740-600 Ma (Ring, 1993). The dates from the SMC are consistent with Pan-African ages (1000-570 Ma) suggesting movement along this transcontinental structure occurred during the Pan-African deformation in central Africa.

Ring (1993) deduced dextral shear displacement in the Chimarilo zone from both mesoscopic and microscopic structures. Shear sense evaluation in the MDZ, from the Chisamba area has shown dextral shear movement, consistent with the sense of shear determined in the Chimarilo zone. The sense of shear in the Schleisen zone according to Daly (1986) is sinistral. However, Hoffman (1991) established dextral shear movement in the SMC on the basis of regional tectonic reconstruction. The MDZ is associated with

secondary structures whose shear displacement reflects the overall shear sense on the main structure. The Chinyunyu zone is a dextral shear zone considered to be a secondary structure of the MDZ (Simpson, 1967; Katongo, 1991, Fig 8.2 a). This is supported by a K-Ar age of  $500 \pm 20$  Ma (Snelling et. al., 1972). The previously accepted sinistral sense in the MDZ does not conform to the disposition and sense of shear in the Chinyunyu zone. The dextral sense of shear in the Chinyunyu zone can only be explained by a dextral shear displacement in the MDZ. The sinistral Chindeni zone is believed to be part of the MDZ (De Swardt et al., 1965). However, its orientation with respect to MDZ suggests that it is probably a secondary structure. The orientation and sense of shear of both the Chinyunyu and Chindeni zones about the MDZ can be explained in terms of Riedel shears (Fig. 8.2 B), in a dextral shear regime. The Chinyunyu zone is considered to represent the synthetic Riedel shear (R) while the Chindeni zone developed as an antithetic Riedel shear (R').

The ENE-WSW sub-horizontal plunging stretching lineation mapped in the Chisamba-MDZ area indicate similar tectonic transport direction to both the Lufilian and Zambezi belts. Recent age dates ranging between 550 to 500 Ma, from the Zambezi belt in Zimbabwe indicate that the main phase deformation in the Zambezi belt occurred in the same time range as the Lufilian Arc (Dirks et al., 1998). This implies that the MDZ acted as a transform between the two mobile belts. The model adopted for the tectonic development of the MDZ corroborates that of Daly (1988) but infers dextral rather than sinistral shear movement (Fig. 8.1). The correspondence of timing of transcurrent shearing along the MDZ and regional folding of the Katanga implies that both modes of

deformation relate to a transpressive shear regime (Johns et al., 1989; Hanson et al., 1993).

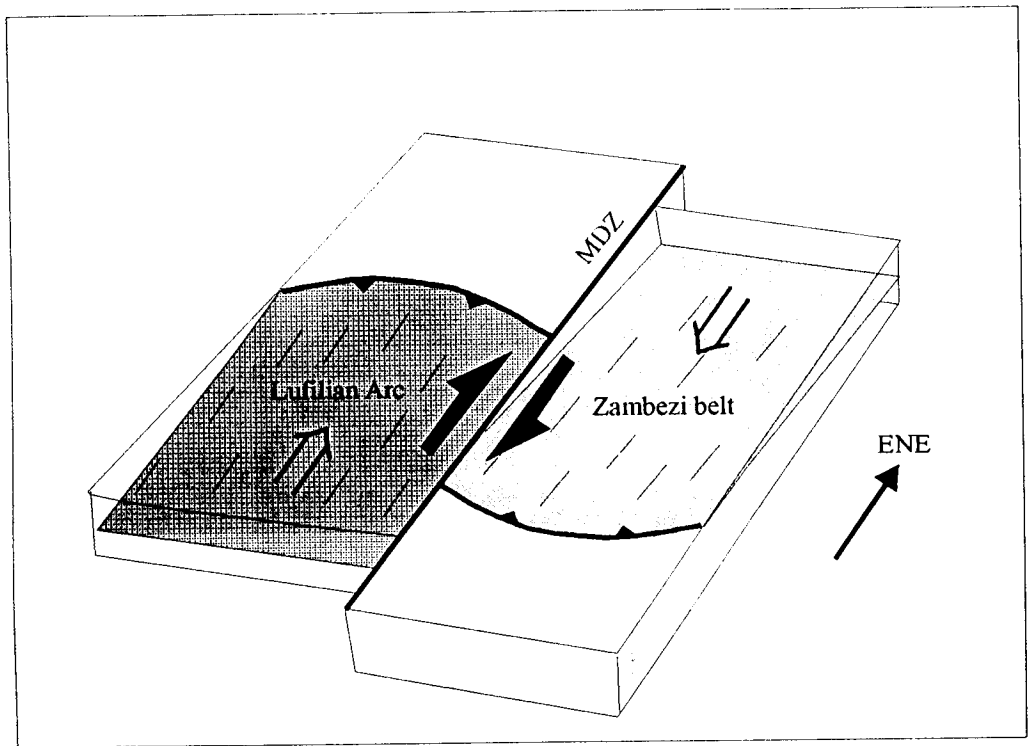


Fig.8.1: Tectonic model showing dextral MDZ separating the Lufilian Arc and Zambezi belt of different geotectonic histories. Open arrows indicate thrust transport.

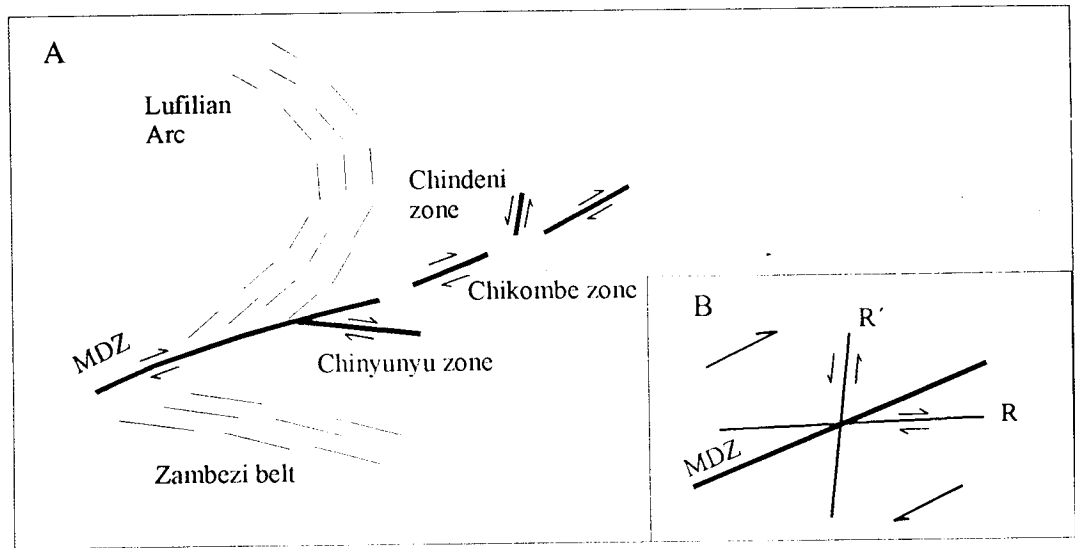


Fig. 8.2 : a) Structural setting of theMDZ and associated second order structures, b) Orientation and sense of shear of second order structures consistent with a Riedel shear pattern. R': Chindeni zone; R: Chinyunyu zone.

## REFERENCES

- Abell, R. S., 1970.** The geology of the Nansenga River area. Explanation of Degree Sheet 1526, NE Quarter: Report of the Geological Survey of Zambia, 25: 62p
- Barr, M. W. C., 1974.** The pre-Karoo geology of the Rufusa area, Zambia, with special reference to structure and metamorphism. (Unpublished) Ph.D thesis. University of Leeds.
- Barr, M. W. C., 1976.** Crustal shortening in the Zambezi Belt. Philosophical Transactions of the Royal Society of London, A280: 555-56
- Barr, M. W. C. and Drysdall, A. R., 1972.** The geology of the Sasare area. Explanation of Degree Sheet 1331, SW Quarter. Report of the Geological Survey of Zambia 30: 73p
- Beach, A. 1980.** Retrogressive metamorphic processes in shear zones with special reference to the Lewisian Complex. Journal of Structural Geology, 2: 257-263
- Blundy, J. D., and Holland, T. J. B., 1990.** Calcic-amphibole equilibria and a new amphibole-plagioclase geothermometer. Contributions to Mineralogy and Petrology, 104: 208-224
- Bucher, K., and Frey, M., 1994.** Petrogenesis of Metamorphic Rocks. Springer-Verlag, Berlin Heidelberg: 318p
- Cahen, L, Snelling, N. J., Delhal, J. and Vail, J. R., 1984.** The geochronology of Africa. Clarendon Press, Oxford: 512p
- Cosi, M., De Bonis, A., Gosso, G., Hunziker, J., Martinotti, G., Maratto, S., Robert, J. P. and Ruhlman, F., 1992.** Late Proterozoic thrust tectonics, high-pressure metamorphism and uranium mineralisation in the Domes area, Lufilian Arc, northwestern Zambia. Precambrian Research, 58:215-240

**Coward, M. P., 1983.** The tectonic history of the Damara Belt. Special publication of the Geological society of South Africa, 11: 409-421.

**Coward, M. P. and Daly, M. C., 1986.** Crustal lineaments and shear zones in Africa: Their relationship to plate movement. Precambrian Research, 24: 27-45

**Daly, M. C., 1988.** Crustal shear zones in central Africa: A kinematic approach to Proterozoic tectonics. Episodes, volume 11, No. 1: 5-11

**Daly, M. C., 1986.** Crustal shear zones and thrust belts: Their geometry and continuity in central Africa. Philosophical Transactions of the Royal Society of London, A317: 111-128

**Deer, W. A., Howie, R. A., and Zussman, J., 1966.** An introduction to the rock forming minerals. Longman, London: 528p

**De Kock, G. S., 1996.** Implications of a new age for the post-tectonic Donkerhuk Granite in the Damara belt of Namibia. IGCP 363 Palaeoproterozoic of sub-equatorial Africa (Abstracts volume): p20

**De Swardt, A. M. J., Drysdall, A. R. and Garrard, P., 1964.** Precambrian geology and structures in central northern Rhodesia. Geological Survey of Northern Rhodesia memoir, No.2: 82p

**De Swardt, A. M. J., Garrard, P. and Simpson, J. G., 1965.** Major zones of transcurrent dislocation and superposition of orogenic belts in parts of central Africa. Geological Society of America Bulletin, volume 76, No. 1: 89-102

**Dirks, P. H. G. M., Jelsma, H. A., Vinyu, M., and Munyanyiwa, H., 1998.** The structural history of the Zambezi belt in northeast Zimbabwe: Evidence for crustal extension during early Pan-African. South African Journal of Geology. 1001(1): 1-16

- Drysdall, A. R., and Stillman, C. J., 1966.** Scapolite from the Katanga carbonate rocks of the Lusaka district. Records of the Geological Survey of Northern Rhodesia, 10: 20-24
- Garrard, P., 1968.** The geology of the Chainama hills area. Explanation of Degree Sheet 1528, NW Quarter. Report of the Geological Survey of Zambia, 24: 80p
- Graham, C. M. and Powell, R., 1984.** A garnet-hornblende geothermometer and applications to Pelona schist, southern California. Journal of Metamorphic Geology, 2: 13-32
- Hanmer, S. and Passchier, C., 1991.** Shear sense indicators: A review. Geological Society of Canada, Paper No. 90-17
- Hanson, R. E., Wardlaw, M. S., Wilson, T. J., and Mwale, G., 1993.** U-Pb zircon ages from the Hook Granite Massif and Mwembeshi Dislocation: Constraints on Pan-African deformation, plutonism and transcurrent shearing in central Zambia. Precambrian Research 63: 183-209
- Hanson, R. E., Wilson, T. J. and Wardlaw, M. S., 1988.** Deformed batholiths in the Pan-African Zambezi belt: Age and implications for regional Proterozoic tectonics. Geology 16: 1134-1137
- Hippertt, J. F. M., 1993.** 'V'-pull -apart microstructures: A new shear sense indicator. Journal of Structural Geology, volume 15, No.12: 1393-1403
- Hirth, G., and Tullis, J., 1992.** Dislocation creep regimes in quartz aggregates. Journal of Structural Geology, volume 14, No. 2: 145-159
- Hobbs, B. E., Means, W. D., and William, P. F., 1976.** An outline of structural geology. John Wiley, New York: 571p



**Hoffman, P. F., 1991.** Did the break up of Laurentia turn Gondwana inside out? *Science* 252: 1409-1412

**Johnson, C. C., Liyungu, K., Mabuku, S., Mwale, G., Sakungo, F., Tembo, D., Vallance, G., Barr, M. W. C., 1989.** The stratigraphy and structural framework of eastern Zambia: Results of a geotraverse. *Journal of African Earth Sciences*. Volume 9, No.9: 123-136

**Kamona, A. F., 1993.** The carbonate-hosted Kabwe Pb-Zn deposit, central Zambia. Ph.D. Thesis (unpublished). University of Aachen, Germany

**Kasolo, P. C., 1992.** Fluid channeling and gold mineralisation within the late Proterozoic Mwembeshi shear zone, Zambia. Ph.D. Thesis (unpublished) University of Southampton.

**Katongo, C., 1991.** The geology of the Namwengi area. Unpublished MG 511 project report. University of Zambia. Lusaka

**Kohn, M. J., and Spear, F. S., 1989.** Empirical calibration of geobarometers for the assemblage, garnet+hornblende+plagioclase+quartz. *American Mineralogist*, 75: 77-84

**Leake, B. E., 1978.** Nomenclature of amphiboles. *Mineralogical Magazine*, volume 42: 533-563

**Lister, G. S and Snoke, A. W., 1984.** S-C mylonite. *Journal of Structural Geology*, 6: 617-638

**Liyungu, A. K., 1986.** Correlation of the Zambezi belt rocks with those to the north of the Mwembeshi Dislocation Zone. UNESCO. *Geology for Economic Development*. Newsletter 5: 173-177

**Mbumba, E., 1990.** Mineralisation at major continental shear zones: Implications for the Mwembeshi zone, Zambia. M. Sc. Thesis (unpublished). University of London.

- Mendelsohn, F., (Editor), 1961.** The geology of the Northern Rhodesia Copperbelt. Macdonald: 523p
- Moore, T. A., 1964.** The Geology of the Chisamba area. Explanation of Degree Sheet 1428, SW Quarter. Report of the Geological Survey of Zambia, 14: 32p
- Munyanyiwa, H., 1983.** The petrological and trace element study of the Mulungushi meta-volcanic rocks. (Unpublished) MG510 project report. University of Zambia, Lusaka.
- Munyanyiwa, H., 1985.** The geochemistry and metamorphism of calc-silicate rocks, marbles and amphibolites in a portion of the Zambezi belt, southern Zambia. M. Sc Thesis (unpublished) University of Zambia.
- Newman, D and A. G. Smith, inpress.** The Geology of the Chipembi area. Explanation of Degree Sheet 1428, SE Quarter. Reoprt of the Geological Survey of Zambia, in press.
- Ng'ambi, O., Boelrijl, N. A. I. M., Priem, H. N. A., and Daly, M. C., 1986.** Geochronology of the Mkushi gneiss complex, central Zambia. Precambrian Research, 32: 279-295
- Passchier, C. W., and Simpson, C., 1986.** Porphyroblast systems as kinematic indicators. Journal of Structural Geology, 8: 831-844
- Passchier, C. W., and Trouw, R. A. J., 1996.** Microtectonics. Springer-Verlag, Berlin: 289p
- Perchuk, L. L., Aronovich, L. Y., Podleskii, K. K., Lavrent'eva, I. V., Gerasimov, V. Y. U., Fedk'in, V. V., Kitsul, V. I., Karsakov, L. P. and Berdnikov, N. V., 1985.** Precambrian granulites of the Aldan Shield, eastern Siberia, USSR Journal of Metamorphic Geology, 3: 265-310
- Pettijohn, F. J., 1975.** Sedimentary rocks. Third edition. Harper, New York: 628p

- Phillips, K. A., 1958.** The geology and metalliferous deposits of the Luri Hills area (Mumbwa district). Explanation of degree sheet 1527 NW quarter. Report of the Geological Survey of Zambia, 4: 67p
- Porada, H., 1989.** Pan-African rifting and orogenesis in southern to equatorial Africa and eastern Brazil. Precambrian Research, 44: 103-136
- Prasad, R. and Vrana, S., 1972.** The intrusives of the Chombwa area with special reference to the eclogites. Records of the Geological Survey of Zambia, 4: 131-137
- Price, N. J., and Cosgrove, J. W., 1990.** Analysis of geological structures. Cambridge University Press. London: 502p
- Ramsay, T. G., and Huber, M. I., 1983.** The techniques of modern structural geology I: strain analysis. Academic press, London: 307p
- Ramsay, C. R. and Ridgeway, J., 1977.** Metamorphic patterns of Zambia and their bearing on problems of Zambian tectonic history. Precambrian Research, 4: 321-372.
- Roedder, E., 1984.** Fluid inclusions: Review. Mineralogical Society of America, 12
- Reichwalder, P., 1978.** The gneiss complex and Mpanshya group in: The geology of the Luano valley. Explanation of degree sheet 1429SW and SE quarters. Report of the Geological Survey of Zambia, 61: 85p
- Ring, U. 1993.** Aspects of the kinematic history and mechanism of superposition of the Proterozoic mobile belts of eastern-central Africa (northern Malawi and southern Tanzania). Precambrian Research, 62: 207-226
- Shepherd, J. P., Rankins, A. H, and Alderton, D. H. M., 1985.** A practical guide to fluid inclusion studies. Blackie and sons. Glasgow:

**Sibson, R. H., 1977.** Fault rocks and fault mechanisms. *Journal of the Geological Society of London*, 13: 191-213

**Simpson, J. G., Drysdall, A. R. and Lambert, H. H. J., 1963.** The geology and ground water resources of Lusaka area. Explanation of degree sheet 1528 NW quarter. Report of the Geological Survey of Zambia, 6: 59p

**Simpson, J. G., 1967.** The geology of the Chinyunyu area. Explanation of degree sheet 1529 NW quarter. Report of the Geological Survey of Zambia, 19: 70p

**Simpson, J. G., 1962.** The geology of the Mwembeshi River area. Explanation of degree sheet 1527 NE quarter. Report of the Geological Survey of Zambia, 11: 29p

**Simpson, C. and Schmid, S., 1983.** An evaluation of criteria to deduce the sense of movement in sheared rocks. *Bulletin of the Geological Society of America*, 94: 1281-1288

**Simpson, C., and Wintch, R. R., 1989.** Evidence of deformation-induced K-feldspar replacement by myrmekite. *Journal of metamorphic geology*, 7: 261-275

**Sliwa, A., 1981.** Final report on Mumbwa PL 152. Minex report (unpublished)

**Smith, A. G., 1963.** The geology of the country around Mazabuka and Kafue. Explanation of degree sheet 1527, SE quarter and 1528, SW quarter. Report of the Geological Survey of Northern Rhodesia, 2: 32p

**Smith, A. G., 1966.** The geology of the Kapiri-Mposhi area. Explanation of degree sheet 1328 SE quarter. Report of the Geological Survey of Zambia, 12: 32p

**Snelling, N. J., Johnson, R. L., and Drysdall, R. L., 1972.** The geochronology of Zambia. *Records of the Geological Survey of Zambia*, 12: 19-30

**Spear, F. S., 1993.** Metamorphic phase equilibria and pressure-temperature-time paths. *Mineralogical Society of America Monograph*. Washington D. C: 799p

- Spry, A., 1969.** Metamorphic textures. Pergamon Press, London: 350p
- Stillman, C. J., 1965.** The geology of the Musofu river and Mkushi areas. Explanation of degree sheet 1329, part of NW and SW quarters. Report of the Geological Survey of Zambia, 12: 52p
- Stillman, C. J., and Simpson, J. G., 1963.** 'Muva' sequences southeast of the Copperbelt and in the southern part of the Central Province. Records of the Geological Survey of Zambia, 9: 1-9
- Soto, J. I., 1993.** Ptmafic: Software for thermobarometry and activity calculations with mafic and ultramafic assemblages. American Mineralogist, volume 78: 840-844
- Tembo, F., 1994.** The geology, geochemistry and tectonic significance of metagabbroic rocks in the Lufilian arc of Zambia. Ph.D. Thesis (unpublished). Goettingen University, Germany.
- Thieme, J. G., Johnson, R. L., 1981.** Geological map of the Republic of Zambia. 1:1,000,000. Geological Survey of Zambia
- Thieme, J. G., 1984.** Geological map of the Lusaka area. 1:250,000 geological map series, sheet no. SD-35-15
- Tullis, J., and Yund, R. A., 1985.** Dynamic recrystallisation of feldspar: A mechanism of ductile shear zone formation. Geology, 13: 238-241
- Unrug, R., 1983.** The Lufilian Arc: A microplate in the Pan-African collision zone of the Congo and Kalahari cratons. Precambrian Research, 21: 181-196
- Vernon, R. H., 1991.** Questions about myrmekite in deformed rocks. Journal of Structural Geology, 13: 979-985

**Vrana, S., Prasad, R. and Fediukova, E., 1975.** Metamorphic kyanite eclogites in the Lufilian Arc of Zambia. *Contributions Mineralogy Petrology*, 51: 1-22

**Williams, H. Francis, J. T. and Gilbert, C. M., 1982.** Petrography. An introduction to the study of rocks in thin sections. Second edition. W. H. Freeman and Company. San Francisco: 626p

**Wilson, T. J., Hanson, R. E. and Wardlaw, M. S., 1993.** Meso- and Neoproterozoic tectonics of southern Africa in relation to Gondwana assembly. *EOS* 73 (14): 369.

## APPENDIX

### FLUID INCLUSION DATA

#### Explanation of abbreviations in appendix

Lsv	-	liquid- solid-vapour inclusions
Thsvl	-	temperature of homogenisation of lsv fluid inclusion to liquid
Thsvv	-	temperature of homogenisation of LSV fluid inclusion to vapour
Thaqv	-	temperature of homogenisation of aqueous fluid inclusion to vapour
Thaql	-	temperature of homogenisation of aqueous fluid inclusion to liquid
Ts	-	temperature of dissolution of halite
TmCO <sub>2</sub>	-	temperature of melting of CO <sub>2</sub>
ThCO <sub>2</sub>	-	temperature of homogenisation of liquid and vapour CO <sub>2</sub>
ThH <sub>2</sub> O-CO <sub>2</sub>	-	temperature of homogenisation of H <sub>2</sub> O and CO <sub>2</sub>
Td	-	temperature of decrepitation
Thtot	-	Temperature of total homogenisation of LSV fluid inclusions
Wt% NaCl	-	Salinity of fluid inclusion

Table IA-1: SAMPLE KK59

	Thsvl	Thsvv	Thaqv	Thaql	Ts	TmCO <sub>2</sub>	ThCO <sub>2</sub>	ThH <sub>2</sub> O-CO <sub>2</sub>	Td
1	309.10	338.20	214.10	309.10	309.80	-57.30	14.80	322.10	215.30
2	194.70	338.20	308.20		269.80	-57.30	18.10	405.20	217.20
3	195.70	428.50	448.10		295.50	-57.30	11.80	438.50	269.80
4	309.10	476.10	418.20		261.50	-57.30	17.00	369.30	241.40
5	276.90	489.40	328.80		262.30	-57.20	24.70	344.60	536.30
6	300.10	462.80	335.60		284.20	-57.30	21.30	275.10	
7	281.10	401.20	405.20		275.50	-57.30	27.00	275.10	
8		452.30	438.50		248.70	-57.30	17.20	338.90	
9		342.20			248.20	-57.20	26.50	260.80	
10		415.80			290.40	-57.10	7.50	300.50	
11		241.70			255.70	-57.20	23.10	242.40	
12		284.20			294.30		18.30	294.40	
13		332.60			275.50		18.30	289.30	
14		390.60			194.70		13.30	239.60	
15		395.60			188.20		22.80	306.70	

16		385.30			219.10		22.50	244.10	
17		280.10			293.80		15.70	284.30	
18		326.70			207.90		20.40	295.70	
19		332.10			315.50		16.30	256.00	
20		418.20			349.70		18.40	345.60	
21		321.90			285.20		14.80	320.10	
22		494.30			297.30		21.00	285.50	
23		240.40			276.90		20.80	474.80	
24					281.10		24.80	246.60	
25					300.10		19.30	321.60	
26					202.90		19.40	321.60	
27					315.50		19.40	318.20	
28					251.30		24.40	240.40	
29					293.90		25.80	506.70	
30					262.80		25.40	325.70	
31					287.50		24.70	295.70	
32					277.10		22.80	245.10	
33					298.10		24.10	323.70	
34					301.20		22.80	180.60	
35					255.10		24.10	257.60	
36					308.70		25.40	366.70	
37					293.20		25.00	240.30	
38					294.50		24.30		
39					269.30		21.80		
40					251.20		22.70		
41							20.10		
42							16.90		
43							18.00		
44							26.60		
45							22.70		
46							26.30		
47							27.30		



48							29.10		
49							22.50		
50							22.40		
51							30.50		
52							28.30		
53							27.60		
54							28.10		
55							28.00		
56							27.60		
57							27.50		
58							27.60		
59							28.60		
60							27.50		
61							28.50		
62							27.90		
63							27.90		
64							28.70		

Table IA-2: SAMPLE KK 59

	Th <sub>tot</sub> °C	T <sub>s</sub> °C	Wt% NaCl
1	494.3	261.5	35.5
2	290.4	309.1	37.4
3	338.2	284.2	37.0
4	321.9	275.5	36.4
5	428.5	294.3	37.7
6	476.1	275.5	36.4
7	194.7	194.2	31.6
8	188.2	195.1	31.3
9	462.8	219.1	32.9
10	536.3	315.5	39.4
11	452.3	349.7	42.4
12	285.4	342.4	37.1
13	415.8	297.3	38.0
14	276.9	276.9	36.5
15	300.1	300.1	38.2
16	332.6	315.5	39.4
17	390.6	313.9	39.3
18	395.6	281.3	34.8
19	385.3	293.9	37.7
20	326.7	277.1	36.5
21	332.2	298.1	38.0
22	322.1	255.1	35.0
23	438.5	308.7	38.8

Table IB-1: SAMPLE CK 37

	Thlvsl	Thlvsv	Thaql	Thaqv	Ts	Td
1	198.90	466.20	220.70	325.60	310.00	369.80
2	335.60	340.60	243.70	290.20	126.00	368.80
3	260.20	421.80	248.70	475.50	160.00	466.80
4	310.00	340.60	243.70	198.70	320.20	282.20
5	473.60	391.60	230.80	282.30	155.70	490.80
6	279.00		161.80	507.70	130.20	421.80
7	340.20		249.80	522.20	231.50	400.10
8	260.70		273.80	255.20	310.00	199.30
9	356.80		394.80	281.60	268.30	260.60
10	361.20		247.70	490.80	473.60	500.90
11	283.40		237.90	271.20	394.60	548.20
12	355.60		247.20	548.20	385.60	413.60
13	360.20		348.60		279.00	413.60
14	210.20		226.60		247.70	410.60
15			247.20		340.20	363.20
16			233.60		260.70	434.40
17			217.20		260.70	454.80
18			212.80		361.20	298.80
19			206.20		283.40	178.70
20			206.70		360.20	440.00
21			194.20		417.20	370.60
22			235.90		385.50	427.60
23			263.60		391.20	399.20
24			242.20		33.50	425.60
25			232.20		490.30	253.20
26			205.60			399.20
27			199.80			399.20
28			299.20			337.70
29			295.70			260.70
30			202.50			337.70

31			264.70			369.90
32			292.80			391.60
33						394.20
34						414.60
35						406.50
36						454.20
37						408.60
38						330.30
39						355.60
40						450.60
41						424.60
42						380.90
43						355.60
44						500.10
45						224.10
46						410.10
47						360.20
48						244.60
49						368.10
50						308.70
51						210.50
52						358.50

Table IB-2: SAMPLE KK 37

	Th <sub>tot</sub> °C	T <sub>s</sub> °C	Wt% NaCl
1	198.9	155.7	29.9
2	260.2	130.2	28.9
3	310.0	310.0	38.9
4	473.0	473.0	56.2
5	453.3	453.3	53.7
6	440.2	230.5	33.5
7	279.0	279.0	36.6
8	340.2	340.2	41.5
9	260.7	260.7	35.4
10	221.3	221.3	33.0
11	356.8	356.8	43.0
12	361.2	361.2	43.5
13	344.2	344.2	41.9
14	283.4	283.4	36.9
15	315.7	315.7	39.4
16	360.2	360.2	43.4
17	417.2	417.2	49.4
18	490.3	490.3	58.5